

**KCNT1-Associated Epileptic Encephalopathies in Mouse Models:  
Phenotypic Characterization and Targeted Therapeutic Interventions**

Inaugural Dissertation

zur

Erlangung des Doktorgrades

Dr. nat. med.

der Medizinischen Fakultät

und

der Mathematisch-Naturwissenschaftlichen Fakultät

der Universität zu Köln

vorgelegt von

Timuçin Baş

aus Şişli, Türkei

Copy Star Copyshop, Köln

2025

Betreuer/in: Prof. Dr. Dirk Isbrandt

Referent/in: Prof. Dr. Tatiana Korotkova

Prof. Dr. Matteo Bergami

Datum der mündlichen Prüfung: 31.03.2025

# Contents

List of Figures .....	VIII
List of Tables.....	X
List of Abbreviations .....	XI
Abstract (English).....	XIV
Abstract (German) .....	XV
1.   Introduction .....	1
1.1   Epilepsy and Genetic Factors.....	1
1.2   KCNT1: Structure and Function.....	2
1.2.1   Structure and Expression Patterns in the Nervous System.....	2
1.2.2   Role in Regulating Neuronal Excitability .....	3
1.3   <i>KCNT1</i> Mutations and Associated Epilepsy Syndromes .....	4
1.3.1   Spectrum of KCNT1-Associated Epilepsies.....	4
1.3.2   Autosomal Dominant Nocturnal Frontal Lobe Epilepsy (ADNFLE).....	4
1.3.3   Epilepsy of Infancy with Migrating Focal Seizures (EIMFS).....	5
1.3.4   Other Associated Epileptic Encephalopathies .....	6
1.3.5   Genotype-Phenotype Relationships .....	6
1.4   Molecular Mechanisms of <i>KCNT1</i> Mutations.....	7
1.4.1   Types of Mutations .....	7
1.4.2   Gain-of-Function Nature of Most Epilepsy-Associated Mutations .....	8
1.4.3   Effects on Channel Properties .....	8
1.5   Pathophysiology of KCNT1-Associated Epilepsies.....	9
1.5.1   Hypothesized Mechanisms of Epileptogenesis.....	9
1.5.2   The Role of Increased Potassium Conductance in Neuronal Hyperexcitability	10
1.5.3   Differential Effects on Inhibitory and Excitatory Neurons .....	10

1.6	Comorbidities of KCNT1-Associated Epilepsies.....	11
1.6.1	Associated Intellectual Disabilities .....	11
1.6.2	Psychiatric Features and Behavioural Issues .....	11
1.6.3	Potential Cardiac Arrhythmias and SUDEP Risk .....	11
1.7	Current Treatment Strategies and Challenges .....	12
1.7.1	Resistance to Conventional Antiepileptic Drugs .....	12
1.7.2	Potential Targeted Therapies .....	12
1.7.3	Need for Personalized Treatment Approaches.....	13
1.8	Future Directions and Research Gaps.....	14
1.8.1	Ongoing Research into KCNT1 Channel Function and Regulation .....	14
1.8.2	Development of Novel Therapeutic Targets .....	14
1.8.3	Potential for Gene Therapy or Precision Medicine Approaches .....	14
1.9	Identification and Modeling of <i>KCNT1</i> Mutations .....	15
1.10	Identification and Validation of KCNT1 Blockers .....	16
1.10.1	Pimozide as a Potential Therapeutic Agent for KCNT1-associated Epilepsy..	17
1.10.2	Carvedilol as a Potential Therapeutic Agent for KCNT1-associated Epilepsy	18
1.11	The Aims and Scope of the Study .....	19
2.	Materials and Methods.....	20
2.1	Animal Husbandry and Generation of Animal Models.....	20
2.2	Genotyping .....	20
2.3	Telemetric Electrocorticogram (ECoG).....	23
2.3.1	Surgical Protocol for Telemetric Implants .....	23
2.3.2	Analysis of ECoG Recordings .....	25
2.4	KCNT1 Blockers Administration .....	27
2.4.1	Pimozide Treatment in Heterozygous KCNIN Adult Mice.....	27
2.4.2	Pimozide Treatment in Homozygous KCNRQ Adult Mice .....	28

2.4.3	Carvedilol Treatment in Heterozygous KCNIN Adult Mice.....	29
2.4.4	Carvedilol Treatment in Heterozygous KCNIN Neonatal Mice .....	29
2.5	Immunohistochemistry.....	30
2.5.1	Sample Preparation .....	31
2.5.2	Staining Procedures .....	32
2.5.3	Image Acquisition and Analysis .....	34
2.6	Body Weight Development and Behavioural Tests .....	35
2.6.1	Somatosensory Reflex Tests in Neonatal Animals .....	36
2.6.2	Open Field.....	36
2.6.3	Elevated Plus Maze.....	37
2.6.4	Y-Maze .....	37
2.6.5	Object Location Memory.....	38
2.6.6	Object Recognition Memory .....	39
2.6.7	Step-Through Passive Avoidance .....	39
2.6.8	The Analysis of Behavioural Experiments.....	40
3.	Results.....	41
3.1	Spontaneous Seizures in KCNT1 Mutant Models .....	41
3.2	Altered Cortical Oscillations During Interictal Periods .....	43
3.3	Severe Sleep Architecture Disruptions .....	46
3.4	Genotype Effects on Development, Behavior and Cognition .....	48
3.4.1	Impaired Development and Sensory-Motor Function .....	48
3.4.2	Locomotion and Habituation Deficits .....	49
3.4.3	Reduced Anxiety-Like Behavior .....	50
3.4.4	Working Memory Deficits.....	51
3.4.5	Intact Recognition Memory.....	53
3.4.6	Impaired Long-Term Memory.....	54

3.5	Morphological Changes Associated with Epileptic Activity .....	55
3.5.1	Altered Perineuronal Nets in the Dentate Gyrus Molecular Layer .....	55
3.5.2	Increased NPY Expression in Mossy Fibers .....	56
3.5.3	Enhanced Reactive Astroglia in the Hippocampus .....	58
3.6	Pimozide Treatment in Adult KCNT1 Mutants .....	59
3.6.1	Pimozide Treatment in Adult KCNIN Heterozygous Animals .....	59
3.6.2	Pimozide Treatment in Adult KCNRQ Homozygous Animals .....	62
3.7	Carvedilol Treatment in Adult KCNIN Mutants .....	64
3.8	Preventive Carvedilol Treatment in Neonatal KCNIN Mutants .....	67
3.8.1	Positive Effects of Early Carvedilol Treatment on Seizures and Cortical Excitability .....	67
3.8.2	Mild Sleep Architecture Alterations Unaffected by Carvedilol Treatment .....	70
3.8.3	Reduction in Anxiety-Like Behavior Following Carvedilol Treatment .....	71
3.8.4	Perineuronal Nets Remain Unaltered by Carvedilol Treatment .....	72
3.8.5	Normal Astroglia Levels in Juvenile KCNIN Heterozygotes .....	73
4.	Discussion .....	75
4.1	KCNT1 Mutations Cause Severe Epileptic Phenotypes, Altered Oscillatory Dynamics, and Disrupted Sleep Architecture .....	76
4.2	Developmental and Behavioural Deficits Reflect Genotype-Specific Neurological Impairments .....	78
4.3	Morphological Changes Correlate with Network Hyperexcitability .....	80
4.4	KCNT1 Blocker Treatment in Adult Mice Fails to Reverse Epileptic Phenotypes .....	82
4.5	Early Treatment Reduces the Severity of Epileptic Phenotypes .....	83
4.6	Synaptic Transmission Alterations Highlight E/I Balance Shift in KCNT1 Mutants .....	85
4.7	Future Directions .....	88
5.	Conclusion .....	91

References .....	93
Acknowledgement .....	102
Statutory Declaration .....	103

## List of Figures

Figure 1: Proposed mechanism of hSlo2.2 channel closed and open states. ....	2
Figure 2: Activation of Slack channels by cytoplasmic sodium .....	4
Figure 3: The mutation positions identified by previous studies. ....	5
Figure 4. Functional characterization of KCNT1 mutations .....	16
Figure 5: Surgical Setup and Electrode Position. ....	25
Figure 6: Automated brain state detection using AccuSleep. ....	27
Figure 7: Regions of interest (ROI) analysed for immunohistochemistry quantifications.....	35
Figure 8: Spontaneous seizures and interictal activity in KCNT1 mutant models. ....	41
Figure 9: Seizure incident variability in KCNIN and KCNRQ mutant models. ....	43
Figure 10: The analysis of interictal cortical oscillations in KCNIN heterozygous animals. .	44
Figure 11: The analysis of interictal cortical oscillations in KCNRQ homozygous animals. .	45
Figure 12: Severe disruptions in sleep architecture in KCNRQ homozygous and moderate alterations in KCNIN heterozygous mutant models. ....	47
Figure 13: Genotype-specific effects on body weight development and somatosensory reflexes in KCNIN and KCNRQ models. ....	49
Figure 14: Increased locomotion and impaired habituation in KCNIN animals and reduced locomotion and increased anxiety-like behavior in KCNRQ homozygous males. ....	50
Figure 15: Reduced anxiety-like behavior in KCNIN heterozygous and KCNRQ homozygous animals. ....	51
Figure 16: KCNRQ homozygous male animals exhibit working memory impairments in the Y-Maze, while KCNIN animals maintain intact memory performance. ....	52
Figure 17: Intact recognition memory in KCNRQ animals. ....	53
Figure 18: Epileptic KCNIN heterozygous and KCNRQ homozygous animals exhibit impaired memory in the Step-Through Passive Avoidance Test. ....	54
Figure 19: Altered perineuronal nets in the dentate gyrus molecular layer, with enhanced WFA signal intensity in KCNRQ homozygous and KCNIN heterozygous animals. ....	56

Figure 20 Increased NPY signal intensity in the mossy fibers is pronounced in KCNRQ homozygous animals and shows higher variability in KCNIN heterozygotes. ....	57
Figure 21: Enhanced astrocytic reactivity in the hippocampal area of KCNRQ homozygous animals and a trend toward increased astrogliosis in KCNIN heterozygotes. ....	59
Figure 22: Pimozide treatment did not affect seizure incident rates in adult KCNIN heterozygous animals. ....	60
Figure 23 Chronic pimozide treatment normalized the aberrant beta oscillations during REM sleep in adult KCNIN heterozygous animals. ....	61
Figure 24: Pimozide treatment did not affect seizure frequency in adult KCNRQ homozygous animals. ....	63
Figure 25: Chronic pimozide treatment did not alter interictal oscillations in adult KCNRQ homozygous animals. ....	64
Figure 26: Chronic carvedilol treatment did not affect seizure frequency in adult KCNIN heterozygous animals. ....	65
Figure 27: Chronic carvedilol treatment did not alter interictal oscillations in adult KCNIN heterozygous animals. ....	66
Figure 28: Early carvedilol treatment prevents seizures in a subset of juvenile KCNIN heterozygous animals. ....	68
Figure 29: Early carvedilol treatment shows a trend toward reduced cortical excitability in juvenile KCNIN heterozygous animals. ....	69
Figure 30: Mild alterations in sleep architecture in juvenile KCNIN heterozygous animals with no significant effect of carvedilol treatment. ....	71
Figure 31: Carvedilol treatment reduces anxiety-like behavior in juvenile KCNIN heterozygous animals. ....	71
Figure 32: Increased perineuronal nets in the dentate gyrus molecular layer of non-treated KCNIN heterozygous animals are not prevented by carvedilol treatment. ....	73
Figure 33: Normal Astroglia Levels in Juvenile KCNIN Heterozygotes. ....	74
Figure 34: Pronounced synaptic transmission alterations in the sensory-motor cortex layer 2/3 of KCNRQ homozygote animals. ....	85

## List of Tables

Table 1: Primer Sequences for Genotyping KCNIN and KCNRQ Animals. ....	21
Table 2: Reagents for the PCR and qPCR Reaction Setups. ....	22
Table 3: Thermal Cycling Program for KCNIN. ....	22
Table 4: Thermal Cycling Program for KCNRQ. ....	23
Table 5: Thermal Cycling Program for KCNIN-qPCR. ....	23
Table 6: Synaptic transmission alterations in KCNT1 mutants. ....	86

## List of Abbreviations

ANOVA = analysis of variance

ASM = anti-seizure medication

bp = base pairs

CA = cornu ammonis

Ca<sup>2+</sup> = calcium

cm = centimeter

D.I. = discrimination index

DEE = developmental and epileptic encephalopathy

dNTP = deoxyribonucleotide triphosphate

DSI = Data Science International

E/I = excitation/inhibition

ECoG = electrocorticogram

EDTA = ethylenediaminetetraacetic acid

EIEE = early infantile epileptic encephalopathies

EPM = elevated plus maze

EPSC = excitatory postsynaptic current

EPSP = excitatory postsynaptic potential

FW = forward

*foof* = fitting-oscillations-and-one-over-f

GABA = gamma-aminobutyric acid

GFAP = glial fibrillary acidic protein

h = hour

H<sub>2</sub>O = water

HCl = hydrogen chloride

i.p. = intraperitoneal

IPSC = inhibitory postsynaptic current

IPSP = inhibitory postsynaptic potential

ITI = intertrial interval

K<sup>+</sup> = potassium

KCNIN = KCNT1<sup>pI296N</sup>

KCNRQ = KCNT1<sup>pR911Q</sup>

LANUV = Landesamt für Natur, Umwelt und Verbraucherschutz

mA = milliamperes

min = minutes

mEPSC = miniature excitatory postsynaptic current

mIPSC = miniature inhibitory postsynaptic current

Mut = mutant

Na<sup>+</sup> = sodium

NaCl = sodium chloride

NOEE = neonatal-onset epileptic encephalopathy

NPY = neuropeptide Y

ns = not significant

OLM = object location memory

ORM = object recognition memory

PD = postnatal day

PCR = polymerase chain reaction

PSD = power spectrum density

PV+ = parvalbumin-positive

Pyr = pyramidal neurons

REM = rapid eye movement

Rev = reverse

RMP = resting membrane potential

s = seconds

sEPSC = spontaneous excitatory postsynaptic current

sIPSC = spontaneous inhibitory postsynaptic current

SOM+ = somatostatin-positive

SWS = slow-wave-sleep

SWRs = sharp-wave ripples

t = time

T<sub>m</sub> = melting temperature

TEA = tris acetate ethylenediaminetetraacetic acid

TLE = temporal lobe epilepsy

UV = ultraviolet

vs. = versus

WFA = *Wisteria floribunda* agglutinin

WT = wild type

## Abstract (English)

Developmental and epileptic encephalopathies (DEE) are severe neurodevelopmental disorders characterized by refractory seizures, cognitive deficits, and behavioral abnormalities. Among these, KCNT1-associated DEE are caused by gain-of-function (GoF) mutations in the *KCNT1* gene, encoding the sodium-gated potassium channel  $K_{Na1.1}$  (Slack). These mutations disrupt neuronal excitability, leading to profound impairments in brain development and function. Despite the severity of these disorders, treatment options remain extremely limited, and there are no approved therapies specifically targeting *KCNT1* mutations. This thesis investigates the pathophysiological mechanisms underlying KCNT1-associated epilepsy and evaluates potential therapeutic interventions using two novel knock-in mouse models harboring patient-derived *KCNT1* mutations, p.I335N (KCININ) and p.R950Q (KCNRQ), which exhibit distinct GoF properties.

Comprehensive phenotypic characterization of these models revealed spontaneous generalized seizures, significant hippocampal pathology, and pronounced behavioral abnormalities. Histological analyses demonstrated reactive astrogliosis, enhanced perineuronal net density in the dentate gyrus, and elevated neuropeptide Y expression in the hippocampal mossy fibers, indicative of extensive hippocampal network remodeling. Behavioral experiments revealed increased locomotion, reduced anxiety-related behavior, and impaired memory performance. Electrocorticography (ECoG) recordings uncovered significant disruptions in sleep architecture and interictal network activity, including reductions in cortical theta power during both sleep and wakefulness. Together, these findings establish the face and construct validity of these mouse models for KCNT1-associated epileptic encephalopathies.

To address the limited efficacy of existing treatment options, brain-permeable KCNT1 channel blockers were identified through high-throughput screening of FDA-approved compounds and validated on KCNT1 channels in vitro. Chronic treatment with these blockers in adult mice failed to ameliorate seizure phenotypes, highlighting the importance of targeting earlier developmental periods. Notably, treatment administered during the neonatal period increased the proportion of seizure-free animals but did not prevent the alterations in interictal network activity, emphasizing the need for therapeutic interventions that address the early stages of epileptogenesis. This study provides a detailed characterization of KCNT1-associated epilepsy models, elucidates their underlying pathophysiology, and highlights important challenges of developing therapies for these disorders. These findings underscore the urgent need for precision medicine approaches targeting developmental windows to address the unmet clinical need for effective treatments.

## Abstract (German)

Entwicklungs- und epileptische Enzephalopathien (*developmental and epileptic encephalopathies*, DEE) sind schwere neurologische Entwicklungsstörungen, die durch refraktäre Anfälle, kognitive Defizite und Verhaltensanomalien gekennzeichnet sind. KCNT1-assoziierte DEE werden durch Gain-of Function (GoF)-Mutationen im KCNT1-Gen verursacht, das für den Natriumaktivierten Kaliumkanal  $K_{Na}1.1$  (Slack) kodiert. Diese Mutationen stören die neuronale Erregbarkeit, was zu tiefgreifenden Beeinträchtigungen von Gehirnentwicklung und -funktion führt. Trotz der Schwere dieser Störungen sind die Behandlungsmöglichkeiten nach wie vor äußerst begrenzt, und es gibt keine zugelassenen Therapien, um *KCNT1*-Mutationen gezielt zu behandeln. In dieser Arbeit werden die pathophysiologischen Mechanismen untersucht, die der KCNT1 assoziierten Epilepsie zugrunde liegen, und potenzielle therapeutische Interventionen an zwei neuen Knock-in-Mausmodellen, die von Patienten stammende KCNT1-Mutationen tragen, p.I335N (KCIN) und p.R950Q (KCNRQ), die unterschiedliche GoF-Eigenschaften aufweisen, evaluiert.

Eine umfassende phänotypische Charakterisierung dieser Modelle ergab spontane generalisierte Anfälle, eine signifikante Pathologie des Hippocampus und ausgeprägte Verhaltensanomalien. Histologische Analysen zeigten eine reaktive Astroglie, erhöhte perineuronale Netzdichten im *Gyrus dentatus* und eine erhöhte Neuropeptid Y Expression in den Moosfasern des Hippocampus, was auf einen umfassenden Umbau des Hippocampus Netzwerks hindeutet. Die Bewertung des Verhaltensexperimente ergaben eine gesteigerte Lokomotion, ein vermindertes angstbedingtes Verhalten und eine beeinträchtigte Gedächtnisleistung. Elektrokortikographieaufnahmen (ECoG) ergaben signifikante Störungen der Schlafarchitektur und der interiktalen Netzwerkaktivität, einschließlich einer Verringerung kortikaler Thetaoszillationen sowohl im Schlaf als auch im Wachzustand. Zusammengefasst belegen diese Ergebnisse die Validität der Mausmodelle für KCNT1-assoziierte epileptische Enzephalopathien.

Um die begrenzte Wirksamkeit bestehender Behandlungsmöglichkeiten zu verbessern, wurden hirnpereable KCNT1-Kanalblocker in einem Hochdurchsatz-Screening FDA-zugelassener Substanzen identifiziert und an KCNT1-Kanälen *in vitro* validiert. Die chronische Behandlung erwachsener Mäuse mit diesen Blockern führte nicht zu einer Verbesserung des Anfallsphänotyps, was zeigt, wie wichtig es ist, in früheren Entwicklungsphasen anzusetzen. Eine Behandlung während der Neugeborenenperiode erhöhte zwar den Anteil anfallsfreier Tiere, verhinderte aber nicht die Veränderungen in der interiktalen Netzwerkaktivität, was die Notwendigkeit therapeutischer Maßnahmen in den frühen Stadien der Epileptogenese weiter unterstreicht. Diese Studie liefert eine detaillierte Charakterisierung von KCNT1-assoziierten Epilepsiemodellen, klärt die zugrunde liegende Pathophysiologie auf und zeigt wichtige Herausforderungen bei der Entwicklung von Therapien für diese Erkrankungen auf. Diese Ergebnisse unterstreichen den dringenden Bedarf an präzisionsmedizinischen Ansätzen, die auf Entwicklungsfenster abzielen, um den ungedeckten klinischen Bedarf an wirksamen Behandlungen zu decken.

# 1. | Introduction

## 1.1 | Epilepsy and Genetic Factors

Epilepsy is a complex and chronic neurological disorder, characterized by the recurrence of unprovoked seizures resulting from abnormal electrochemical activity in the brain. It represents one of the most common neurological conditions globally, affecting approximately 1-3% of the global population over their lifetime, with significant heterogeneity in its etiology, clinical presentation, and response to treatment (Boillot and Baulac 2016; McTague et al. 2016). Seizures, the hallmark of epilepsy, can manifest in diverse forms, from focal events, which originate in a specific brain region, to generalized seizures, which involve widespread cortical networks (McTague et al. 2016). The clinical spectrum ranges from brief lapses in consciousness to severe convulsions. While traditionally, epilepsy has been attributed to structural, infectious, or metabolic causes, genetic factors have emerged as pivotal in understanding many forms of the disorder, particularly early-onset and refractory epilepsies (Villa and Combi 2016).

The core feature of epilepsy is the brain's predisposition to generate abnormal electrochemical discharges, which disrupt normal neural activity. These discharges result from an imbalance between excitatory and inhibitory neurotransmission, leading to the clinical manifestations of seizures (McTague et al. 2016). Depending on the brain regions involved, seizures may affect motor, sensory, autonomic, or cognitive functions (Gao et al. 2022). Severe forms of epilepsy, such as **epileptic encephalopathies**, are particularly devastating. These syndromes, which often present in infancy or early childhood, are characterized by frequent, pharmacoresistant seizures and are frequently associated with developmental delays and cognitive impairments (Helbig and Ellis 2020; Villa and Combi 2016). For instance, Dravet syndrome, which begins in the first year of life, is marked by polymorphic seizure types and profound neurodevelopmental deterioration (McTague et al. 2016; Helbig and Ellis 2020). The link between epilepsy and cognitive decline in such syndromes suggests that the epileptic activity itself contributes to the developmental regression, beyond the impact of the underlying brain pathology (McTague et al. 2016).

Ion channels, particularly potassium and sodium channels, have been a central focus of epilepsy research. Mutations in potassium channel genes, such as *KCNT1*, *KCNQ2*, and *KCNQ3*, have been identified as key contributors to various epileptic syndromes (Boillot and Baulac 2016; Villa and Combi 2016). These channels are integral to maintaining the

electrochemical stability of neurons, and mutations can disrupt the flow of potassium ions, leading to neuronal hyperexcitability and the generation of seizures. For example, **KCNT1-associated epileptic encephalopathy**, a severe form of epilepsy is characterized by early onset, frequent seizures, and significant developmental delays (McTague et al. 2016; Gao et al. 2022).

## 1.2 | KCNT1: Structure and Function

### 1.2.1 | Structure and Expression Patterns in the Nervous System

The *KCNT1* gene encodes a sodium-activated potassium ( $K_{Na}$ ) channel, commonly referred to as SLACK (Sequence Like a Calcium-Activated  $K^+$  channel) or Slo2.2. This channel belongs to the Slo family of potassium channels and is activated by elevations in intracellular sodium concentration (Kameyama et al. 1984; Bhattacharjee et al. 2003). Structurally, KCNT1 shares key characteristics with other potassium channels, comprising six transmembrane segments (S1-S6) and a pore loop between the S5 and S6 segments that forms the ion-conducting pathway of the channel (J. Zhang et al. 2023) (Figure 1). It has a large intracellular C-terminal domain, which contains two regulators of conductance for potassium (RCK) domains essential for modulating the gating mechanism of the channel, allowing for fine-tuning of potassium ion conductance in response to changes in cellular sodium levels. The binding of  $Na^+$  ions induces conformational changes, leading to channel activation and subsequent potassium efflux (Kaczmarek 2013; Niday and Tzingounis 2018).

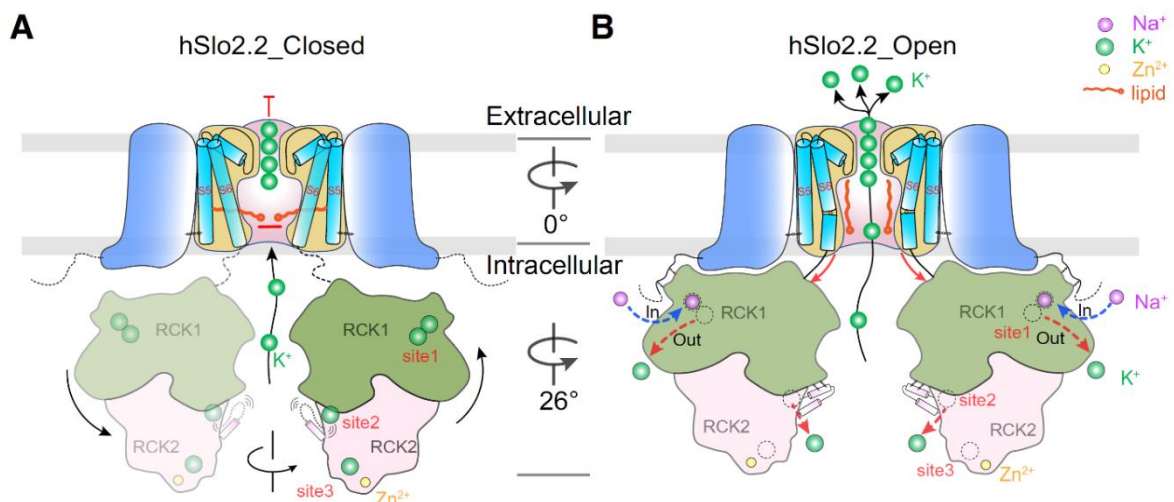


**Figure 1: Proposed mechanism of hSlo2.2 channel closed and open states. (A)** Under conditions of low intracellular  $Na^+$  concentration, potassium ions ( $K^+$ ) occupy binding Sites 1–3, stabilizing the gating ring domain in a closed conformation. This configuration allows the gating ring domain to interact loosely with the transmembrane domain (TMD), enabling rotational movement of the gating ring relative to the TMD. **(B)** As intracellular  $Na^+$  concentration increases,  $Na^+$  replaces  $K^+$

at Sites 1 and 2, prompting an expansion and rotation of the gating ring domain. This conformational change causes the gating ring to dock onto the TMD, leading to the opening of the inner gate (*J. Zhang et al. 2023*).

KCNT1 channels exhibit widespread expression throughout the central and peripheral nervous systems, where they play a crucial role in regulating neuronal excitability (Bhattacharjee, Gan, and Kaczmarek 2002). Notably, KCNT1 expression is abundant in brain regions involved in controlling rhythmic neuronal firing and synaptic plasticity, including the hippocampus, cortex, and thalamus (Rizzi, Knaus, and Schwarzer 2016). This extensive distribution underscores the channel's role in maintaining the physiological functions of both excitatory and inhibitory neurons. The channels are particularly important in regions requiring precise control of firing patterns and are implicated in maintaining the balance between excitation and inhibition within neural circuits (Kaczmarek 2013; Lim et al. 2016). Additionally, their expression across various neuron types, including those involved in inhibitory signaling, highlights their integral role in maintaining network stability (Niday and Tzingounis 2018).

### **1.2.2 | Role in Regulating Neuronal Excitability**

The KCNT1 channel plays a pivotal role in modulating neuronal excitability by facilitating potassium ion efflux under conditions of elevated intracellular sodium, such as during trains of action potentials (Bhattacharjee et al. 2003; Yuan et al. 2003) (Figure 2). This potassium efflux is essential for the repolarization of neurons following action potentials, helping to prevent sustained neuronal depolarization. Through the regulation of potassium conductance, KCNT1 channels serve to terminate action potentials and prevent excessive neuronal firing, thereby ensuring controlled neuronal activity (Kaczmarek 2013; Joshi 2022).

The after-hyperpolarization phase is essential for limiting the frequency of neuronal firing, particularly in neurons that exhibit burst-firing patterns. By modulating this phase, KCNT1 channels help prevent excessive or uncontrolled neuronal firing and facilitate neuronal recovery between successive action potentials. Consequently, these channels are crucial for maintaining neuronal excitability and overall network stability (Kaczmarek 2013; Niday and Tzingounis 2018; Joshi 2022).

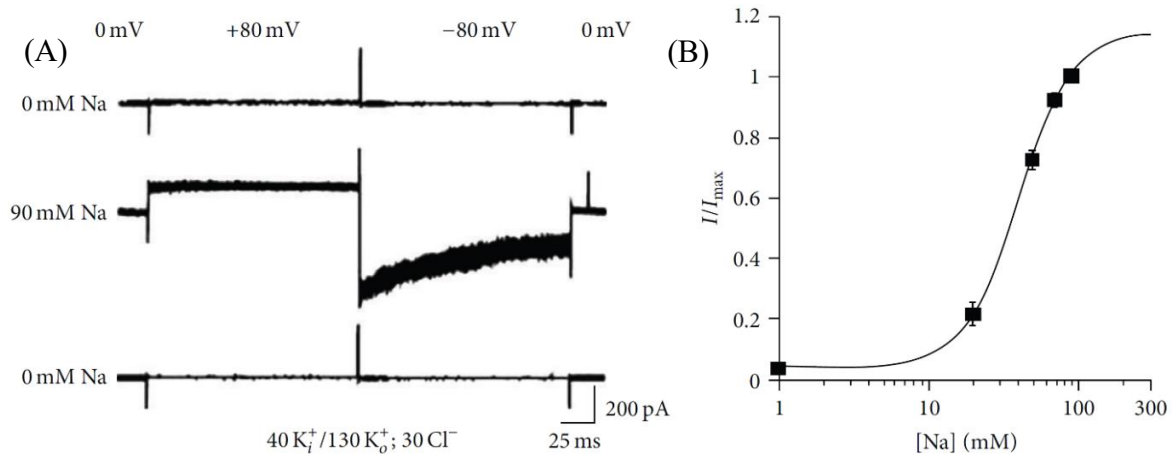


**Figure 2: Activation of Slack channels by cytoplasmic sodium.** (A) Representative recordings of macroscopic Slack currents at 0 mV and -80 mV from an excised inside-out patch in Slack-transfected CHO cells, shown in both the presence and absence of 90 mM sodium. (B) Sodium concentration-response curve illustrating the activation of Slack currents in excised patches. Currents were normalized to those observed at 90 mM sodium Figure modified from (Bhattacharjee *et al.* 2003).

### 1.3 | *KCNT1* Mutations and Associated Epilepsy Syndromes

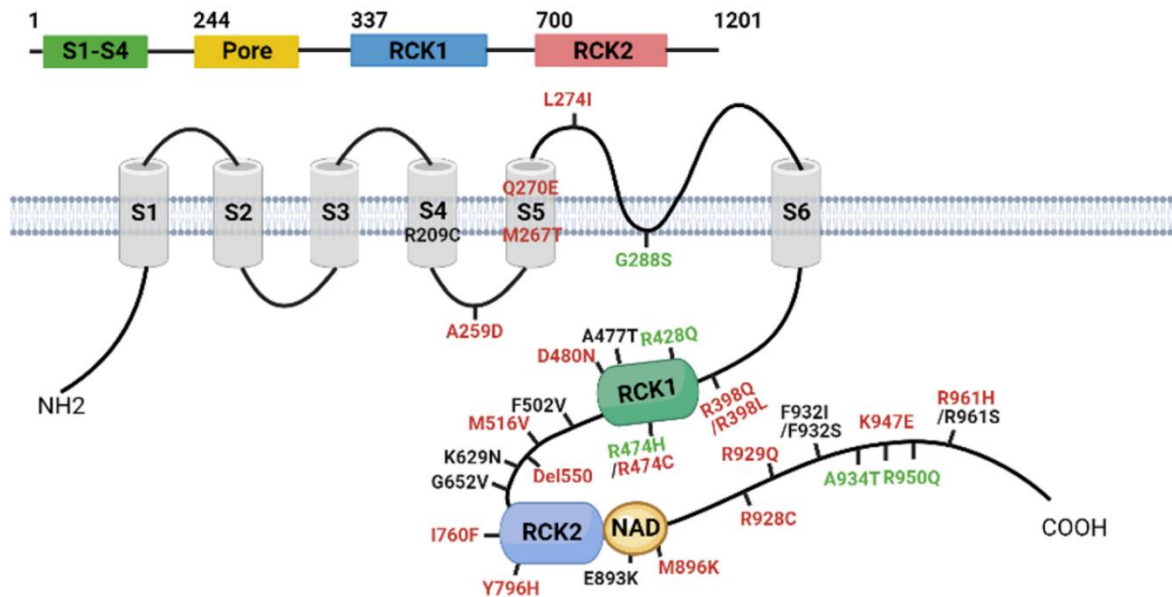
#### 1.3.1 | Spectrum of *KCNT1*-Associated Epilepsies

Mutations in the *KCNT1* gene are implicated in a wide range of epilepsy syndromes, predominantly through gain-of-function mutations that increase neuronal network excitability (Barcia *et al.* 2012; Heron *et al.* 2012) (Figure 3). The principal syndromes associated with *KCNT1* mutations include Autosomal Dominant Nocturnal Frontal Lobe Epilepsy (ADNFLE), also termed Autosomal Dominant Sleep-Related Hypermotor Epilepsy (ADSHE), and Epilepsy of Infancy with Migrating Focal Seizures (EIMFS) (Ishii *et al.* 2013; Rizzo *et al.* 2016; Barcia *et al.* 2019). Additionally, *KCNT1* mutations have been linked to other early-onset epileptic encephalopathies, such as West Syndrome, Ohtahara Syndrome, and focal epilepsies with later onset (Rizzo *et al.* 2016; Cataldi *et al.* 2019; Kohli, Ravishankar, and Nordli 2020).

#### 1.3.2 | Autosomal Dominant Nocturnal Frontal Lobe Epilepsy (ADNFLE)

**Clinical Characteristics and Age of Onset:** ADNFLE, or ADSHE, is characterized by clusters of nocturnal seizures, which can range from simple arousals to complex hyperkinetic episodes with dystonic posturing. These seizures primarily occur during non-REM sleep and manifest as sudden, often violent motor activity. Age of onset is generally late childhood to adolescence, with *KCNT1*-associated cases showing a higher incidence of cognitive

impairments and psychiatric comorbidities, such as anxiety and attention deficits. Case studies have documented instances of familial KCNT1-associated ADFLE, with varying



levels of severity within affected families (Borlot et al. 2020; Fang et al. 2021; Lu et al. 2022).

**Figure 3: The mutation positions identified by previous studies.** Highlighting the positions of mutations reported in studies on quinidine therapy. Mutation positions are color-coded to reflect varied therapeutic outcomes with quinidine. Green denotes mutation sites associated with patients who experienced mixed or controversial therapeutic results, black indicates mutation sites associated with effective outcomes, and red represents mutation sites where quinidine therapy was ineffective (Liu et al. 2023).

### 1.3.3 | Epilepsy of Infancy with Migrating Focal Seizures (EIMFS)

**Clinical Characteristics and Age of Onset:** EIMFS, also known as malignant migrating partial seizures of infancy, is a severe early-onset epileptic encephalopathy marked by migrating focal seizures. These seizures generally present within the first six months of life and exhibit a distinctive migratory pattern, shifting across different cortical regions and often accompanied by autonomic symptoms such as apnea and cyanosis. The condition is highly refractory to conventional antiepileptic therapies, leading to profound developmental delays and significant cognitive impairment over time. EIMFS typically manifests within the first weeks or months of life, with most patients experiencing severe developmental delays and failing to reach major milestones due to the disorder's refractory nature. Recent treatment attempts, including quinidine, cannabidiol, and the ketogenic diet, have demonstrated limited

efficacy, and achieving consistent seizure control remains challenging for most cases (Ishii et al. 2013; Barcia et al. 2019; Borlot et al. 2020; Fang et al. 2021; Yang et al. 2022).

### 1.3.4 | Other Associated Epileptic Encephalopathies

In addition to ADNFLE and EIMFS, *KCNT1* mutations have been associated with several other early-onset epileptic encephalopathies, including:

- **West Syndrome:** Characterized by infantile spasms and a distinctive hypsarrhythmic EEG pattern, West Syndrome in the context of *KCNT1* mutations often involves developmental regression. Treatment response is variable, with most cases exhibiting limited seizure control (Rizzo et al. 2016; Kohli, Ravishankar, and Nordli 2020).
- **Ohtahara Syndrome:** Known also as early infantile epileptic encephalopathy, Ohtahara Syndrome typically manifests in the neonatal period and is marked by a suppression-burst EEG pattern. This condition frequently progresses to other severe epilepsy syndromes, with minimal therapeutic options available (Cataldi et al. 2019; Borlot et al. 2020).
- **Focal Epilepsies with Later Onset:** Certain patients with *KCNT1* mutations develop focal epilepsy later in childhood or adolescence. These cases are generally less severe than early-onset forms but may include behavioral and psychiatric comorbidities. Structural brain abnormalities, such as delayed myelination and cortical atrophy, have been documented in some cases, underscoring the heterogeneity of *KCNT1*-associated epilepsies (Fang et al. 2021; Lu et al. 2022; Yamamoto et al. 2023).

### 1.3.5 | Genotype-Phenotype Relationships

Mutations in the *KCNT1* gene give rise to a diverse array of epilepsy syndromes, characterized by considerable variability in clinical presentations. This diversity in phenotype is observed not only across different families but also within affected families, suggesting that these mutations can produce a spectrum of clinical outcomes ranging from mild focal seizures to severe, pharmaco-resistant epilepsy with significant neurodevelopmental impairments (Barcia et al. 2019; T. S. Gertler et al. 2022; T. Gertler et al. 2018).

The clinical heterogeneity associated with *KCNT1* mutations is further illustrated by the variability in seizure types, age of onset, and accompanying neurological complications among affected individuals. Electroencephalographic (EEG) patterns exhibit substantial diversity, with suppression-burst and hypsarrhythmic patterns frequently documented in

cases of EIMFS (Lim et al. 2016; Barcia et al. 2019). This phenotypic variability complicates efforts to establish direct genotype-phenotype correlations, underscoring the need for individualized genetic and clinical evaluations in patients with *KCNT1*-associated disorders (T. Gertler et al. 2018).

The substantial variation in clinical outcomes observed among individuals with *KCNT1* mutations indicates that both genetic modifiers and environmental factors likely play a role. Somatic mosaicism and epistatic interactions have been proposed as genetic modifiers contributing to this phenotypic diversity. For example, cases of somatic mosaicism in the asymptomatic parents of children with EIMFS suggest that the proportion of cells harbouring the mutation may influence the severity of the phenotype. Moreover, the genetic background with unique combination of allelic variants throughout the genome results in distinct resilience against pathologic effect of mutations. Additionally, mutations in other epilepsy-associated genes, such as *SCN1A* and *GABRG2*, display similar variability, suggesting that interactions between genes may shape the clinical manifestations of *KCNT1* mutations (Lim et al. 2016; Barcia et al. 2019).

Environmental factors, such as early-life exposures and nutritional status, are also believed to influence the phenotypic expression of *KCNT1*-associated epilepsy. Variability in treatment responses further emphasizes the importance of environmental influences, as some individuals show minimal improvement with standard anticonvulsant therapies or dietary interventions. These differences in treatment efficacy underscore the necessity of considering environmental factors when managing *KCNT1*-associated epilepsy (Lim et al. 2016; Barcia et al. 2019).

## **1.4 | Molecular Mechanisms of *KCNT1* Mutations**

### **1.4.1 | Types of Mutations**

The majority of pathogenic *KCNT1* mutations reported are missense mutations, which involve single nucleotide changes that substitute one amino acid for another. Mutations such as p.R428Q and p.A934T have been demonstrated to increase the channel's open probability and alter its response to intracellular sodium, resulting in elevated potassium currents and abnormal neuronal firing patterns (Barcia et al. 2012; Heron et al. 2012).

In addition to missense mutations, in-frame deletions are also observed, though they occur less frequently. In-frame deletions lead to the removal of one or more amino acids without

disrupting the protein's reading frame. These deletions may affect critical functional domains of the SLACK channel, such as the C-terminal regulatory region, which subsequently alters channel gating properties or impacts interactions with regulatory molecules (Kim et al. 2014; Tang et al. 2016).

### **1.4.2 | Gain-of-Function Nature of Most Epilepsy-Associated Mutations**

A defining feature of many epilepsy-associated *KCNT1* mutations is their gain-of-function (GOF) nature. Pathogenic variants typically increase SLACK channel activity, leading to an excessive outflow of potassium ions that disrupts normal neuronal excitability. Functional studies using heterologous systems, such as *Xenopus laevis* oocytes and HEK cells, have consistently shown that most epilepsy-related *KCNT1* variants induce hyperactivity in the channel by enhancing sodium sensitivity or by modifying the current-voltage relationships. This GOF mechanism is linked with prolonged channel opening times or increased channel conductance, contributing to the altered excitability of neurons that underlies severe epilepsy phenotypes (Hinckley et al. 2023).

The phenotypic diversity associated with *KCNT1* mutations is influenced by the extent of the gain-of-function effects exerted by specific variants. For example, mutations associated with EIMFS, such as p.R428Q and p.A934T, have been reported to produce significantly higher current amplitudes than those linked to ADNFLE, suggesting a correlation between mutation effects and disease severity. Patients with mutations that induce stronger GOF effects often present with more severe clinical features, such as early-onset seizures, developmental delays, and profound neurological impairment (Barcia et al. 2019; McTague et al. 2018).

### **1.4.3 | Effects on Channel Properties**

#### **Increased Current Amplitude**

Pathogenic gain-of-function mutations in *KCNT1* are commonly associated with increased potassium current amplitudes, which substantially enhance the activity of the sodium-activated potassium channel  $K_{Na1.1}$ . This effect has been observed in several studies, including those employing heterologous expression systems and neuronal cultures derived from human-induced pluripotent stem cells (iPSCs). For example, the P924L mutation leads to a several-fold increase in  $K_{Na}$  currents, which, in human iPSCs, is directly correlated with elevated neuronal firing rates and greater action potential generation (Quraishi et al. 2019;

Wu, Quraishi, et al. 2024). Increased current amplitude in these mutant channels results from increased channel open probability, thereby augmenting potassium outflow and re/hyperpolarizes the membrane potential. Consequently, the increased potassium currents might lead to either sustained hyperpolarized state resulting reduced firing rates or facilitates action potentials by recovering Na<sup>+</sup> channels from inactivation.

### **Changes in Sodium Sensitivity**

Mutations in *KCNT1* also frequently enhance the channel's sensitivity to intracellular sodium. Enhanced sodium sensitivity is crucial as it can lead to increased potassium currents even under basal conditions where sodium levels are relatively low. This mechanism has been illustrated in the R455H mutation, which shows heightened responses to sodium, driving further potassium efflux and reinforcing neuronal hyperexcitability (Shore et al. 2020; T. S. Gertler et al. 2022). In murine models, the elevated sodium sensitivity resulting from these gain-of-function mutations has been linked to higher firing frequencies and the development of seizure phenotypes typical of severe epileptic encephalopathies (Shore et al. 2024).

## **1.5 | Pathophysiology of KCNT1-Associated Epilepsies**

### **1.5.1 | Hypothesized Mechanisms of Epileptogenesis**

The pathophysiology of KCNT1-associated epilepsies is hypothesized to involve gain-of-function mutations that lead to aberrant potassium conductance, significantly altering neuronal excitability and network synchrony. These mutations in the *KCNT1* gene result in hyperactive sodium-activated potassium channels, which disrupt the normal repolarization and firing patterns of neurons. This disruption is thought as a paradoxical GoF with increased hyperpolarizing potassium current creating an environment conducive to hypersynchronous activity, a hallmark of epileptogenesis (Quraishi et al. 2019; Wu, Quraishi, et al. 2024). Experimental models of *KCNT1* mutations indicate that these hyperactive channels increase the likelihood of spontaneous action potential generation, particularly in regions of the brain with high KCNT1 expression, such as the cortex and hippocampus. This increased firing rate is consistent with findings in various *in vivo* and *in vitro* models that demonstrate how *KCNT1* mutations contribute to the development of seizure-prone neural circuits through an imbalance in network excitability (Shore et al. 2020, 2024).

### **1.5.2 | The Role of Increased Potassium Conductance in Neuronal Hyperexcitability**

The amplified  $K_{Na}$  currents resulting from these mutations enhance potassium outflow during the afterhyperpolarization (AHP) phase of action potentials. Under normal physiological conditions, potassium currents help stabilize the membrane potential by hyperpolarizing the cell after firing, thus preventing excessive neuronal activation. However, the enhanced conductance seen in *KCNT1* mutations accelerates the repolarization phase, reducing the action potential duration and shortening the refractory period between action potentials, thereby facilitating repetitive firing (Shore et al. 2020; T. S. Gertler et al. 2022). Experimental studies have shown that this excessive  $K_{Na}$  conductance either promotes sustained neuronal firing in glutamergic neurons or suppresses the normal activity in GABAergic interneurons which contributes to network hypersynchrony (Quraishi et al. 2019; Wu, Quraishi, et al. 2024).

### **1.5.3 | Differential Effects on Inhibitory and Excitatory Neurons**

*KCNT1* mutations exhibit differential effects on excitatory and inhibitory neurons, contributing to an imbalance in the excitatory and inhibitory (E/I) dynamics that is essential for maintaining normal cortical function. In excitatory neurons, these mutations, such as Y796H, lead to an increased  $K_{Na}$  current that becomes prominent at higher membrane potentials, facilitating rapid action potential repolarization. This mechanism supports sustained high-frequency firing in excitatory neurons, thereby increasing overall excitatory drive within neural circuits (Shore et al. 2020; T. S. Gertler et al. 2022). In contrast, in inhibitory neurons, *KCNT1* mutations induce  $K_{Na}$  currents that activate at subthreshold voltages, causing a hyperpolarized resting potential and raising the rheobase, the minimum current required to generate an action potential. Consequently, inhibitory neurons with *KCNT1* mutations exhibit a reduced firing rate, impairing their ability to counterbalance excitatory signals. Studies have shown that PV+ interneurons are particularly affected, exhibiting a marked decrease in excitability due to *KCNT1* mutations, which leads to a significant reduction in inhibitory output and a subsequent increase in network excitability (Wu, Quraishi, et al. 2024; Shore et al. 2024; T. S. Gertler et al. 2022). This differential effect between excitatory and inhibitory neurons disrupts the E/I balance, which is a critical factor

in the development of epileptogenic networks in KCNT1-associated epilepsy syndromes (Wu, Quraishi, et al. 2024; Shore et al. 2020).

## **1.6 | Comorbidities of KCNT1-Associated Epilepsies**

### **1.6.1 | Associated Intellectual Disabilities**

Intellectual disability is a frequent comorbidity in patients with *KCNT1* mutations, likely due to the role of the sodium-activated potassium channel in regulating neuronal excitability and synaptic function (Matt et al. 2021; Wu, El-Hassar, et al. 2024). Individuals with EIMFS often experience profound developmental delays, with the majority of patients failing to achieve major motor and cognitive milestones. Studies suggest that intellectual impairment in KCNT1-associated epilepsy is primarily due to cortical development deficits which may disrupt normal brain functioning during critical periods. Additionally, mutations in *KCNT1* can impair other neurodevelopmental pathways, further compounding cognitive deficits (Kim et al. 2014; Bonardi et al. 2021).

### **1.6.2 | Psychiatric Features and Behavioural Issues**

Patients with KCNT1-associated epilepsy frequently exhibit a range of psychiatric and behavioural issues. Anxiety, autism spectrum disorder (ASD)-like features, and social difficulties are among the most commonly reported. These behavioural symptoms are hypothesized to arise from the dysregulated neuronal excitability induced by *KCNT1* mutations, which may impair cortical circuits involved in emotion regulation and social behaviour. Mouse models deficient in Slack channels have demonstrated alterations in anxiety-like behaviours, suggesting that *KCNT1* mutations may disrupt limbic structures like the amygdala, which are involved in emotional processing (Bausch et al. 2015, 2018; Q. Zhang et al. 2022).

### **1.6.3 | Potential Cardiac Arrhythmias and SUDEP Risk**

Extracerebral manifestations of *KCNT1* mutations, including cardiac arrhythmias, have been increasingly recognized as contributing to the risk of sudden unexpected death in epilepsy (SUDEP) (Kuchenbuch et al. 2019). The presence of Slack channels in cardiac tissue suggests that these channels may play a role in cardiac electrophysiology. Mutations in *KCNT1* may lead to arrhythmic events, as documented in several case studies where patients with KCNT1-associated epilepsy also exhibited dilated cardiomyopathy or atrioventricular

conduction abnormalities (Kohli, Ravishankar, and Nordli 2020; Yamamoto et al. 2023). The combination of frequent seizures and potential cardiac involvement underscores the importance of comprehensive monitoring and may warrant further investigation into targeted interventions to mitigate SUDEP risk in this patient population.

## **1.7 | Current Treatment Strategies and Challenges**

### **1.7.1 | Resistance to Conventional Antiepileptic Drugs**

KCNT1-associated epilepsy syndromes, such as EIMFS and ADNFLE, frequently exhibit resistance to conventional antiepileptic drugs (AEDs) (Miziak and Czuczwar 2022; D. Xu et al. 2022). This resistance is likely due to specific gain-of-function (GOF) mutations in *KCNT1*, which lead to hyperactive sodium-activated potassium channels that are not effectively targeted by traditional AEDs, which typically act on sodium or calcium channels. Consequently, the standard pharmacological approach, including AEDs like valproate and levetiracetam, often fails to achieve adequate seizure control in these patients (Helbig and Ellis 2020; Delanty and Cavalleri 2017).

### **1.7.2 | Potential Targeted Therapies**

Given the pharmaco-resistant nature of KCNT1-associated epilepsies, recent research has focused on identifying more effective targeted therapies. Quinidine, a class I antiarrhythmic drug, was initially identified as a potential therapy due to its ability to inhibit SLACK ( $K_{Na1.1}$ ) channels (Figure 3). However, its clinical use is limited by safety concerns, including QT prolongation, and inconsistent efficacy across different *KCNT1* mutations (M Qunies and A Emmitte 2022; Iraci et al. 2024).

- **VU0606170:** This selective SLACK channel inhibitor, identified through high-throughput screening, reduces spontaneous calcium oscillations in overactive neurons by specifically targeting the GOF effects of *KCNT1* mutations. Studies indicate that VU0606170 can decrease firing rates in neuronal cultures, suggesting potential as an antiepileptic agent for SLACK-associated disorders (Spitznagel et al. 2020).
- **1,2,4-Oxadiazole Derivatives:** Recently, oxadiazole-based inhibitors have shown promising results. These compounds inhibit SLACK channels with improved selectivity and reduced side effects compared to quinidine. Specifically, VU0935685 and other analogs from this class have demonstrated significant reductions in spontaneous neuronal firing in mouse models, indicating their potential for reducing seizure frequency in KCNT1-associated epilepsy (Qunies et al. 2023).

- **Xanthine Inhibitors:** Another promising class of small molecules includes xanthine derivatives, such as VU0948578, which show efficacy in inhibiting mutant SLACK channels. This class of inhibitors has displayed good selectivity against other ion channels, including hERG, and demonstrates an improved safety profile. Xanthine inhibitors provide a unique avenue for selectively targeting KCNT1-associated epilepsy with minimal off-target effects (Qunies et al. 2024).
- ***In Silico* Designed Compounds:** Using computational approaches, compounds such as CPK20 have been developed to specifically target the pore-forming domain of SLACK channels, offering enhanced metabolic stability and potency over quinidine. These inhibitors were shown to effectively counteract the GOF mutations linked to epileptic phenotypes, such as EIMFS, with fewer cardiac side effects (Iraci et al. 2024).

Overall, these targeted therapies are valuable not only for their direct effects on SLACK channels but also as part of a broader strategy to tailor treatments based on the specific *KCNT1* mutation in each patient. This approach allows for increased efficacy and reduced adverse effects, addressing the limitations of conventional AEDs in treating KCNT1-associated epilepsies. However, considering that these compounds still require to undergo clinical trials, it might take another decade to meet the urgent need of patients.

### 1.7.3 | Need for Personalized Treatment Approaches

The phenotypic diversity and mutation-specific effects observed in KCNT1-associated epilepsies underscore the necessity for personalized treatment approaches. Precision medicine strategies that involve tailoring treatment based on genetic testing and functional studies are increasingly relevant. Additionally, ongoing studies of SLACK channel modulators in combination with existing AEDs have shown potential for enhancing therapeutic efficacy and mitigating drug resistance (Qunies et al. 2024; Griffin et al. 2021). This personalized approach may improve the quality of life for patients with KCNT1-associated epilepsies, particularly those for whom standard treatments have been ineffective. Future research on the pharmacokinetics and long-term effects of these novel inhibitors will be critical in refining these strategies and developing more effective treatment protocols (Qunies et al. 2023; Cole et al. 2020).

## **1.8 | Future Directions and Research Gaps**

### **1.8.1 | Ongoing Research into KCNT1 Channel Function and Regulation**

Ongoing research into KCNT1 channel function has revealed new insights into its role in the central nervous system (CNS), particularly concerning its regulation by intracellular sodium and other cellular metabolites. Advanced studies using high-resolution structural techniques, such as cryo-electron microscopy, have facilitated a detailed understanding of the KCNT1 channel's structural and functional domains, including the critical role of the RCK domain in sodium sensitivity (Hite et al. 2015; J. Xu et al. 2023). Additionally, efforts to understand how gain-of-function (GOF) mutations disrupt normal channel activity are ongoing, with a focus on how these mutations alter gating mechanisms and subunit interactions within heteromeric channels. Understanding these mechanistic details is essential for developing targeted interventions that can mitigate the aberrant excitability resulting from GOF mutations (Goldberg 2021).

### **1.8.2 | Development of Novel Therapeutic Targets**

The challenges associated with conventional drugs, like quinidine, have driven the development of more selective KCNT1 inhibitors (Milligan et al. 2014). Recent studies have identified novel chemotypes and small molecules, such as xanthine derivatives and oxadiazole compounds, that exhibit enhanced selectivity and potency in inhibiting KCNT1 channels without affecting cardiac function (Quines et al. 2023, 2024). For instance, compounds like CPK20, derived from in silico screening, have shown promising selectivity for KCNT1 over cardiac hERG channels, presenting a more favourable safety profile compared to quinidine (Iraci et al. 2024). Furthermore, research into additional compounds, such as bepridil and clofilium, has demonstrated their potential to inhibit hyperexcitable KCNT1 channels effectively, although their clinical application is currently limited by side effects (Rizzo et al. 2016; de Los Angeles Tejada et al. 2012). These studies underscore the need for ongoing drug discovery efforts to develop more potent, KCNT1-specific inhibitors that bypass the drawbacks associated with broad-spectrum ion channel blockers.

### **1.8.3 | Potential for Gene Therapy or Precision Medicine Approaches**

Emerging precision medicine approaches, including antisense oligonucleotides (ASOs), are being explored as innovative therapies for KCNT1-associated epilepsies. ASOs have shown

the ability to selectively silence mutant *KCNT1* alleles, reducing the pathogenic channel activity responsible for seizure generation. Preclinical studies in mouse models have demonstrated that ASO-based gene silencing can decrease seizure frequency and extend survival in animals carrying *KCNT1* mutations (Burbano et al. 2022). Additionally, the expanding field of gene therapy holds promise for developing mutation-specific treatments that address the underlying genetic cause of KCNT1-associated epilepsy. This approach, combined with personalized pharmacotherapy based on a patient's unique mutation profile, may offer a more effective means of managing drug-resistant epilepsies associated with KCNT1. As our understanding of genotype-phenotype correlations in KCNT1 disorders deepens, the prospect of personalized, mutation-targeted therapies becomes increasingly viable, paving the way for tailored treatment strategies that minimize adverse effects while maximizing therapeutic efficacy.

### **1.9 | Identification and Modeling of *KCNT1* Mutations**

To investigate the phenotypic consequences of KCNT1 gain-of-function mutations and evaluate potential therapeutic strategies, two knock-in mouse models were generated using the CRISPR/Cas9 gene-editing system. Patient-derived mutations were introduced into the *Kcnt1* gene locus of CD1 mice. Two mutations were selected based on clinical findings and their electrophysiological impact on channel function: Ile335Asn (I335N) and Arg950Gln (R950Q). Both mutations are located in regions recognized as hotspots for missense mutations within the pore domain and second potassium conductance regulatory domain of the KCNT1 channel, respectively.

The Ile335Asn (p.I335N) mutation was identified in a male patient (born 2012, Munich), who presented with neonatal-onset epilepsy refractory to multiple anticonvulsant therapies, including quinidine, and exhibited severe developmental delay accompanied by microcephaly. Functional recordings in heterologous expression systems using *Xenopus oocytes* revealed that KCNIN homomeric channels did not conduct measurable currents, whereas heteromeric channels showed a current increase of approximately 250% compared to wild-type (WT) (Figure 4).

The Arg950Gln (p.R950Q) mutation was identified in a female patient (born 2006, Tübingen), who developed epilepsy at three months of age, which was also refractory to numerous therapies, including sultiam, carbamazepine, oxcarbazepine, lamotrigine, levetiracetam, lacosamide, and quinidine. This patient exhibited a global developmental

delay with an IQ score of 65. In *Xenopus oocyte* recordings, KCNRQ homomeric channels displayed an approximate 500% current increase, while heteromeric channels showed a 250% increase compared to WT (Figure 4).

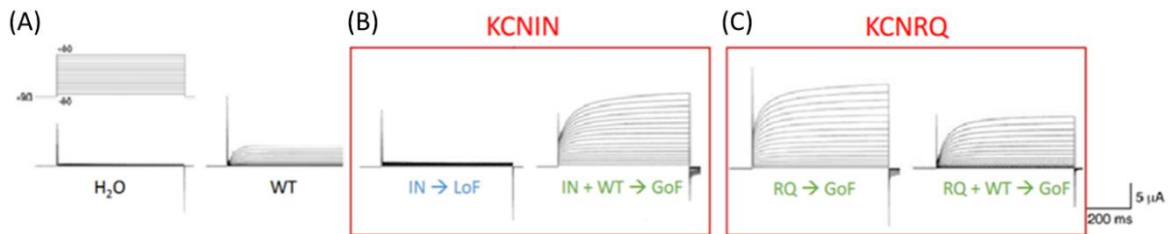


**Figure 4. Functional characterization of KCNT1 mutations** The functional effects of KCNT1 mutations were assessed using two-electrode voltage-clamp recordings in *Xenopus oocytes*. cRNAs encoding KCNT1 variants were injected into oocytes, (A) with H<sub>2</sub>O-injected oocytes and WT KCNT1 serving as controls, showing baseline currents. Compared to WT, (B) heterozygous KCNIN (IN+WT) displayed a significant GoF, while homozygous KCNIN (IN) exhibited almost complete loss-of-function (LoF). (C) For the KCNRQ mutation, heterozygous KCNRQ (RQ+WT) showed the mildest GoF, whereas homozygous KCNRQ (RQ) demonstrated the most severe GoF, with the highest increase in current observed.

These functional findings suggest a hierarchy of severity: the KCNRQ homozygous mutation is predicted to result in the most severe pathological phenotype, followed by the heterozygous KCNIN mutation, while the heterozygous KCNRQ mutation is expected to produce a milder phenotype. Based on these observations, two knock-in mouse models carrying corresponding mutations were generated: CD1.*Kcnt1*<sup>p.I296N/+</sup> (heterozygous mutation corresponding I335N in human sequence), CD1.*Kcnt1*<sup>p.R911Q/+</sup> and CD1.*Kcnt1*<sup>p.R911Q/R911Q</sup> (heterozygous and homozygous mutations corresponding to human R950Q, respectively).

These mouse models serve as suitable tools for studying the pathophysiological mechanisms underlying KCNT1-associated epilepsies and provide a platform for testing novel therapeutic interventions targeting the effects of gain-of-function mutations in KCNT1.

### 1.10 | Identification and Validation of KCNT1 Blockers

Given the urgent need for effective blockers targeting the mutation-induced GoF of KCNT1 channels, a high-throughput drug repurposing screen was performed to identify potential therapeutic candidates. The screen utilized a thallium flux assay established in HEK293 cells stably expressing human KCNT1 channels to detect compounds capable of inhibiting KCNT1-mediated currents.

Following the initial screen, the top six hit compounds were subjected to further validation using patch-clamp electrophysiology to confirm their inhibitory effects on both WT and mutated KCNT1 channels. The selection criteria for candidate blockers included their half-maximal inhibitory concentration, ability to cross the blood-brain barrier, and established safety profiles as FDA-approved drugs.

Two promising compounds, Pimozide and Carvedilol, were chosen for further investigation based on their strong inhibitory effects on KCNT1 channels and favourable pharmacokinetic properties. The following sections provide a brief overview of these two compounds, their physiological roles, and their potential as therapeutic agents for KCNT1-associated epilepsies.

### **1.10.1 | Pimozide as a Potential Therapeutic Agent for KCNT1-associated Epilepsy**

Pimozide is a diphenylbutylpiperidine derivative and a dopamine D2 receptor antagonist approved for the treatment of Tourette syndrome and resistant psychotic disorders. Its primary mechanism of action is through dopaminergic receptor blockade in the CNS, leading to a suppression of motor and phonic tics, as well as psychotic symptoms (TEVA PHARMACEUTICALS 2008).

In addition to its role in the dopaminergic system, pimozide has been shown to affect voltage-gated potassium channels (TEVA PHARMACEUTICALS 2008). This property is particularly relevant to KCNT1-associated epileptic encephalopathies, where GoF mutations result in hyperactivity of KCNT1 channels. By inhibiting these channels, pimozide has the potential to restore disrupted neuronal excitability, thereby reducing seizure activity.

Pimozide is extensively metabolized in the liver, primarily by CYP3A4 and, to a lesser extent, CYP2D6 enzymes (Chapron et al. 2020). It has a long elimination half-life (approximately 55 hours), which may contribute to sustained therapeutic effects but also necessitates careful dose monitoring (TEVA PHARMACEUTICALS 2008; AA Pharma Inc. 2014). Despite its therapeutic benefits, pimozide carries a known risk for QT interval prolongation and cardiac arrhythmias, particularly at high doses or when combined with CYP3A4 inhibitors. This highlights the need for cautious dose optimization when considering its repurposing for KCNT1-associated epilepsy (TEVA PHARMACEUTICALS 2008).

The ability of pimozide to cross the blood-brain barrier and its well-characterized safety profile make it a strong candidate for repurposing in KCNT1-associated epileptic encephalopathies. Its known physiological effects on potassium channels and dopaminergic systems provide a mechanistic rationale for its potential therapeutic efficacy.

### **1.10.2 | Carvedilol as a Potential Therapeutic Agent for KCNT1-associated Epilepsy**

Carvedilol is a non-selective  $\beta$ -adrenergic receptor blocker widely used in the treatment of congestive heart failure, hypertension, and post-myocardial infarction management (Benkel et al. 2022). Carvedilol has been shown to interact with voltage-gated potassium channels and influence neuronal excitability (Schaefer et al. 1998). This feature is particularly relevant for KCNT1 GoF mutations, where excessive potassium channel activity leads to neuronal hyperexcitability and seizures. The inhibitory effect of carvedilol on these channels, combined with its ability to cross the blood-brain barrier, highlights its therapeutic potential in reducing seizure burden in KCNT1-associated epilepsies.

In addition to its  $\beta$ -adrenergic blockade, carvedilol interacts with serotonin 5-HT<sub>2A</sub> receptors as a functional antagonist, influencing pathways associated with neurotransmitter regulation in the CNS (Murnane et al. 2019). This dual mechanism may provide broader modulation of neuronal excitability, further supporting its role in managing hyperexcitability disorders like KCNT1-associated epileptic encephalopathies.

Carvedilol is extensively metabolized in liver by CYP2D6 and CYP3A4, however how effectively it distributes throughout the body and further metabolization in and clearance from CNS still remains elusive (Benkel et al. 2022; Schaefer et al. 1998). Additionally, its safety profile, particularly the potential for dose-dependent QT interval prolongation at higher concentrations, underscores the need for cautious dose optimization during further preclinical and clinical evaluations.

Overall, carvedilol's ability to inhibit potassium channel activity at lower concentrations, combined with its blood brain barrier permeability makes it a promising candidate for repurposing as a therapeutic agent in KCNT1-associated epileptic encephalopathy.

## 1.11 | The Aims and Scope of the Study

Ion channelopathies, which arise from dysfunctions in ion channels critical for neuronal signalling, profoundly impact brain development and function. Genetic mutations disrupting the delicate balance of neuronal excitability often lead to severe neurodevelopmental disorders, such as epileptic encephalopathies. Among these, mutations in the KCNT1 gene, encoding the SLACK potassium channel, are recognized as key contributors to early-onset epileptic encephalopathies. These mutations generate a hyperexcitable neuronal environment, triggering seizures and impairing essential brain developmental processes.

Despite increasing recognition of KCNT1-associated epileptic encephalopathies, therapeutic options remain severely limited. The intractable nature of seizures, coupled with severe developmental delays and associated comorbidities, highlights the urgent need for targeted treatment strategies. Conventional anticonvulsant therapies have proven largely ineffective, emphasizing the necessity of addressing the underlying pathophysiology of KCNT1 mutations.

This thesis aims to evaluate the phenotypic consequences of specific single-point KCNT1 mutations and investigate the therapeutic potential of targeted pharmacological interventions. By using mouse models carrying patient-derived mutations, this work systematically characterizes key aspects of the disease, including body growth, neural activity via ECoG, brain morphology, and behavioural outcomes. Establishing such a detailed baseline is essential for understanding the disease progression and for determining treatment efficacy.

In addition to characterization, this study focuses on testing two pharmacological blockers selected for their potential to mitigate the gain-of-function effects of KCNT1 mutations. The blockers are evaluated across multiple domains, including brain morphology, ECoG-recorded brain activity, and behaviour. The ultimate goal is to determine whether these targeted treatments can effectively reduce seizure burden and improve developmental outcomes.

Given the critical lack of effective therapies for KCNT1-associated epilepsies, this research is both timely and essential. By combining phenotypic characterization with therapeutic evaluations, the findings of this study aim to advance our understanding of KCNT1

dysfunction and contribute to the development of innovative therapeutic strategies that may significantly improve clinical outcomes for affected individuals.

## 2. | Materials and Methods

### 2.1 | Animal Husbandry and Generation of Animal Models

All animals (mice, *Mus musculus*) were housed in type II long plastic cages placed in isolators (SCANBUR) under standard housing conditions. These conditions included a temperature of  $21 \pm 2^\circ\text{C}$ , approximately 50% relative humidity, and *ad libitum* access to water and rodent chow (Altromin Spezialfutter GmbH, Germany). The mice were transferred to clean cages weekly and maintained on an inverted 12:12 dark-light cycle, with lights turning on at 10 PM.

Two knock-in mouse lines were generated by the *In vivo Research Facility* of CECAD, University of Cologne (head: Prof. Branko Zevnik) using the CRISPR/Cas9 genome-editing technique to carry patient-derived heterozygous point mutations in the KCNT1 gene. These mutations, p.I335N and p.R950Q, correspond to de novo mutations associated with human KCNT1-related epileptic encephalopathies. The resulting mouse lines, CD1.*Kcnt1*<sup>p.I296N</sup> (hereafter referred to as KCNIN) and CD1.*Kcnt1*<sup>p.R911Q</sup> (hereafter referred to as KCNRRQ), were maintained on a strain background, CD1. These mutations lead to a gain-of-function in the KCNT1 ion channel, mimicking the human condition. All experiments involving animals were conducted in accordance with ethical guidelines and were approved by the Landesamt für Natur, Umwelt und Verbraucherschutz (LANUV) Nordrhein-Westfalen, Germany.

### 2.2 | Genotyping

**DNA Isolation:** DNA was extracted from ear or tail biopsies collected from mice. Biopsies were lysed overnight in 100  $\mu\text{l}$  lysis buffer (100 mM NaCl, 50 mM Tris/HCl, pH 8.0, 1 mM EDTA, 0.2% Nonidet P-40, 0.2% Tween 20, 0.1 mg/ml Proteinase K) at  $54^\circ\text{C}$  under constant shaking and were inactivated by heating the lysate at  $84^\circ\text{C}$  for 45 minutes. For tail biopsies, Proteinase K was used to ensure a clean, protein-free DNA preparation.

**Polymerase Chain Reaction (PCR):** Genotyping was performed using polymerase chain reaction. Primer sequences specific to the KCNIN and KCNRRQ mutations are listed in Table

1. Reaction mixtures were prepared in a total volume of 50  $\mu$ l, containing the components listed in Table 2. The PCR reactions were carried out using a thermal cycler (Analytik Jena GmbH, Germany) with cycling conditions optimized for each mouse line (Table 3). The annealing temperatures were set according to the melting temperatures of the respective primers.

**Agarose Gel Electrophoresis:** Following PCR, 1.8% agarose gels were prepared by dissolving agarose powder (VWR Life Science, Sigma-Aldrich, Germany) in 1x TAE buffer (40 mM Tris, 10  $\mu$ l acetic acid, 1 mM EDTA, pH 8.0). PCR products (15  $\mu$ l) were mixed with loading dye and loaded into the gel wells alongside 5  $\mu$ l DNA PANladder I (100 bp, PAN-Biotech™, Germany). The DNA fragments were separated electrophoretically at 140 V for 30 minutes and visualized using a CCD camera under UV illumination.

**Restriction Enzyme Digestion:** For KCNIN samples, restriction digestion was performed on the PCR products to identify the presence of the mutation. The reaction mix (Table 4) contained 10  $\mu$ l of crude PCR product, 2  $\mu$ l of CutSmart buffer (10x), 1.5  $\mu$ l of MluCI enzyme (10 U/ $\mu$ l), and 16.5  $\mu$ l of water. Samples were incubated at 37°C for 2 hours. Digested products were analyzed by agarose gel electrophoresis as described above. Successful digestion indicated the presence of the heterozygous or homozygous mutation.

**Quantitative Polymerase Chain Reaction (qPCR):** Quantitative polymerase chain reaction was performed in KCNIN animals when the results from PCR with restriction enzyme digestion were inconclusive. The reaction setup included primers and probes specific for the wild-type and mutant alleles, with each reaction prepared in duplicate in a total volume of 12.5  $\mu$ l. The thermal cycling protocol consisted of an initial denaturation at 95°C, followed by 40 cycles of denaturation and annealing/extension, and a final post-read stage (Table 5). Reactions were run on a QuantStudio 6 Flex Real-Time PCR System. Post-PCR analysis was conducted using QuantStudio Real-Time PCR software, enabling allelic discrimination based on fluorescence signals. Positive and negative controls were included in all runs to ensure the reliability and specificity of the assay.

**Table 1: Primer Sequences for Genotyping KCNIN and KCNRQ Animals.**

Primer/Probe	Sequence	Product Size (bp)
<b>KCNIN-PCR</b>		
MS113 (I296N-fw2)	5'-CCCTGATCTTCCTGTTTC-3'	417 (digested 245 + 172)
MS115 (I296N-rv2)	5'-ATGGTTGCTCTTGTGCGG-3'	417 (digested 245 + 172)

<b>KCNRQ-PCR</b>		
KCNT1 R911Q rev 12	5'-TGAGGTCCAAAAAGGACCAG-3'	326
KCNT1 R911Q WT FW	5'-CTTCCTTGCAGCAAGAACGG-3'	326
MS 122 rev	5'-CCAGCAGGAGAAAGTCAG-3'	248
KCNT1 R911Q mut FW	5'-CTTCCTTGCAGCAAGAACAA-3'	248
<b>KCNIN-qPCR</b>		
KCNIN-qPCR-FW	5'-GACTTTCTCAACTGTGGGCTTC-3'	Allelic Discrimination
KCNIN-qPCR-REV	5'-ACTCACTTGCAGTGGGAGCAC-3'	Allelic Discrimination
KCNIN WT Fam Probe	5'-FAM- CAAGGGTGACACATCTCAGGATGAC- Q-MGB-3'	WT-specific
KCNIN Mut Vic Probe	5'-VIC- CAAGGGTGACACAatTCAGGATGAC- Q-MGB-3'	Mutant-specific

**Table 2: Reagents for the PCR and qPCR Reaction Setups.**

<b>Reagent</b>	<b>PCR Volume per Reaction (<math>\mu</math>l)</b>	<b>qPCR Volume per Reaction (<math>\mu</math>l)</b>
Forward Primer	0.5	0.5
Reverse Primer	0.5	0.5
Probe (WT or Mutant)	—	0.5 each
Dream-Taq Polymerase	0.25	—
Master Mix (2X)	—	6.25
dNTPs (10 mM)	0.5	—
Nuclease-Free Water	41.25	3.75
Buffer (10X)	5.0	—
DNA Template	2.0	0.5
<b>Total Volume</b>	<b>50.0</b>	<b>12.5</b>

**Table 3: Thermal Cycling Program for KCNIN.**

<b>Step</b>	<b>Temperature [°C]</b>	<b>Time</b>	<b>Note</b>
Initial denaturation	95	3 min	
Denaturation	94	34 s	
Annealing	55	45 s	
Elongation	72	60 s	12x, -0.5 °C per cycle
Denaturation	94	35 s	

Annealing	49	30 s	
Elongation	72	60 s	29x
Final elongation	72	5 min	

**Table 4: Thermal Cycling Program for KCNRQ (Green colour represents the wild-type annealing temperature, while red colour represents the mutant annealing temperature).**

Step	Temperature [°C]	Time	Note
Initial denaturation	95	3 min	
Denaturation	94	30 s	
Annealing	68/65	45 s	
Elongation	72	30 s	9x, -1 °C per cycle
Denaturation	94	30 s	
Annealing	59/65	45 s	
Elongation	72	30 s	35x
Final elongation	72	5 min	

**Table 5: Thermal Cycling Program for KCNIN-qPCR.**

Step	Temperature [°C]	Time	Note
Pre-Read Stage	60	30 s	
Initial Denaturation	95	10 min	
Denaturation	95	15 s	40 cycles
Annealing/Extension	60	1 min	40 cycles
Post-Read Stage	60	30 s	

## 2.3 | Telemetric Electrocorticogram (ECoG)

### 2.3.1 | Surgical Protocol for Telemetric Implants

To investigate brain activity and electrographic seizures, telemetric electrocorticogram (ECoG) recordings were performed on either adult mice (10–32 weeks old) or juvenile mice (4–5 weeks old) using implanted radio transmitters (Model HD-X02, ETA-F10, EA-F20 or F20-EET Data Science International, USA). For the juvenile recordings, animals were

considered to reach a minimum body weight of 15 g as a preliminary condition. Recordings were carried out for at least seven days.

Approximately 30 minutes before surgery, mice received buprenorphine (0.025 mg/kg, intraperitoneal) for analgesia. Anesthesia was induced with 3–4% isoflurane in 100% oxygen and maintained at 1–2% during surgery. Animals were positioned in a stereotaxic frame, and body temperature was maintained at 37°C using a heating pad with continuous monitoring via a rectal probe. The surgical site was shaved and disinfected, and a medial skin incision was made to expose the skull.

The skull was cleaned using a cotton swab and hardened with dental cement (OptiBond™, Kerr Dental, Germany) cured with UV light. For transmitters with a single recording electrode, a craniotomy (0.6 mm diameter) was performed above the dorsal hippocampus (1.5 mm lateral and 2 mm caudal to the bregma) for electrode placement. For transmitters with two recording electrodes, additional craniotomies were made in both hemispheres, with the second electrode positioned symmetrically relative to the midline. A reference electrode craniotomy was drilled above the cerebellum (1 mm posterior to lambda and 1–3 mm lateral to the midline). Electrodes were positioned on the dura mater and secured with dental adhesive (Tetric EvoFlow, M+W Dental, Germany).

A subcutaneous pocket was created along the dorsal region of the animal to accommodate the radio transmitter. The transmitter was implanted in this pocket, and the skin was closed using tissue glue (GLUture®, World Precision Instruments, USA). At the end of the surgery, animals received a subcutaneous injection of carprofen (5 mg/kg, Norbrook® Laboratories Limited, Ireland) for postoperative analgesia. Following surgery, animals were allowed to recover for five days, during which they were monitored and scored daily for well-being. Transmitters were activated using a magnet, and animals were placed on receiver platforms (PhysioTel Receiver Model RPC-1, Data Science International) housed within a Faraday cage. Continuous ECoG signals, motor activity, and synchronized video recordings were collected from the home cages over a seven-day period.

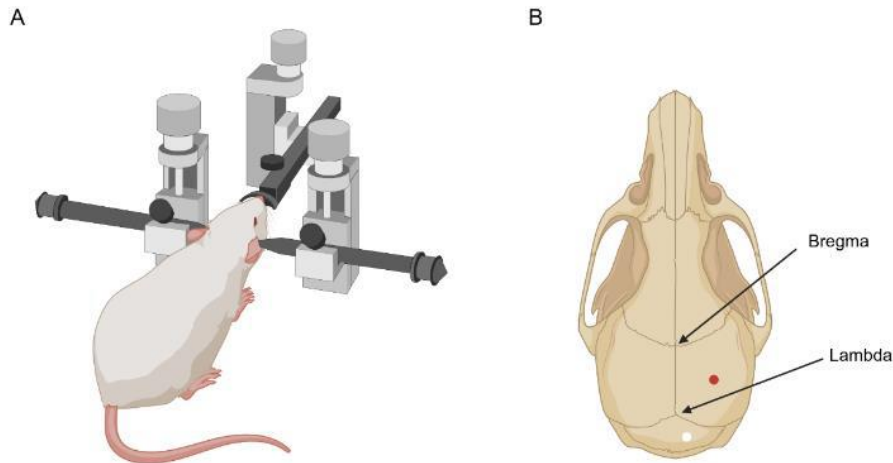


**Figure 5: Surgical Setup and Electrode Position.** (A) Depiction of the stereotaxic frame with the animal secured in position. (B) Illustration of the mouse skull showing key stereotaxic landmarks: bregma and lambda (black arrows). The red dot marks the craniotomy site above the hippocampus (-2.0 mm posterior, 1.5 mm lateral to bregma, dorsal CA1), where the recording electrode was positioned. The white dot indicates the craniotomy site above the cerebellum used for placing the reference electrode.

### 2.3.2 | Analysis of ECoG Recordings

**Data Acquisition:** Electrocorticogram (ECoG) signals were recorded continuously using telemetric transmitters over a period of seven days. Synchronized video recordings of animal behaviour were captured alongside the ECoG signals and stored using Ponemah 6.5 (DSITM, USA) and Media Recorder 4.0 (Noldus, The Netherlands). The recorded data were visualized and preprocessed in NeuroScore (DSITM, USA) to identify epochs of interest and ensure high-quality signals for further analysis.

**The Detection of Seizures:** Seizures were detected using a hybrid approach combining automated detection in NeuroScore and supervised machine learning by AccuSleep (Barger et al. 2019). NeuroScore's spike detection tool applied an absolute threshold between 200  $\mu\text{V}$  and 2000  $\mu\text{V}$  with a spike duration of 0.1–250 ms to identify potential seizure events. Detected events were manually verified to ensure accuracy. Additionally, the supervised algorithm AccuSleep, originally developed for sleep state classification, was extended to classify seizure events based on characteristic patterns of seizures in ECoG recordings.

**Brain State Detection and Power Spectrum Analysis:** Brain states, including REM sleep, slow-wave sleep (SWS), and wakefulness (WAK), were identified using AccuSleep, a supervised machine learning algorithm. AccuSleep was trained to classify brain states with high accuracy by processing ECoG signals and pseudo-EMG signals derived from high-pass filtered ECoG channels. The filtering parameters were tailored to the telemetric transmitters used (80 Hz for HD-X02 and 200 Hz for ETA-F10). Detected brain states were validated against manually scored datasets to ensure classification reliability.

Spectral analysis of ECoG signals was performed to characterize power distribution across different brain states. Power-spectrum-density (PSD) plots were computed using multitaper spectral estimation implemented in the Chronux toolbox, ensuring high-resolution analysis of the power spectrum. Neural power spectra were further parameterized into periodic (oscillatory) and aperiodic components using the FOOOF (fitting oscillations and one over f) algorithm (Donoghue et al. 2020). The aperiodic component, modeled as  $L(f) = b - \log(k+f^\chi)$ , describes the  $1/f$ -like background activity, where  $\chi$  represents the aperiodic exponent potentially reflecting the excitation/inhibition (E/I) balance in neural networks. Periodic oscillations were identified as peaks in the spectrum above the aperiodic component and analysed across theta (3–16 Hz), beta (12–40 Hz), low gamma (36–90 Hz), and high gamma (89–199 Hz) frequency bands. The FOOOF algorithm ensured accurate decomposition of these components by iteratively fitting Gaussian curves to oscillatory peaks. Comparisons of the aperiodic exponent across brain states and experimental groups provided insights into the dynamics of neural excitability and inhibition.

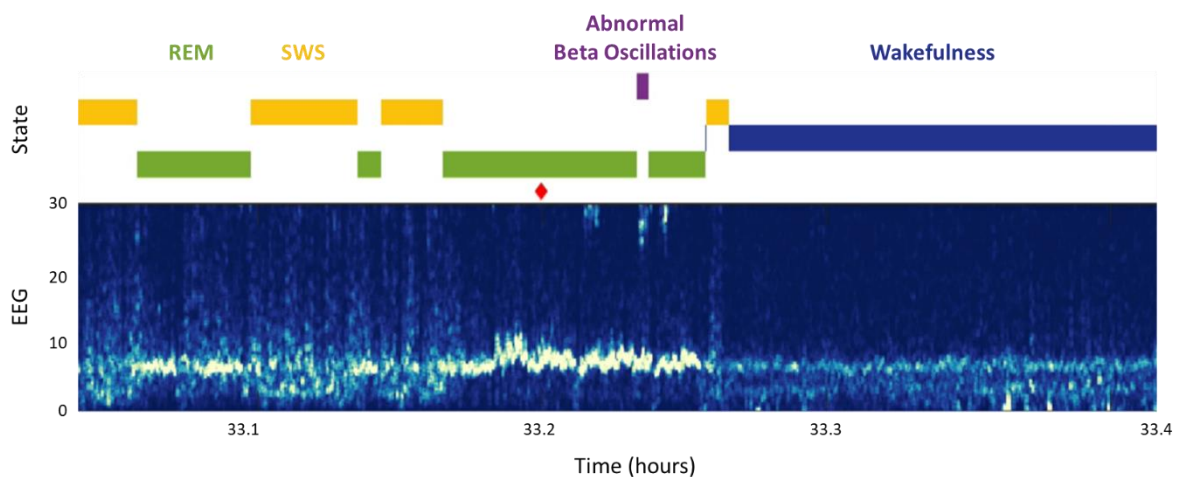


**Figure 6: Automated brain state detection using AccuSleep.** The upper panel displays the brain states detected over time (e.g., REM sleep, SWS and wakefulness), providing an overview of state transitions. The lower panel shows the wavelet spectrogram of the corresponding EEG signals, with time (hours) on the x-axis and frequency (Hz) on the y-axis. Warmer colours indicate higher power in the EEG signal, while cooler colours represent lower power. This visualization highlights the frequency power dynamics associated with different brain states.

**Sleep Architecture Analysis:** Sleep architecture was quantitatively assessed using the brain state classifications provided by AccuSleep. A custom MATLAB script processed detected brain states by filtering and merging events based on predefined thresholds. Minimum durations of 10 seconds were required for REM events, while SWS and WAK events were constrained to a minimum of 60 seconds to exclude transient artefacts. Events failing to meet these criteria were discarded, and closely spaced events were merged to ensure robust classification.

For each brain state, the script computed key metrics, including the total duration (in seconds), the proportion of the total recording time (as a percentage), and the number of discrete events. Additional measures included the mean and median event durations and the frequency of events normalized to hourly intervals. Differences in sleep state distributions across experimental groups were statistically analysed, highlighting alterations in sleep architecture potentially linked to genetic or treatment conditions.

## **2.4 | KCNT1 Blockers Administration**

### **2.4.1 | Pimozide Treatment in Heterozygous KCNIN Adult Mice**

To investigate the effects of Pimozide (Sigma, Germany) on epileptic activity, adult heterozygous KCNIN mice aged 13–17 weeks were treated with the drug via intraperitoneal (i.p.) injections. The treatment protocol consisted of two phases: a vehicle control phase and a drug treatment phase. During the vehicle phase, animals received injections of the vehicle solution (5% DMSO in 0.9% NaCl) twice daily for 5 consecutive days. Pimozide was then dissolved in the same vehicle solution for the treatment phase and administered at doses of 1 mg/kg body weight in the morning and 1.5 mg/kg body weight in the evening.

Blood samples were collected 1.5 hours after the final morning injection on the last day of pimozide treatment to measure serum drug levels. These measurements provided essential

pharmacokinetic data, verifying effective drug delivery and ensuring consistent dosing across experimental groups. After the treatment phase, a washout period of 4 days was implemented, during which no injections were administered, and recordings were paused. ECoG recordings resumed following the washout period to assess post-treatment neural activity and seizure dynamics.

Throughout the treatment, animals remained within the ECoG recording system to maintain a consistent environment, ensuring minimal variability in experimental conditions. This setup allowed for the analysis of epileptic activity during the vehicle phase, drug treatment phase, and the post-washout recording phase. All animals in this study were heterozygous KCNIN mice, ensuring consistency across experimental groups.

#### **2.4.2 | Pimozide Treatment in Homozygous KCNQR Adult Mice**

A second treatment study was conducted to assess the effects of Pimozide in KCNQR homozygous mice aged 14–18 weeks. The experimental design mirrored the protocol used for KCNIN heterozygous mice, with the exception of the Pimozide dosage. Animals were treated via intraperitoneal (i.p.) injections in two phases: a vehicle control phase followed by a drug treatment phase.

During the vehicle phase, animals received injections of the vehicle solution (5% DMSO in 0.9% NaCl) twice daily for 5 consecutive days. This was followed by a 7-day Pimozide treatment phase. Pimozide was dissolved in the vehicle solution and administered twice daily at a dose of 1.5 mg/kg body weight in the morning and 2 mg/kg body weight in the evening. Blood samples were collected 1.5 hours after the final evening injection on the last day of Pimozide administration to measure drug levels in the serum.

A 7-day washout period followed the treatment phase, during which no injections were given, and ECoG recordings were paused. Post-treatment neural activity was assessed through ECoG recordings that resumed immediately after the washout period. Animals were continuously monitored within the recording system during the vehicle and treatment phases, ensuring robust data collection and minimal variability.

### **2.4.3 | Carvedilol Treatment in Heterozygous KCNIN Adult Mice**

A third treatment study was conducted to evaluate the effects of Carvedilol in KCNIN heterozygous mice aged 12–17 weeks. Carvedilol (Adooq Bioscience, CA, USA) was administered continuously via subcutaneously implanted Alzet© Osmotic Pumps (Model 2002, 200 µL capacity, 0.5 µL/h release rate, CA, USA), allowing for sustained drug delivery over the treatment period. The pumps were surgically implanted before the treatment phase on the side opposite the telemetric implant and explanted after the treatment phase to ensure uninterrupted drug delivery.

The dosage of Carvedilol was set at 8 mg/kg body weight. The drug solution was prepared as 30 mg/mL Carvedilol dissolved in 20% w/v hydroxypropyl-β-cyclodextrin (Sigma, Germany) in 1% glacial acetic acid (Sigma, Germany). The vehicle solution consisted of the same preparation without Carvedilol. The treatment protocol included a 7-day vehicle phase, followed by a 7-day Carvedilol administration phase. An additional 7-day Carvedilol administration phase was implemented after optimizing the solution through prolonged ultrasonication to improve drug solubility. Blood samples were collected on the final day of Carvedilol treatment to measure drug levels in the serum.

Following Carvedilol administration, a washout period of 3 days was observed during which no drug was administered. Post-treatment effects were assessed with ECoG recordings conducted over 3 consecutive days following the washout period. Animals were continuously monitored within the ECoG recording system throughout the vehicle, treatment, and recording phases.

### **2.4.4 | Carvedilol Treatment in Heterozygous KCNIN Neonatal Mice**

The fourth treatment study investigated the effects of Carvedilol in neonatal KCNIN heterozygous mice from postnatal day 7 (P7) to P35. Carvedilol was administered via two delivery methods: intraperitoneal injections from P7 to P21 (pre-weaning phase) and chow food embedding from P21 to P35 (post-weaning phase).

During the pre-weaning phase, animals received intraperitoneal injections of Carvedilol twice daily, delivering a total daily dose of 8 mg/kg body weight. The drug solution was prepared as 0.4 mg/mL Carvedilol dissolved in 0.5% w/v hydroxypropyl-β-cyclodextrin in 0.025% glacial acetic acid. From P21 onward, following weaning, Carvedilol was embedded

in chow food (65 mg Carvedilol/kg chow, Altromin Spezialfutter GmbH, Germany), allowing continuous drug delivery as the animals consumed their home cage food. The vehicle solution consisted of the same preparation without Carvedilol, and vehicle-treated animals followed the same protocol as treated animals.

The concentration of carvedilol in the chow was calculated based on monitored food intake in a pilot experiment with a separate cohort of animals. Food consumption was continuously recorded using an automated monitoring system (Infra-e-motion, Hamburg, Germany), which measured food and water intake in the animals' home cages. These measurements, combined with previous estimates of food consumption (Sacco et al. 2017), were used to determine the appropriate concentration of carvedilol in the chow. Final serum carvedilol levels were analysed at the end of the experiment to confirm effective drug delivery and to refine the final formulation of the carvedilol-embedded chow.

ECoG recordings were performed from P29 to P35, once animals reached a minimum body weight of 15 g and were surgically implanted with telemetric devices. The study included wild-type animals, untreated heterozygous animals, vehicle-treated animals, and Carvedilol-treated heterozygous animals, ensuring a comprehensive comparison of treatment effects. Blood samples were collected at the end of the recording period to evaluate drug levels in the serum, and the animals were subsequently perfused for histological analyses.

This protocol enabled a detailed assessment of Carvedilol's effects on neonatal animals, spanning both pre- and post-weaning phases and ensuring continuous drug delivery throughout the critical developmental window.

## **2.5 | Immunohistochemistry**

To investigate structural and cellular differences in the hippocampus between genotypes, and to assess the effects of treatments compared to untreated animals, histological staining was performed on brain sections collected from two groups of animals: untreated animals that had not undergone any experimental procedures, specifically for observing genotype effects and those subjected to telemetry and open-field experiments to evaluate treatment effects. Immunohistochemistry was conducted for Wisteria floribunda agglutinin (WFA), neuropeptide Y (NPY), and glial fibrillary acidic protein (GFAP), each selected to address specific features of epilepsy-associated pathology.

**WFA staining** was employed to label perineuronal nets (PNNs), extracellular matrix structures rich in N-acetylgalactosamine beta 1 (GalNac  $\beta$ 1-3 Gal) residues. PNNs stabilize synaptic connections and have been shown to increase in an activity-dependent manner during epilepsy, particularly in the dentate gyrus of the hippocampus (Chaunsali, Tewari, and Sontheimer 2021).

**NPY staining** was used to visualize mossy fibers and interneurons. NPY serves as a biomarker of epileptic activity due to its inhibitory properties, acting as an endogenous anticonvulsant in response to heightened neuronal excitability (Cattaneo et al. 2020). This staining enabled the assessment of compensatory inhibitory mechanisms within the hippocampus.

**GFAP staining** was used to identify astrocytes, which are upregulated during epilepsy-induced neuroinflammation. This provided insights into the extent of gliosis and its role in hippocampal pathology during epileptic activity (Mochol et al. 2023).

Finally, all sections were counterstained with DAPI using Fluoromount-G (Southern Biotech, USA) to visualize cell nuclei, ensuring accurate localization of structural and cellular markers within the tissue.

### 2.5.1 | Sample Preparation

To prepare brain tissue for staining, animals were perfused and fixed to minimize background fluorescence and unspecific staining from the vasculature. Animals were anesthetized via intraperitoneal injection of 10  $\mu$ l/g ketamine-xylazine solution (10% Ketanest [100 mg/ml, Zoetis], 2% Sedaxylan [20 mg/ml, Bayer] in 0.9% sodium chloride solution). Upon the loss of toe reflexes, the animals were restrained in a supine position on a polystyrene platform. A thoracotomy was performed to expose the heart, and a 25-gauge cannula connected to a PERIMAX peristaltic pump (SPETEC) was inserted into the left ventricle while the right atrium was perforated. The animals were perfused with approximately 10 ml of 1x phosphate-buffered saline (PBS) (8.0 g NaCl, 0.2 g KCl, 1.42 g  $\text{Na}_2\text{HPO}_4$ , 1.78 g  $\text{Na}_2\text{HPO}_4 \cdot 2\text{H}_2\text{O}$  per liter  $\text{H}_2\text{O}$ ), followed by 60 ml of 4% formaldehyde (-FA) solution (phosphate buffered pH 7.0, Roti® Histofix 4%, Roth).

After perfusion, the animals were decapitated, and the brains were carefully removed. Brains were post-fixed in 4% -FA at 4°C for 24 hours and then transferred to PBS containing 0.02%

sodium azide for long-term storage. To ensure optimal conditions for sectioning, brains were returned to 4% -FA one day before dissection.

For the animals used in neonatal treatment study, coronal vibratome sections of 40  $\mu\text{m}$  thickness were prepared from the region of interest (approx. from -0.94 mm to -2.8 mm relative to bregma) to target the hippocampus. Sectioning was performed in PBS, and the resulting sections were collected into 24-well plates containing 1 ml PBS with 0.02% sodium azide per well. The sections were stored at 4°C until further staining procedures.

For the animals used in genotype effect investigation, brain sections for WFA and GFAP staining were prepared using a cryostat. Coronal sections of 20  $\mu\text{m}$  thickness were cut and immediately mounted onto glass slides after sectioning. The slides were stored at -20°C until further staining procedures, ensuring preservation of tissue integrity and antigenicity.

## 2.5.2 | Staining Procedures

### Cryostat Section Staining

Cryostat sections of 20  $\mu\text{m}$  thickness were prepared for WFA and GFAP stainings to investigate genotype effects. Sections were mounted directly onto slides during sectioning and stored at -20 °C until further staining procedures.

**WFA Staining:** Cryostat sections were dried at 37 °C for 30 minutes. The sections were permeabilized three times for 10 minutes in 0.1% TritonX-100 in PBS and then incubated in blocking solution (5% bovine serum albumin [BSA] in PBS) for 1 hour at room temperature (RT). Slides were incubated overnight at 4 °C with biotinylated WFA (1:1000; Sigma #1516) in blocking solution. The next day, slides were permeabilized three times for 10 minutes in PBS 0.1% TritonX-100 and incubated with streptavidin Alexa Fluor 546 (1:500; MP #S11225) in blocking solution for 1 hour at RT. Slides were washed twice with PBS 0.1% TritonX-100 and then were washed twice with PBS, counterstained with DAPI, and coverslipped using Fluoromount-G.

**GFAP Staining:** Cryostat sections were dried at 37 °C for 30 minutes. The sections were washed three times for 5 minutes in PBS and blocked for 1 hour in PBS containing 1% normal goat serum (NGS), 0.3% Triton X-100 and 0.2% BSA. Slides were incubated overnight at 4 °C with rabbit polyclonal anti-GFAP antibody (1:500; DAKO #Z033429) in

PBS containing 1% NGS, 0.3% Triton X-100 and 0.2% BSA. The next day, sections were washed three times in PBS for 15 minutes and incubated with Alexa Fluor 488-conjugated goat anti-rabbit IgG (1:500; Invitrogen #A11034) for 1 hour at RT. Slides were washed three times in PBS for 5 minutes, counterstained with DAPI, and mounted with Fluoromount-G.

### **Vibratome Section Stainings**

Vibratome sections of 40  $\mu\text{m}$  thickness were prepared for NPY, WFA, and GFAP stainings to investigate both genotype effects and treatment responses. Staining was performed free-floating in 24-well plates with mesh carriers, using four sections per well per brain.

For all vibratome stainings, 1x PBS, 0.1% PBST (0.1% Triton X-100 in 1x PBS), and blocking solution (5% NGS in PBS) were prepared. After each step, the mesh carrier containing the sections was transferred to another 24-well plate with the next solution. The staining steps after the exposure of secondary antibody were performed in the dark. After staining, sections were mounted on slides using DAPI Fluoromount-G and stored at 4 °C.

### **General Protocol:**

1. Sections were washed three times for 10 minutes in 0.1% PBST at RT on a shaker.
2. Sections were blocked for 1 hour at RT in blocking solution.
3. Primary antibody incubation was performed overnight at 4 °C in blocking solution.
4. Sections were washed three times for 10 minutes in 0.1% PBST at RT.
5. Secondary antibody incubation was performed for 2 hours at RT in blocking solution.
6. Final washes consisted of two 10-minute washes in PBST and two 10-minute washes in PBS.

**WFA Staining:** For WFA staining, biotinylated WFA (1:500; Sigma #L1516) was used as the primary reagent. After washing, streptavidin Alexa Fluor 546 (1:500; MP #S11225) was used as the secondary reagent to visualize perineuronal nets.

**NPY Staining:** For NPY staining, rabbit anti-NPY antibody (1:1000; ImmunoStar #22940) was used as the primary antibody. After washing, Alexa Fluor 488-conjugated goat anti-rabbit IgG (1:500; Invitrogen #A11034) was used as the secondary antibody.

**GFAP Staining:** For GFAP staining, rabbit anti-GFAP antibody (1:500; DAKO #Z033429) was used as the primary antibody, followed by Alexa Fluor 488-conjugated goat anti-rabbit IgG (1:500; Invitrogen #A11034) as the secondary antibody.

### 2.5.3 | Image Acquisition and Analysis

Fluorescently stained brain sections were analysed using a Zeiss epifluorescence microscope (Axio Imager M2, Zeiss, Germany) equipped with an AxioCam MRc camera (Zeiss, Germany). Images were acquired and processed using ZenPro software (Zeiss, Germany). To ensure consistency and comparability across experimental groups, identical microscope settings, including exposure times and light intensities, were maintained for all animals within each staining protocol. Linear adjustments of contrast were applied uniformly to all images for visualization purposes, quantitation was performed on un-adjusted raw data.

Overview images of whole sections were captured using a 5× objective, while higher-resolution images of the hippocampal region were acquired with a 10× objective. The microscope and software settings were optimized to prevent photobleaching and maintain signal integrity during image acquisition.

Image analysis was performed using ImageJ software (version 1.54f). Regions of interest (ROI) corresponding to specific hippocampal subregions were manually selected for each staining. For WFA, the molecular layer of the dentate gyrus was analysed, while GFAP analysis included the total hippocampus. For NPY, analyses focused on the hippocampal mossy fibers.

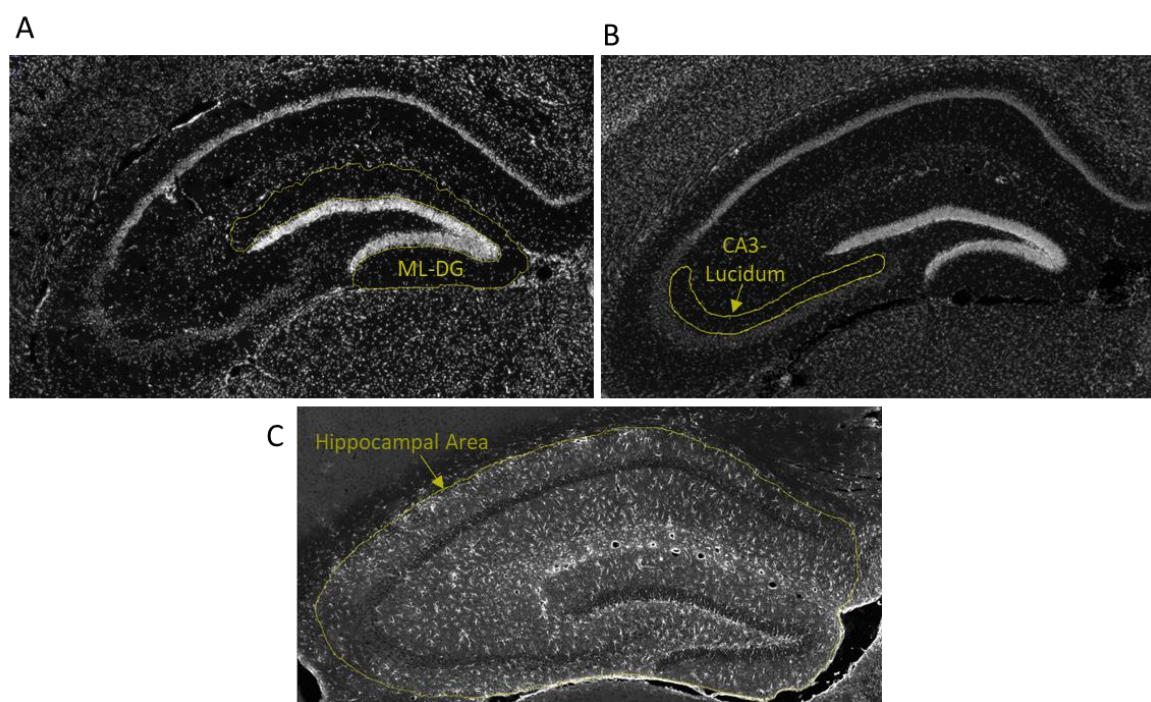


**Figure 7: Regions of interest (ROI) analysed for immunohistochemistry quantifications.** (A) For WFA staining, the molecular layer of the dentate gyrus (ML-DG) was quantified. The mean gray value was compared between experimental groups. (B) For NPY staining, the lucidum of the CA3 region was quantified, focusing on mossy fiber expression level. (C) For GFAP staining, the entire hippocampus was analysed, with comparisons of the mean gray value and the stained area fraction.

Quantitative metrics were extracted as follows:

- **WFA staining:** Mean gray values (mean [pixels]) were calculated for the selected ROI, the molecular layer of the dentate gyrus.
- **GFAP staining:** Mean gray values were calculated for the whole hippocampal area. Additionally, the stained area fraction was determined from binarized images using a threshold set to the mean background intensity plus six times the standard deviation.
- **NPY staining:** Staining intensity in mossy fibers were quantified using mean gray values.

Statistical analyses were performed using GraphPad Prism (version 10.0.2). Data visualization included scatter plots with appropriate statistical comparisons. A non-parametric Kruskal-Wallis test was conducted to compare each group with the non-treated wild-type controls. All statistical tests were two-tailed, with the significance level set at  $P < 0.05$ . Significant differences are denoted by p-values in figures, while non-significant differences ( $p\text{-value} > 0.05$ ) are indicated as "ns".

## 2.6 | Body Weight Development and Behavioural Tests

A series of behavioural tests were conducted to assess body development, motor activity, anxiety-like behaviour, and memory in both KCNIN and KCNRQ mouse lines. Behavioural testing was performed in adult animals of both lines, except for the Object Recognition Memory test, which was not conducted for KCNIN mice. Additionally, juvenile KCNIN animals treated with Carvedilol were exclusively tested using the open field test.

Body weight development was monitored longitudinally for three months in the KCNIN line, whereas body weight measurements for KCNRQ animals were recorded until postnatal day 23 (P23). All behavioural experiments were conducted under standardized conditions. Mice were habituated to the experimenter and testing room before each test, and experiments were carried out during the dark phase of the 12:12 dark-light cycle to align with the animals' natural activity period. To minimize stress and fatigue, at least one rest day was allowed

between experiments. Testing arenas were thoroughly cleaned with 70% ethanol after each trial to eliminate olfactory cues.

At the time of behavioural testing, neonatal mice were between P2 and P8 for early somatosensory reflex assessment, juvenile animals were tested between P29 and P35, and adult animals were aged between 11 and 22 weeks. This comprehensive approach ensured reliable comparisons of behavioural phenotypes across genotypes, treatments, and developmental stages.

### **2.6.1 | Somatosensory Reflex Tests in Neonatal Animals**

Somatosensory reflexes were tested in neonatal mice between postnatal day 2 (P2) and postnatal day 8. The tests included the righting reflex, cliff avoidance reflex, and geotactic reflex. Each reflex test was performed twice for each pup, with an intertrial interval (ITI) of 30 seconds. The latency to complete each task was recorded, and failure to perform the task within 30 seconds was noted as a failure.

**The cliff avoidance reflex** was assessed by placing the pup on a raised platform approximately 10 cm high with its head and front paws positioned at the edge. Successful performance was defined as the pup turning its body approximately 90°, moving its head and front paws away from the edge of the platform.

**The righting reflex** evaluated the pup's ability to turn from a supine position to a normal prone position. Success was determined when the animal successfully turned, and all four paws made contact with the ground.

**The geotactic reflex** was tested by placing the pup on an inclined plexiglass plate set at a 37° angle with its nose facing downward. The task was considered successful when the pup turned 180° to face upward along the incline.

For each test, the latency to successfully complete the task was measured, and the mean and standard error of the mean (SEM) of the two trials were calculated and plotted. These tests provided insight into the development of basic motor and sensory reflexes in neonatal animals.

### **2.6.2 | Open Field**

The open field test was performed to assess the exploratory behaviour and locomotor activity of the animals. The test arena was a white box (50 x 50 x 40 cm), divided into two zones: a

border area (5 cm from the edge) and a central area (20 x 20 cm). Animal behaviour was detected and recorded using EthoVisionXT 17 (Noldus, Wageningen, The Netherlands). Each animal was placed facing the lower left corner of the arena, and recording commenced after a 3-second delay triggered by motion detection.

For adult KCNIN and KCNQR mice, the test was conducted under 25 lux illumination with a total duration of 20 minutes. For juvenile KCNIN animals treated with Carvedilol, the test was performed under 100 lux illumination for a duration of 15 minutes. The following parameters were quantified during the analysis: total distance moved [m], distance moved per time bin [cm], and the percentage of time spent in the center versus border areas.

### **2.6.3 | Elevated Plus Maze**

The elevated plus maze was used to assess anxiety-like behaviour in the mice. The apparatus consisted of a plus-shaped platform elevated 70 cm above the ground, with two open arms (exposed) and two closed arms (surrounded by 15 cm-high opaque walls), along with a central area connecting all arms. The test relies on the natural conflict between exploration of open areas and the preference for the safety of enclosed spaces.

Recordings were performed in complete darkness using infrared light, and tracking was achieved with EthoVisionXT 17. At the start of the test, animals were placed in the center of the maze facing one of the open arms, and behaviour was recorded for 5 minutes. The measured parameters included the time spent in open arms [s], time spent in closed arms [s], and the arm preference index, calculated as:

$$\text{Arm Preference} = \frac{\text{Time in Open Arm} - \text{Time in Closed Arm}}{\text{Time in Open Arm} + \text{Time in Closed Arm}}$$

The arm preference index ranges from -1 (complete avoidance of open arms) to +1 (exclusive preference for open arms), with 0 indicating no preference. This test provides insights into anxiety-related behaviour and exploration tendencies in experimental animals.

### **2.6.4 | Y-Maze**

The Y-maze test was conducted to assess the working memory of animals and innate preference to explore novel environments. The maze was illuminated at 10 lux. Each animal was placed in the center of the Y-maze and allowed to explore the three arms until they completed 23 arm entries or a maximum duration of 15 minutes. For an arm entry to be

considered valid, the animal had to enter at least 5 cm into the arm with its hind legs, and a re-entry was only counted if the animal had fully returned to the center of the maze. The percentage of spontaneous alternations, calculated as the ratio of consecutive entries into all three arms without re-entry into the same arm, and the average transition time [s] were analysed. Animals that did not achieve 23 alternations within the allowed 15 minutes were excluded from the analysis.

### 2.6.5 | Object Location Memory

The long-term spatial memory was assessed using the *Object Location Memory* task, performed under 15 lux illumination in the same arena as the open-field test. The arena was divided into two compartments by a PVC wall with a central opening, enabling the animals to alternate between compartments. Visual landmarks were affixed to the walls within the arena to provide spatial cues. The paradigm consisted of two phases: an *exposure trial* (10 minutes) and a *recall trial* (10 minutes), separated by a 24-hour inter-trial interval, during which mice were returned to their home cages.

In the exposure (or training) trial, two identical objects (e.g., plastic bottles filled with dark blue dye) were placed at designated positions in two corners of the arena. Mice were placed in one compartment of the arena, facing the opening to the adjacent compartment, and allowed to explore the objects freely. During the recall (or testing) trial, conducted 24 hours later, one of the two objects was displaced to a novel location while the other remained fixed. The animals' inherent tendency to explore novel spatial stimuli was quantified by analysing the time spent interacting with the objects. Object interaction was defined as the mouse's nose being within a 2 cm radius of the object.

Behavioural parameters, including distance moved [m], mean velocity [cm/s], and time [s] spent in the object zones, were recorded and analysed using EthoVision XT 17. The discrimination index (DI), calculated as  $(Object^{displaced} - Object^{fixed} / Object^{displaced} + Object^{fixed})$ , was used to determine the preference for the displaced object, with values ranging from 1 (complete preference for the displaced object) to -1 (complete preference for the fixed object) and a value of 0 indicating no preference. Animals that failed to explore both objects or did not alternate between the compartments were excluded from the analysis.

### 2.6.6 | Object Recognition Memory

The long-term recognition memory was assessed using *Object Recognition Memory* task. The test was conducted in the same arena and under the same conditions as the object location memory experiment. The experimental design included an exposure (or training) trial and a recall (or testing) trial, with the recall trial performed 24 hours after the exposure trial. During the exposure trial, two identical objects (plastic bottles filled with blue dye solution) were placed in the arena. For the recall trial, one of the objects was replaced with a 3D-printed pyramid with blunt spikes on its surface, serving as the novel object.

The experiment aimed to evaluate the animals' intrinsic tendency to explore novel stimuli. The parameters distance moved [m], mean velocity [cm/s], and time [s] spent in the object zone were quantified using EthoVision XT 17. Object interaction was defined as the time spent with the mouse's nose within 2 cm of the object. The discrimination index ( $DI = (Object_{novel} - Object_{familiar}) / (Object_{novel} + Object_{familiar})$ ) was calculated to indicate preference between the novel object ( $DI = 1$ ) and the familiar object ( $DI = -1$ ), with no preference represented by a  $DI$  of 0. Animals that explored only one object without transitioning to the other side of the arena were excluded from the analysis.

### 2.6.7 | Step-Through Passive Avoidance

The Step-Through Passive Avoidance test was used to assess learning and memory in mice by exploiting their innate preference for dark environments. The apparatus consisted of a two-compartment box with a grid floor: a smaller illuminated compartment (18 cm × 18.5 cm, 26 cm high, 50 lx) and a larger dark compartment (18 cm × 18.5 cm, 26 cm high, <0.5 lx), connected by a sliding door (5 cm × 5 cm).

During the acquisition trial on the first day, mice were placed in the illuminated compartment, and after 2 minutes, the sliding door was opened. The latency to enter the dark compartment was measured once the mouse encountered the open door and entered with all four paws. Upon entering, the door was closed, and a mild foot shock (2 s, 0.75 mA) was delivered. Mice were then returned to their home cages immediately after the shock.

The retention trial was performed 24 hours later to evaluate memory retention. The procedure was identical except that the sliding door was opened 30 seconds after placing the mouse in the illuminated compartment, and no foot shock was administered. Mice were observed for a maximum of 180 seconds. The latency to enter the dark compartment was

measured, with mice that did not enter the compartment assigned a latency score of 180 seconds. For mice that entered the dark compartment, the time spent in the dark compartment and the number of transitions between the compartments were recorded. This test enabled the assessment of the animals' ability to learn and remember an aversive stimulus while analysing their behavioural response to the environment.

### **2.6.8 | The Analysis of Behavioural Experiments**

Behavioural experiments were recorded using EthoVisionXT 17. The raw data were exported from EthoVisionXT and analysed in GraphPad Prism for statistical testing and data visualization. A non-parametric Kruskal-Wallis test was used to compare experimental groups with the wild-type control group for both KCNIN and KCNRQ lines. All statistical tests were two-tailed, and significance was determined

at  $P < 0.05$ . Significant differences are indicated with  $p$ -values in the figures, while comparisons without  $p$ -values represent non-significant differences (ns;  $P > 0.05$ ).

For open field experiments, an additional two-way ANOVA was performed to assess time-dependent changes in the distance moved within each group. Significance was set at  $P < 0.05$ . In the Y-Maze experiment, a one-sample Wilcoxon test was conducted to determine whether performance significantly exceeded the chance level of 50%, ensuring that observed alternations reflected memory-based choices rather than random exploration.

### 3. | Results

#### 3.1 | Spontaneous Seizures in KCNT1 Mutant Models

To investigate the occurrence and characteristics of spontaneous seizures in KCNT1 mutant models, telemetric video-ECoG recordings were performed. A total of 22 adults (10–32 weeks old) KCNIN heterozygous animals, 6 adults (9 weeks old) KCNIN homozygous animals, 7 adult (17–29 weeks old) KCNRQ heterozygous animals and 7 adults (14–19 weeks old) KCNRQ homozygous animals were recorded. Figure 8 highlights the representative seizure events recorded in heterozygous KCNIN and homozygous KCNRQ animals. The setup involved subcutaneously implanted radio transmitters for continuous cortical activity monitoring (Figure 8A). Spontaneous seizures in KCNIN heterozygotes were characterized by high-amplitude, rhythmic discharges in the raw ECoG signal (Figure 8B, top).

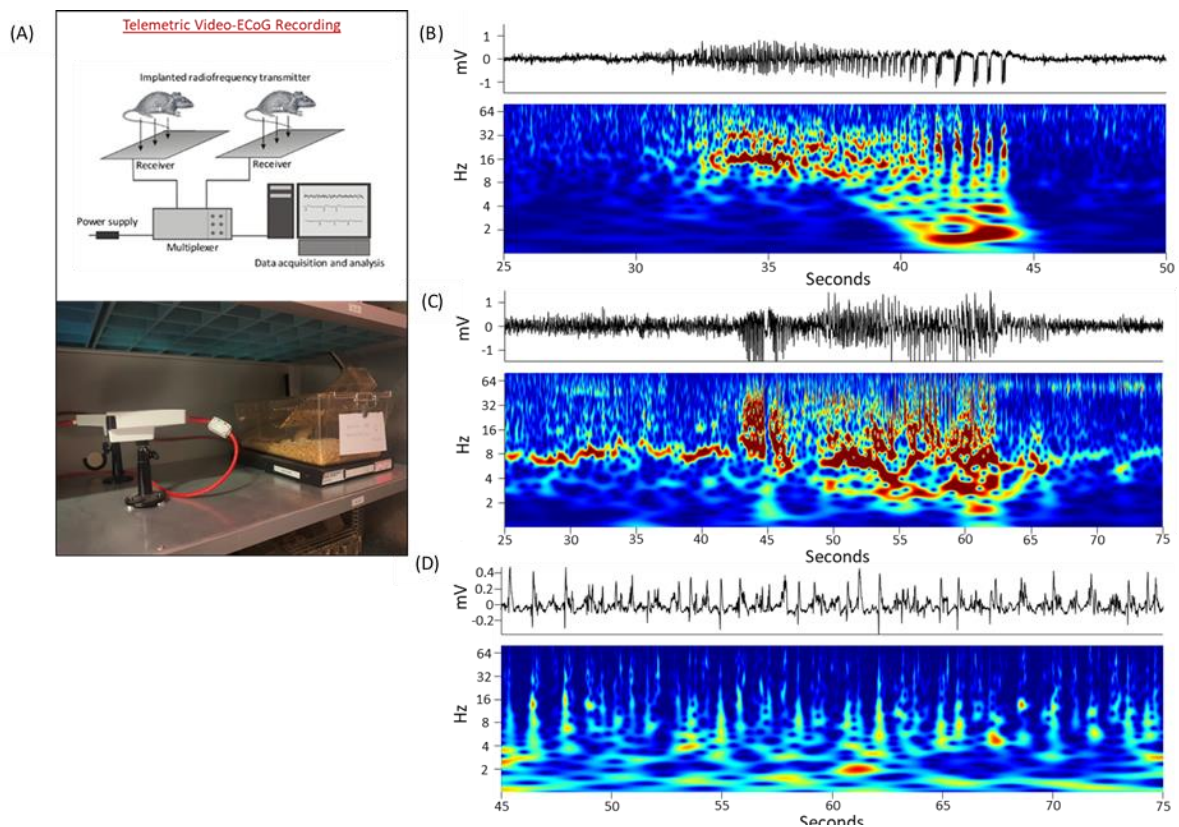


**Figure 8: Spontaneous seizures and interictal activity in KCNT1 mutant models.** (A) Telemetric video-ECoG recording setup to collect cortical activity via subcutaneously implanted radio transmitters. (B) Representative example of a spontaneous seizure event in a heterozygous KCNIN animal. Top: Raw ECoG signal in mV of a seizure activity. Bottom: Time-frequency wavelet spectrogram showing the power distribution across time and frequencies (warm colors represent high power; cold colors represent low power). (C) Representative example of a spontaneous seizure event in a homozygous KCNRQ animal, structured as described in (B). (D) Example of interictal activity recorded in the homozygous KCNRQ model, structured as described in (B).

The corresponding time-frequency spectrogram revealed that prominent power at beta frequency range at the beginning of the seizures and ending up with low frequency oscillations, indicating a generalized tonic-clonic seizures (Figure 8B, bottom). In the example seizure, the animal had a seizure after SWS and the behaviour of the animal started with a head nodding and continued with bilateral forelimb clonus (Racine Scale=4). The seizures of KCNIN heterozygous animals were also followed by short postictal depression phase. Similarly, seizures in KCNRQ homozygotes were displaying distinct beta bursts at the beginning, and ending up with slow oscillations. In contrast to KCNIN heterozygous animals, they had prolonged ictal events and postictal phase (Figure 8C). In the example seizure, the animal arrested to seizure after a REM sleep period and demonstrated rearing behaviour and falling to the side (Racine Scale=5). Notably, KCNRQ homozygous animals showed absence seizures longer than 5 minutes. During these periods, the animals were not responsive to any external stimuli. Additionally, interictal activity in KCNRQ homozygotes was marked by sporadic epileptic discharges, further emphasizing the hyperexcitable state of the cortical network (Figure 8D).

Figure 9 provides a quantitative assessment of seizure incident variability across recording days. Heat maps of KCNIN heterozygotes demonstrated moderate seizure frequency, with variability among individual animals (Figure 9A). In contrast, KCNRQ homozygotes exhibited higher seizure frequencies, with greater day-to-day fluctuations and more pronounced inter-animal variability (Figure 9B). (KCNIN heterozygous animals:  $0.77 \pm 0.12$

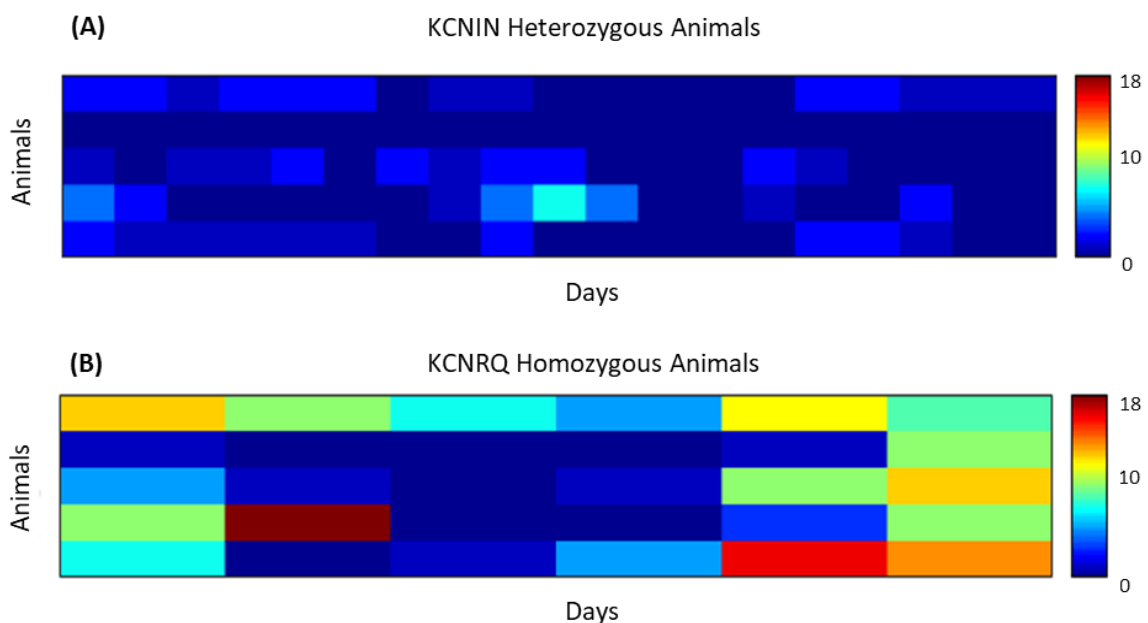


**Figure 9: Seizure incident variability in KCNIN and KCNRQ mutant models.** Heat maps illustrating seizure frequency variability across days of recording in KCNT1 mutant animals. **(A)** Heterozygous KCNIN animals. **(B)** Homozygous KCNRQ animals. Each column represents a recording day, and each row represents an individual animal. Warm colors indicate higher seizure frequency, while colder colors indicate lower seizure frequency.

seizures per day, KCNRQ homozygous animals:  $5.73 \pm 0.98$  seizures per day). Notably, recordings from KCNIN homozygous and KCNRQ heterozygous animals revealed no spontaneous seizure activity. These findings underscore the severity of the epileptic phenotype in KCNRQ homozygotes compared to KCNIN heterozygotes.

Overall, these results establish that both KCNIN and KCNRQ mutant models exhibit spontaneous seizures, with KCNRQ homozygotes displaying a more severe and variable seizure phenotype. The observed interictal and ictal patterns suggest distinct electrophysiological signatures for these models, providing insights into the phenotypic variability of KCNT1-associated epileptic encephalopathies.

### 3.2 | Altered Cortical Oscillations During Interictal Periods

To examine the impact of KCNT1 mutations on cortical oscillatory activity during interictal periods, the power spectral densities (PSDs) of ECoG recordings were analyzed. Figure 10 depicts oscillatory changes in KCNIN heterozygous animals, while Figure 11 illustrates similar data for KCNRQ homozygous animals. As described in Methods section 2.2.2 (Fig. 6), inter-ictal brain states such as REM (paradoxical) sleep, SWS, and wake periods/epochs were identified by a supervised machine learning algorithm, AccuSleep (Barger et al. 2019), and were manually validated.

In KCNIN heterozygotes, there was a trend towards reduced theta power during REM sleep and SWS (Figure 10A-B). Beta oscillations, which are typically absent during sleep in wild-type animals, were prominently observed in the mutant animals (Figure 10C). Interestingly, the power of these beta oscillations was even elevated compared to the sporadic occurrences in wild-type animals. The contingency analysis for the occurrences of beta oscillations during REM sleep revealed no significant dependence of beta occurrence from genotype (Chi-square test,  $p=0.74$ ). Additionally, the aperiodic exponent, which may be a proxy for cortical excitation/inhibition balance, was markedly reduced, particularly during sleep events (Figure 10E), indicating impaired inhibition.

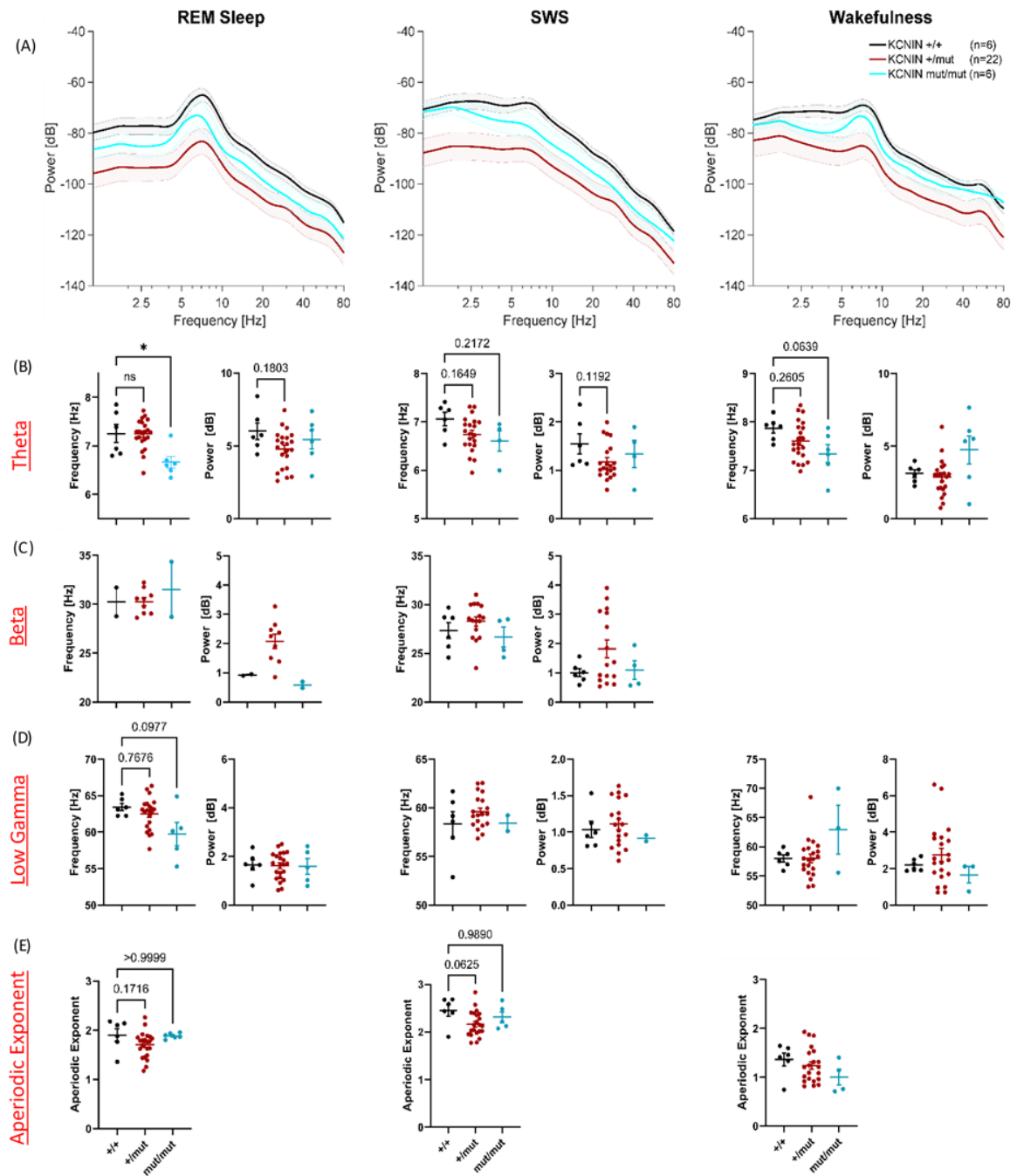


**Figure 10: The analysis of interictal cortical oscillations in KCNIN heterozygous animals. (A)** Power spectral density (PSD) plots showing power (dB) and frequency (Hz) for heterozygous and homozygous KCNIN animals during REM sleep, SWS, and wakefulness. Shaded areas represent mean  $\pm$  SEM, with the number of animals indicated in the legend. **(B–D)** Scatter plots for theta **(B)**, beta **(C)**, and low gamma **(D)** oscillations, showing frequency peaks and corresponding power values for REM sleep (left column), SWS (middle column), and wakefulness (right column). Each dot represents an individual animal, with  $\pm$  SEM plotted. **(E)** Alterations in the aperiodic exponent across brain states, reflecting changes in cortical excitability. Statistical analysis was performed using one-way ANOVA Kruskal-Wallis tests (ns = not significant, \*  $p < 0.05$ ).

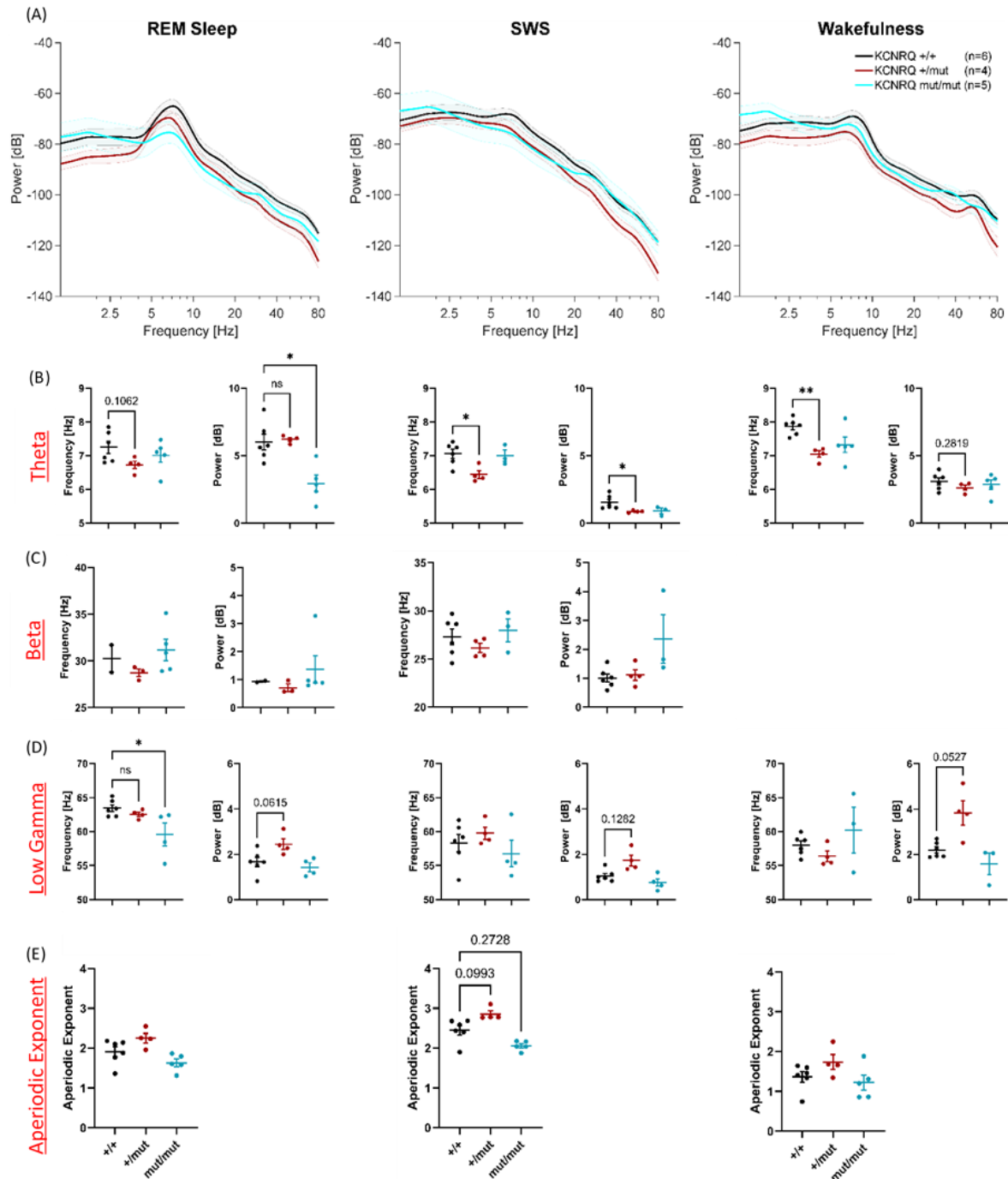


**Figure 11: The analysis of interictal cortical oscillations in KCNRQ homozygous animals. (A)** PSD plots showing power (dB) and frequency (Hz) for heterozygous and homozygous KCNRQ animals during REM sleep, SWS, and wakefulness. Shaded areas represent mean  $\pm$  SEM, with the number of animals indicated in the legend. **(B–D)** Scatter plots for theta **(B)**, beta **(C)**, and low gamma **(D)** oscillations, showing frequency peaks and corresponding power values for REM sleep (left column), SWS (middle column), and wakefulness (right column). Each dot represents an individual animal, with  $\pm$  SEM plotted. **(E)** Alterations in the aperiodic exponent across brain states, reflecting changes in cortical excitability. Statistical analysis was performed using one-way ANOVA Kruskal-Wallis tests (ns = not significant, \*  $p < 0.05$ , \*\*  $p < 0.01$ ).

In KCNRQ homozygotes, oscillatory impairments were more pronounced (Figure 11A). A reduction in theta power during REM sleep was also observed in KCNRQ homozygous animals, further indicating disruptions in this key oscillatory activity. Beta oscillations appeared unexpectedly during sleep stages, with higher power in KCNRQ homozygous animals that exhibited spontaneous seizures (Figure 11B-C). The contingency analysis for the occurrences of beta oscillations during REM sleep revealed a significant dependence of beta occurrence from genotype (Chi-square test,  $p=0.02$ ). The gamma frequency shift observed during REM sleep was unique to epileptic KCNRQ homozygous animals (Figure 11D). However, I did not observe significant alterations in the aperiodic exponent for KCNRQ animals (Figure 11E).

Overall, these results demonstrate that KCNT1 mutations profoundly disrupt cortical oscillatory dynamics during interictal periods. KCNIN heterozygotes displayed a trend toward reduced theta power and an increase in beta oscillations during sleep. Similarly, KCNRQ homozygotes exhibited a significant reduction in REM theta power, an unexpected prominence of beta oscillations during sleep stages, and a distinct gamma frequency shift during REM sleep. These findings highlight the more severe network function alterations in KCNRQ homozygotes and suggest genotype-specific mechanisms underlying cortical excitability and epileptogenesis.

### **3.3 | Severe Sleep Architecture Disruptions**

Sleep architecture analyses were performed exclusively for KCNIN heterozygous and KCNRQ homozygous animals, both of which exhibited spontaneous seizures. In KCNRQ homozygotes, the percentage of time spent in REM sleep was significantly reduced (Figure 12A, middle), and this decrease was accompanied by an increase in wakefulness (Figure 12C, middle), while the duration of SWS epochs was significantly increased (Figure 12B, left). Additionally, the number of REM and SWS epochs per 12-hour period was markedly decreased (Figure 12A-B, right), indicating fragmented and unstable sleep patterns. These disruptions were statistically significant, as confirmed by one-way ANOVA Kruskal-Wallis tests ( $***p < 0.001$ ).

KCNIN heterozygous animals displayed more moderate changes in sleep architecture. REM sleep percentage trended to be reduced compared to wild-type animals and, thus, was less severe than that observed in KCNRQ homozygotes (Figure 12A, middle). Likewise, SWS

episodes tended to be longer (Figure 12B, left), and the frequency of REM and SWS episodes showed a trend of moderate reduction (Figure 12A-B, right). These findings indicate that while both genotypes exhibit sleep disturbances, KCNRQ homozygotes experience more profound impairments.

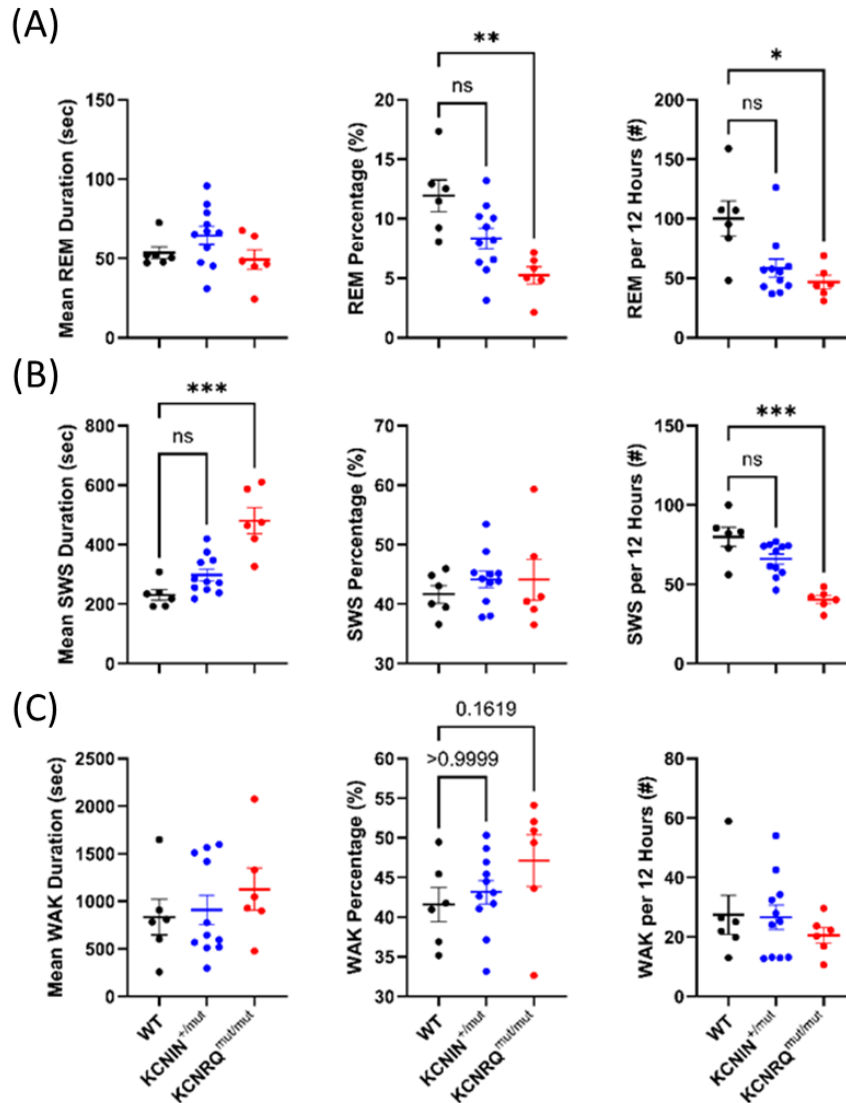


**Figure 12: Severe disruptions in sleep architecture in KCNRQ homozygous and moderate alterations in KCNIN heterozygous mutant models.** (A) REM sleep, (B) SWS, and (C) wakefulness were analyzed for mean epoch duration (left), percentage of total recording time spent in each state (middle), and number of episodes per 12-hour period (right). Homozygous KCNRQ animals exhibit significantly reduced REM percentage, increased SWS duration, and a higher percentage of time spent awake. The number of sleep episodes decreased, reflecting severe disruptions in sleep architecture. Heterozygous KCNIN animals show milder alterations, including a lower percentage of REM sleep, longer SWS episodes, and moderately decreased sleep episode frequency. Data are presented as mean  $\pm$  SEM, with statistical significance assessed using one-way ANOVA Kruskal-Wallis tests (ns = not significant, \*  $p < 0.05$ , \*\*  $p < 0.01$ , \*\*\*  $p < 0.001$ ). These results underscore the impact of KCNT1 mutations on sleep stability, with homozygous KCNRQ animals showing more profound impairments than heterozygote KCNIN.

Overall, these results underscore the significant role of KCNT1 mutations in altering sleep architecture. The severe reduction in REM percentage coupled with increased SWS duration could be an indication of compensatory regulation of network dynamics. This observation suggests a potential mechanistic link between reduced ratio of REM sleep and epileptogenesis, further emphasizing the impact of KCNT1 mutations on sleep and cortical dynamics.

### **3.4 | Genotype Effects on Development, Behavior and Cognition**

#### **3.4.1 | Impaired Development and Sensory-Motor Function**

To elucidate the impact of KCNT1 mutations on developmental and motor functions, I assessed body weight progression and somatosensory reflexes in KCNIN heterozygous and KCNRQ homozygous animals (Figure 13). Representative images of WT and KCNRQ homozygous animals revealed marked phenotypic differences, with the latter showing reduced body size and hunched posture under anesthesia (Figure 13A). Over a three-month monitoring period, both KCNIN heterozygous and KCNRQ homozygous animals gained significantly less weight compared to WT controls (Figure 13B), demonstrating a strong genotype-dependent effect on body weight development.

Somatosensory reflexes were evaluated through the righting reflex, cliff avoidance, and geotactic reflex tests (Figure 13C, E, G). Latency analyses revealed no significant differences across genotypes or sexes, except for the cliff avoidance test, where female KCNRQ homozygous animals showed significantly prolonged latencies compared to WT controls (Figure 13F). These findings suggest a moderate sex-specific impairment of sensory-motor integration in female KCNRQ homozygotes.

Overall, these results underscore a pronounced genotype effect on developmental growth in both lines and selective sensory-motor deficits in KCNRQ homozygotes.

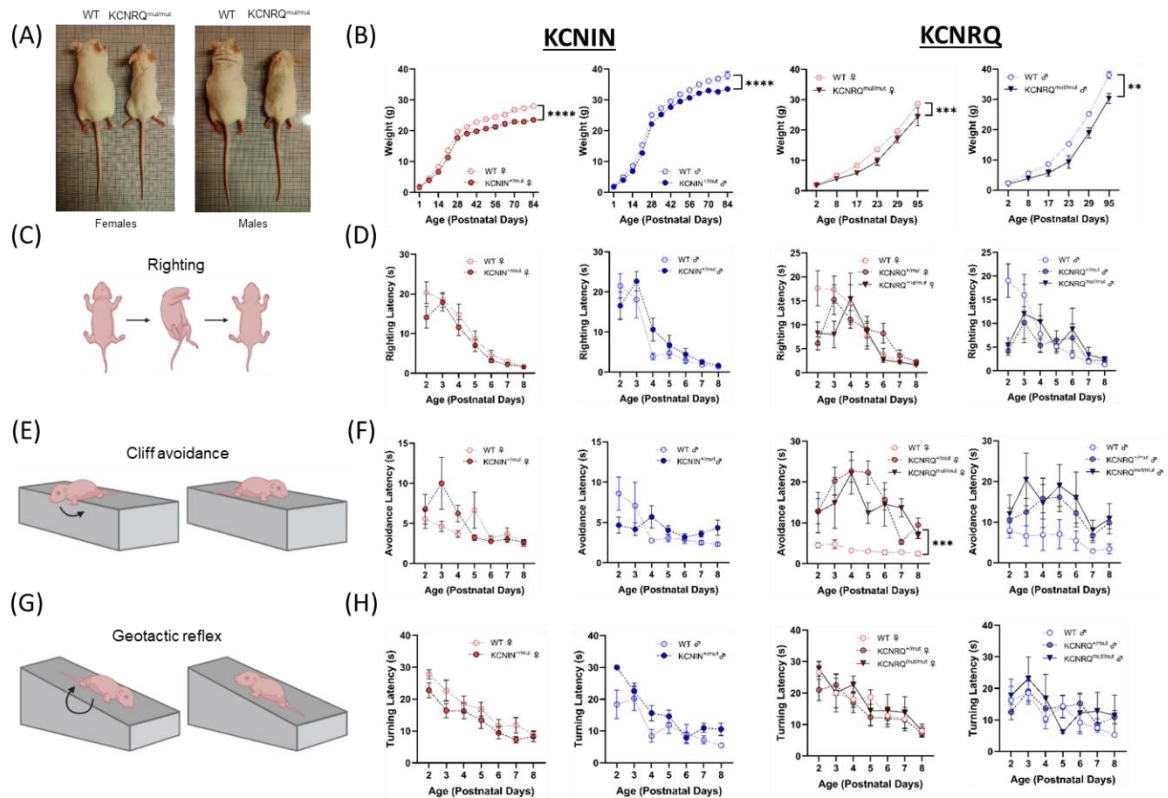


**Figure 13: Genotype-specific effects on body weight development and somatosensory reflexes in KCNIN and KCNRQ models.** (A) Representative images of WT and KCNRQ animals, highlighting phenotypic differences. (B) Body weight development over time for KCNIN heterozygous and KCNRQ homozygous animals, both monitored for three months. Both epileptic mutant models showed significantly impaired body weight development compared to WT animals, reflecting a strong genotype effect. (C, E, G) Illustrations of somatosensory reflex tests, including righting reflex (C), cliff avoidance (E), and geotactic reflex (G), which assess motor coordination and sensory-motor integration. (D, F, H) Reflex test results: latencies for righting (D), cliff avoidance (F), and geotactic reflex (H), organized by genotype and sex, with the number of animals used for all analyses shown in panel D. No significant differences in reflex performance were observed across genotypes or sexes, except for the cliff avoidance test in KCNRQ mutant animals, where significantly prolonged latencies were detected. Data are presented as mean  $\pm$  SEM, with statistical analyses performed using two-way repeated-measures ANOVA (\*\*  $p < 0.01$ , \*\*\*  $p < 0.001$ , \*\*\*\*  $p < 0.0001$ ).

### 3.4.2 | Locomotion and Habituation Deficits

To investigate the influence of KCNT1 mutations on locomotion, habituation and anxiety, open-field tests were conducted on KCNIN and KCNRQ animals (Figure 14). The experiments with KCNIN animals were conducted in collaboration with Dr. Fabio Morellini (ZMNH, Hamburg). KCNIN heterozygotes displayed significantly increased total distance moved compared to WT controls (Figure 14B), indicative of increased locomotion. Additionally, these animals exhibited sustained activity over time, reflecting impaired habituation (Figure 14C). Despite increased locomotion, no significant differences were

observed in the time spent in the center of the arena compared to WT animals, suggesting the absence of anxiety-like behavior (Figure 14D).

In contrast, KCNRQ homozygous males showed reduced total distance moved (Figure 14E) and increased thigmotaxis, spending more time near the arena walls (Figure 14G). These results indicate reduced locomotion and heightened anxiety-like behavior. Heterozygous and homozygous KCNRQ females displayed reduced habituation over time (Figure 14F) without significant anxiety-related behavior.

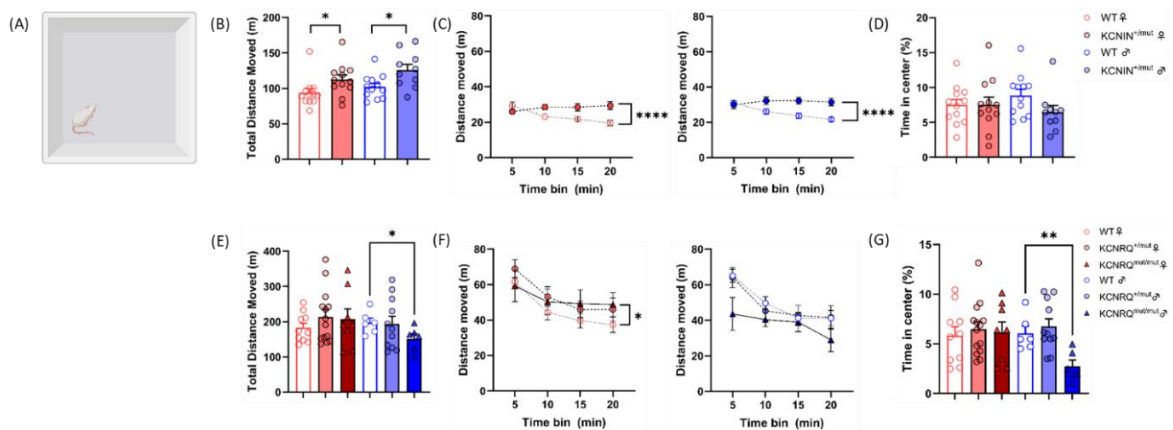


**Figure 14: Increased locomotion and impaired habituation in KCNIN animals and reduced locomotion and increased anxiety-like behavior in KCNRQ homozygous males.** (A) Schematic view of the open field test arena (created with BioRender.com). (B, C, D) KCNIN animals showed increased total distance moved (B), sustained activity over time indicating reduced habituation (C), and no significant differences in time spent in the center of the arena compared to WT (D), reflecting increased locomotion and impaired habituation without anxiety-like behavior. (E, F, G) KCNRQ homozygous males exhibited reduced total distance moved (E) and increased thigmotaxis, spending more time near the walls than in the center (G), indicating reduced locomotion and anxiety-like behavior. Heterozygous and homozygous KCNRQ females displayed reduced habituation (F) but no significant anxiety-related behavior. Statistical analyses: Mann-Whitney U test for total distance moved (B, E), two-way ANOVA for distance moved over time (C, F), and unpaired t-test for time in the center (D, G). Each dot represents an individual animal, with data presented as mean  $\pm$  SEM (note that smaller error bars may be obscured by the mean symbols). (\*  $p < 0.05$ , \*\*  $p < 0.01$ ).

### 3.4.3 | Reduced Anxiety-Like Behavior

To further evaluate anxiety-like behavior, Elevated Plus Maze (EPM) tests were conducted on KCNIN and KCNRQ animals (Figure 15). The assessment of KCNIN animals was performed by our collaborator, Dr. Fabio Morellini (ZMNH, Hamburg). The EPM is a widely used behavioral assay to assess anxiety-like tendencies, based on the animal's willingness to explore open and elevated spaces. KCNIN heterozygotes spent significantly more time in the open arms (OA) of the maze compared to WT controls, indicating a

reduction in anxiety-like behavior (Figure 15B). This behavior suggests that the mutation may alter the balance of exploratory drive and risk aversion in these animals.

Similarly, KCNRQ homozygotes demonstrated an even greater preference for the open arms, spending significantly more time in these areas compared to both WT and KCNRQ heterozygotes (Figure 15C). This pronounced reduction in anxiety-like behavior highlights a potential genotype-specific modulation of emotional processing and risk assessment. Interestingly, KCNRQ heterozygotes showed no significant differences in arm preference compared to WT animals, suggesting that the homozygous mutation might uniquely influence anxiety-like behavior.

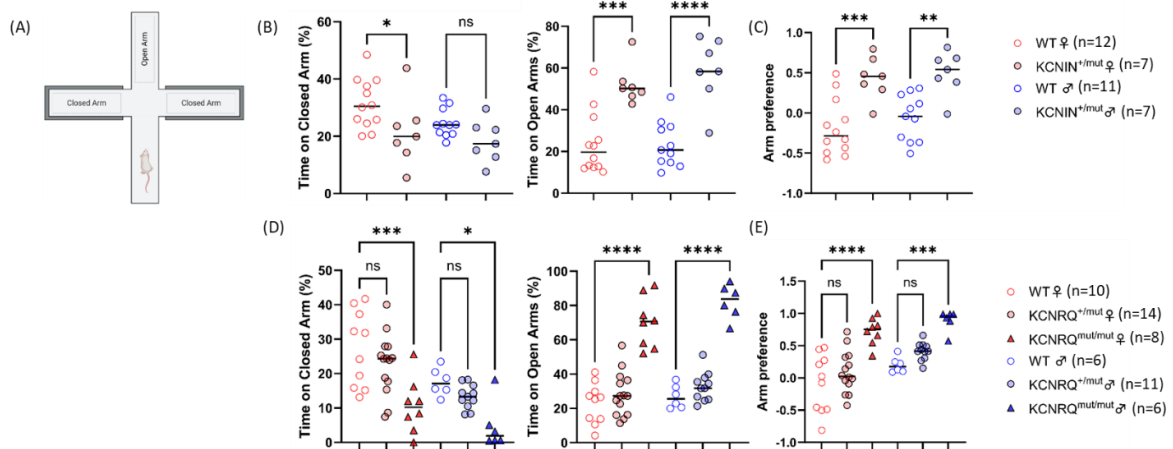


**Figure 15: Reduced anxiety-like behavior in KCNIN heterozygous and KCNRQ homozygous animals.** (A) Schematic view of the Elevated Plus Maze (EPM) with two closed arms (CA) and two open arms (OA) (created by BioRender.com). (B) Cumulative time spent in the CA and OA by KCNIN animals, with heterozygote mutants spending significantly more time in the OA compared to WT animals, indicative of reduced anxiety-like behavior. (C) Cumulative time spent in the CA and OA by KCNRQ animals, with homozygous mutants exhibiting an even stronger preference for the OA compared to WT and heterozygous animals, reflecting a pronounced reduction in anxiety-like behavior. KCNRQ heterozygous animals showed no significant differences in arm preference compared to WT animals. Arm preference values for both KCNIN and KCNRQ animals are consistent with their time allocation. Red symbols represent females, and blue symbols represent males, with filled symbols denoting mutant animals. Data are presented as mean  $\pm$  SEM, with statistical analyses performed using ordinary one-way ANOVA (ns = not significant, \*  $p < 0.05$ , \*\*  $p < 0.01$ , \*\*\*  $p < 0.001$ , \*\*\*\*  $p < 0.0001$ ).

### 3.4.4 | Working Memory Deficits

To assess working memory, Y-Maze tests were performed on KCNIN and KCNRQ animals (Figure 16). The experiments with KCNIN animals were performed by our collaborator, Dr. Fabio Morellini (ZMNH, Hamburg). The Y-Maze measures an animal's innate tendency to alternate between arms, which relies on intact working memory and spatial navigation. The

experiments conducted by our collaborator, Dr. Fabio Morellini (ZMNH, Hamburg) with KCNIN heterozygotes demonstrated preserved working memory, as their alternation percentages were comparable to WT controls (Figure 16B). However, their time per transition was significantly reduced compared to WT animals, likely reflecting their increased locomotion phenotype observed in the open field test (Figure 16C). This behavior may indicate a heightened exploratory drive rather than cognitive deficits.

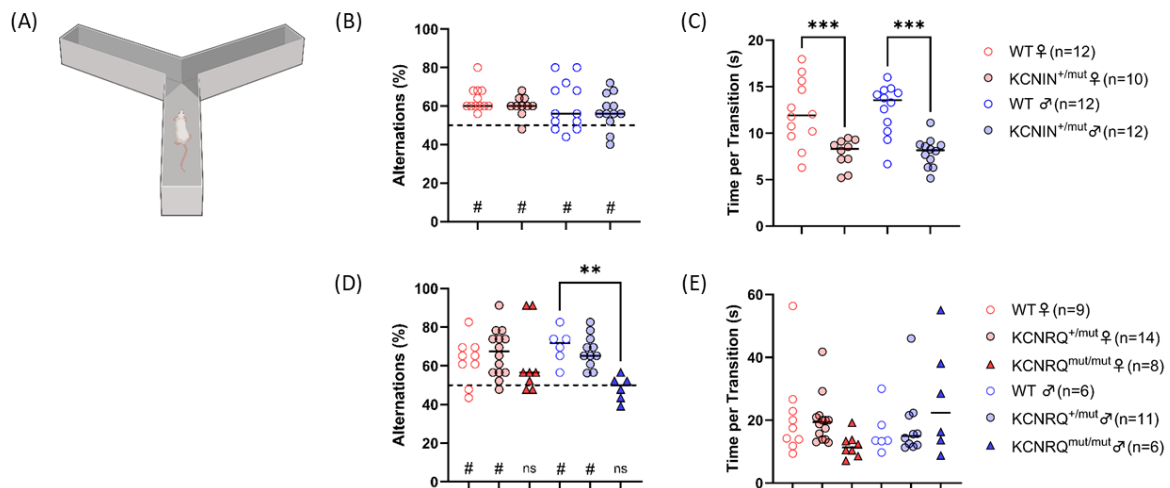


**Figure 16: KCNRQ homozygous male animals exhibit working memory impairments in the Y-Maze, while KCNIN animals maintain intact memory performance.** (A) Schematic view of the Y-Maze apparatus, used to assess working memory and the innate preference to explore novel environments. (B, C) Results for KCNIN animals: (B) Alternation percentage, showing that heterozygous mutants performed similarly to WT animals, indicating intact working memory. (C) Time per transition in seconds was significantly reduced in KCNIN heterozygous mutants compared to WT, likely due to their increased locomotion phenotype observed in the open field test. (D, E) Results for KCNRQ animals: (D) Alternation percentage showed a significant reduction in homozygous males compared to WT and heterozygotes, reflecting working memory impairments. Female homozygotes also exhibited a trend toward reduced performance, although this was not statistically significant. (E) Time per transition showed no significant differences between WT and KCNRQ mutant animals, suggesting comparable exploratory behavior. Red symbols represent females, blue symbols represent males, and filled symbols denote mutant animals. Data are presented as mean  $\pm$  SEM, with statistical analyses performed using one-way ANOVA (\*\*  $p < 0.01$ , \*\*\*  $p < 0.001$ ). For arm alternations, the test was successful when animals performed above chance level of 50 % (ns = not significant, #  $p < 0.05$ , one-sample Wilcoxon test).

In contrast, KCNRQ homozygous males exhibited significant impairments in working memory. Alternation percentages were markedly lower in homozygous males compared to both WT and KCNRQ heterozygotes, suggesting a genotype-specific disruption in cognitive function (Figure 16D). While female homozygotes showed a trend toward reduced alternation percentages, these differences were not statistically significant. Interestingly, no significant differences in time per transition were observed between KCNRQ homozygotes and WT animals, suggesting that their exploratory behavior remained unaffected (Figure

16E). These findings highlight a dissociation between exploratory activity and cognitive performance, with working memory deficits only being present in male KCNRQ homozygotes. performance, with working memory deficits only being present in male KCNRQ homozygotes.

### 3.4.5 | Intact Recognition Memory

Spatial and recognition memory were evaluated using the Object Location Memory (OLM) and Object Recognition Memory (ORM) tests (Figure 17). The OLM test assesses spatial memory by measuring an animal's preference for a displaced object, leveraging their innate curiosity. In the experiment with KCNRQ and KCNIN animals, WT animals did not exhibit a clear preference for displaced objects, which limits the reliability of conclusions regarding spatial memory in these experiments (Figure 17B-C). With the results of OLM experiments, it is not possible to draw a conclusion regarding the effect of the mutations for spatial memory in our animal models.

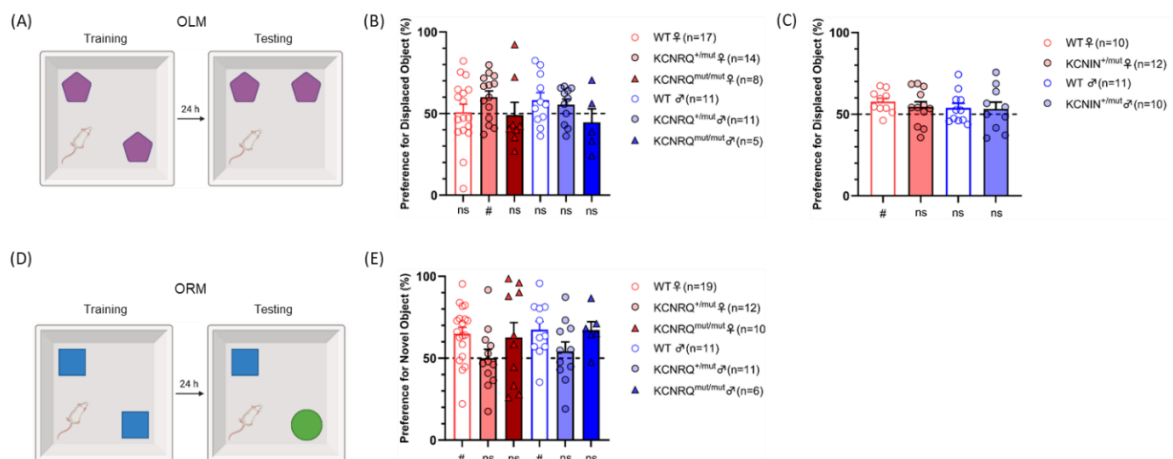


**Figure 17: Intact recognition memory in KCNRQ animals.** (A) Schematic representation of the Object Location Memory (OLM) test, which assesses spatial memory by measuring preference for displaced objects. (B, C) Preference for displaced objects in the OLM test: (B) KCNRQ animals and (C) KCNIN animals. (D) Schematic representation of the Object Recognition Memory (ORM) test, which evaluates recognition memory by measuring preference for novel objects. (E) Preference for novel objects in the ORM test for KCNRQ animals: no significant differences were observed between WT, heterozygous, and homozygous animals, indicating preserved recognition memory. The number of animals used for each experiment is depicted in brackets. Red symbols represent females, blue symbols represent males, and filled symbols denote mutant animals. Data are presented as mean ± SEM, with statistical analyses performed using one-way ANOVA. The tests were successful when animals performed above chance level of 50 % (ns = not significant, # p < 0.05, one-sample Wilcoxon test).

The ORM test is an experimental design to evaluate recognition memory in rodent models. The WT animals demonstrated a clear preference for novel objects which confirms the

reliability of the results regarding object memory assessments in the experiments conducted. KCNRQ animals which show spontaneous seizures demonstrated equal preferences for novel objects compared to WT, confirming intact recognition memory (Figure 17E). On the other hand, KCNRQ heterozygous animals demonstrated a trend towards lower preference for novel object recognition indicating an effect of the mutation on network dynamics.

The results of OLM tests point that further investigation is required to elucidate the spatial memory capabilities in these animals. The findings of ORM test are underlining the importance of dissociating the effect of mutations on the network dynamics and the occurrence of seizures.

### 3.4.6 | Impaired Long-Term Memory

Long term memory was assessed through Step-Through Passive Avoidance tests on KCNIN heterozygous and KCNRQ homozygous animals (Figure 18). This test evaluates associative learning and long-term memory by measuring the latency to enter a dark compartment where the animal previously received a mild aversive stimulus. Reduced latency to avoid the dark compartment reflects impaired memory retention.

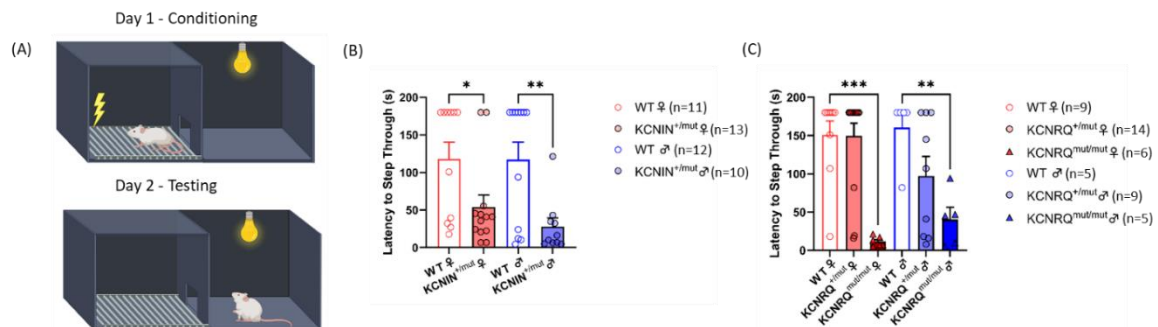


**Figure 18: Epileptic KCNIN heterozygous and KCNRQ homozygous animals exhibit impaired memory in the Step-Through Passive Avoidance Test.** (A) Schematic representation of the Step-Through Passive Avoidance apparatus, used to assess learning and memory by measuring the latency to enter the dark compartment after receiving an aversive stimulus. (B) Latency to step through into the dark compartment for KCNIN animals: heterozygous mutants exhibited significantly reduced latencies compared to WT animals, reflecting impaired memory retention. (C) Latency to step through into the dark compartment for KCNRQ animals: homozygous mutants with epileptic phenotypes showed significantly reduced latencies compared to WT animals, indicating memory impairments, while non-epileptic heterozygous animals performed similarly to WT animals. The number of animals used for each experiment is shown in brackets. Red symbols represent females, blue symbols represent males, and filled symbols denote mutant animals. Data are presented as mean  $\pm$  SEM, with statistical analyses performed using one-way ANOVA (\*  $p < 0.05$ , \*\*  $p < 0.01$ , \*\*\*  $p < 0.001$ ).

KCNIN heterozygotes exhibited significantly reduced latencies to enter the dark compartment compared to WT controls, suggesting deficits in their ability to retain the memory of the aversive stimulus (Figure 18B). Similarly, KCNRQ homozygotes with epileptic phenotypes demonstrated markedly reduced latencies compared to WT animals, indicating memory impairments (Figure 18C). Interestingly, non-epileptic KCNRQ heterozygotes performed comparably to WT controls, highlighting the potential role of seizure activity in exacerbating memory deficits.

The reduced latency times observed in the Step-Through Passive Avoidance test highlight significant impairments in memory retention in epileptic KCNIN heterozygous and KCNRQ homozygous animals. These findings emphasize the role of KCNT1 mutations in disrupting inhibitory avoidance memory, likely contributing to the observed deficits in retaining aversive experiences. The clear difference between epileptic and non-epileptic mutant animals underscores the potential influence on network dynamics responsible for memory processes in these models.

### **3.5 | Morphological Changes Associated with Epileptic Activity**

#### **3.5.1 | Altered Perineuronal Nets in the Dentate Gyrus Molecular Layer**

The hippocampus was selected as the primary focus due to its critical role in the neural circuits affected by KCNT1 mutations and its relevance to epileptic phenotypes. Specifically, perineuronal net (PNN) integrity in the dentate gyrus molecular layer was investigated due to their role in maintaining excitatory-inhibitory balance and preventing hyperexcitability by staining with Wisteria floribunda agglutinin (WFA) (Figure 19). Representative images showed increased WFA signal intensity in both KCNIN heterozygous and KCNRQ homozygous animals compared to WT controls, with KCNRQ homozygotes exhibiting the most pronounced enhancement (Figure 19A). Quantitative analysis of WFA signal intensity confirmed a significant increase in both mutant lines, with KCNRQ homozygotes showing a more severe phenotype than KCNIN heterozygotes (Figure 19B). These findings suggest that KCNT1 mutations alter PNN density, potentially stabilizing the network dynamic via increased activity of inhibitory neurons against excessive inputs from entorhinal cortex in these animals (Cabungcal et al. 2013; Wen et al. 2018).

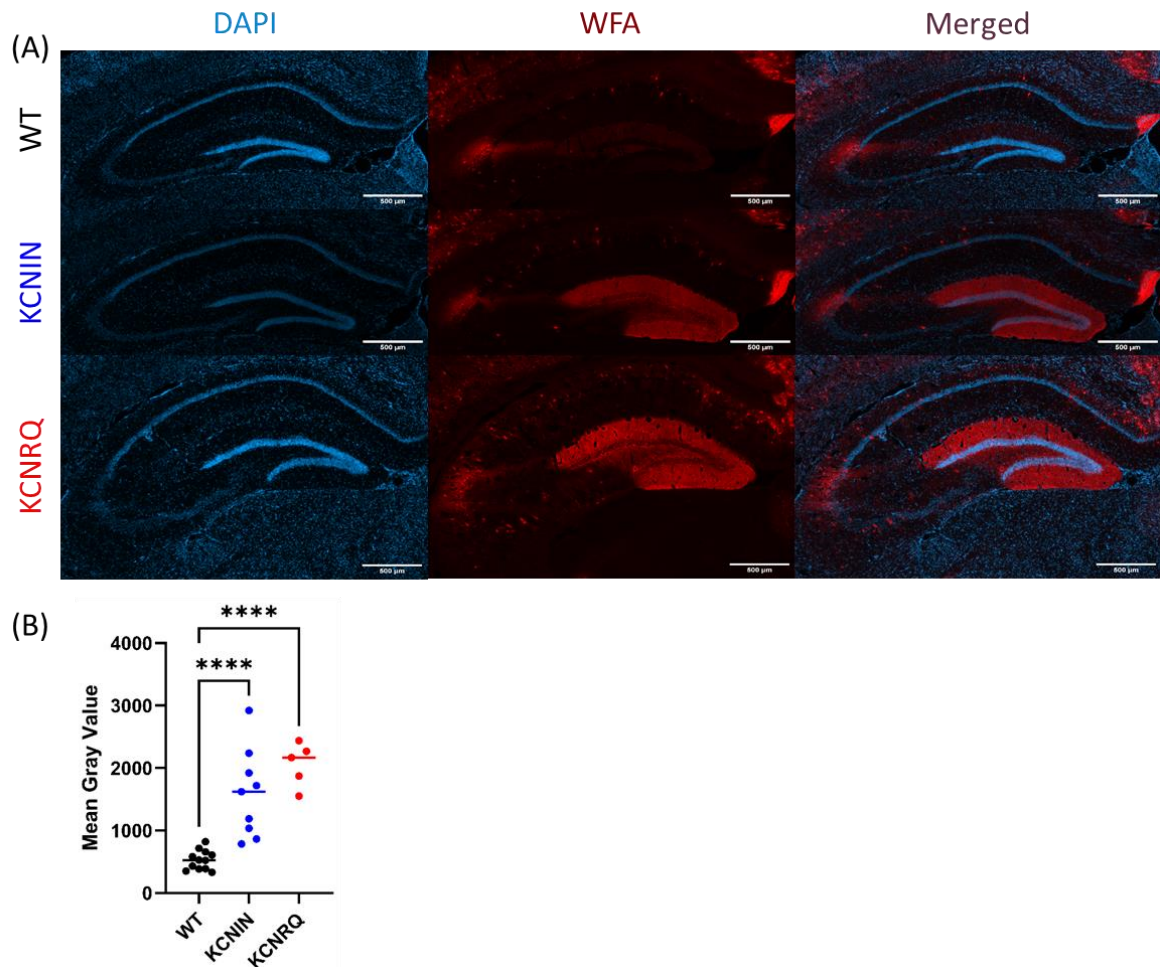


**Figure 19: Altered perineuronal nets in the dentate gyrus molecular layer, with enhanced WFA signal intensity in KCNRQ homozygous and KCNIN heterozygous animals.** (A) Example images of the dentate gyrus molecular layer stained with DAPI (first column), WFA (second column), and merged images (third column). WT images are shown in the first row, KCNIN heterozygote images in the second row, and KCNRQ homozygote images in the third row, illustrating increased WFA signal intensity in both lines. (B) Mean gray value comparisons of WFA signal intensity: both KCNIN heterozygous and KCNRQ homozygous animals exhibited increased WFA intensity compared to WT animals, with KCNRQ homozygotes showing a more severe phenotype and KCNIN heterozygotes displaying a similar but less pronounced increase. Animal numbers used for the analysis are WT (n = 12), KCNIN (n = 9), and KCNRQ (n = 5). Data are presented as mean ± SEM, with statistical analyses performed using one-way ANOVA (\*\*\*\* p < 0.0001).

### 3.5.2 | Increased NPY Expression in Mossy Fibers

Neuropeptide Y (NPY) levels were evaluated due to its role in modulating neuronal excitability and providing an anticonvulsant effect (Cattaneo et al. 2020). Increased NPY expression is often observed as a compensatory response to hyperexcitation, reflecting changes in network activity and seizure susceptibility. The analysis was performed in CA3 lucidum where the mossy fibers are extended to assess potential alterations associated with

epileptic activity (Figure 20). Representative images revealed increased NPY signal intensity in both KCNIN heterozygous and KCNRQ homozygous animals, with the most pronounced effect observed in KCNRQ homozygotes (Figure 20A).

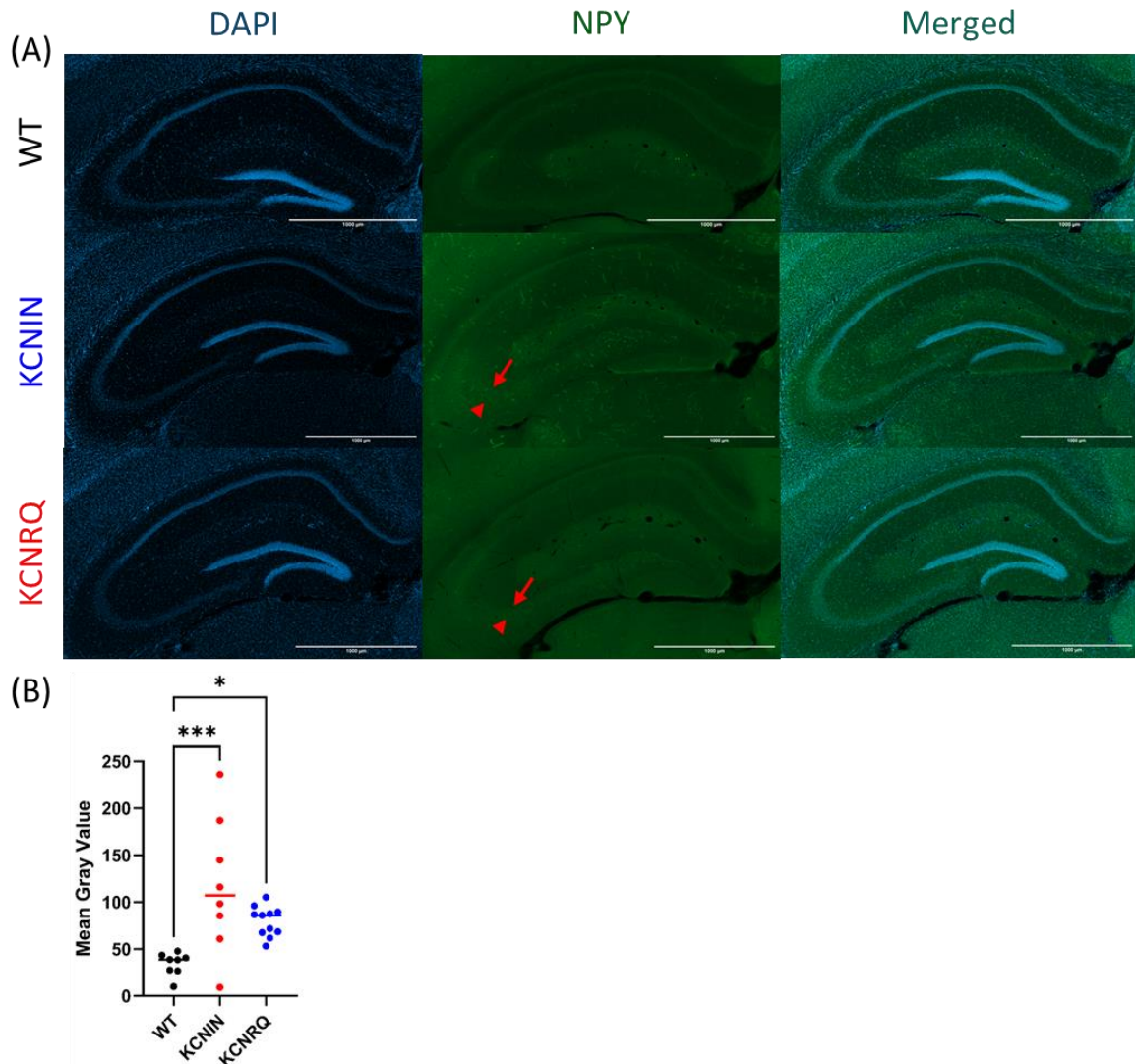


**Figure 20 Increased NPY signal intensity in the mossy fibers is pronounced in KCNRQ homozygous animals and shows higher variability in KCNIN heterozygotes.** (A) Example images of the mossy fiber region stained with DAPI (first column), NPY (second column), and merged images (third column). Red arrows indicate the location of the mossy fibers. WT images are shown in the first row, KCNIN heterozygote images in the second row, and KCNRQ homozygote images in the third row, illustrating increased NPY signal intensity in both lines. (B) Mean gray value comparisons of NPY signal intensity: while the mean signal intensity was higher in KCNIN heterozygous animals compared to WT, the effect was more pronounced in KCNRQ homozygous animals. KCNIN heterozygous animals exhibited greater individual variability in signal intensity, consistent with their broader epileptic phenotype. Animal numbers used for the analysis are WT (n = 8), KCNIN (n = 8), and KCNRQ (n = 11). Data are presented as mean  $\pm$  SEM, with statistical analyses performed using one-way ANOVA (\* p < 0.05, \*\*\* p < 0.001).

Quantitative comparisons of NPY signal intensity showed a significant increase in KCNRQ homozygotes and a milder, yet highly variable, increase in KCNIN heterozygotes compared

to WT controls (Figure 20B). These data indicate genotype-specific alterations in NPY expression, which may reflect differences in seizure frequency and severity between and within each of the two mutant lines.

### 3.5.3 | Enhanced Reactive Astrogliosis in the Hippocampus

Reactive astrogliosis was examined as an epileptic biomarker due to astrocyte activation in response to hyperexcited neurons (Hayatdavoudi et al. 2022). The histological examination was performed by staining for glial fibrillary acidic protein (GFAP) in the hippocampal region (Figure 21). Representative images demonstrated increased GFAP signal intensity in both mutant lines, with KCNRQ homozygous animals showing markedly elevated levels (Figure 21A). Quantitative analysis of GFAP signal intensity confirmed a significant increase in KCNRQ homozygotes, while KCNIN heterozygotes exhibited a trend toward higher values that did not reach statistical significance (Figure 21B). Additionally, analysis of the GFAP area fraction revealed a significant increase in KCNRQ homozygotes, indicating widespread astrogliosis, whereas KCNIN heterozygotes showed a non-significant

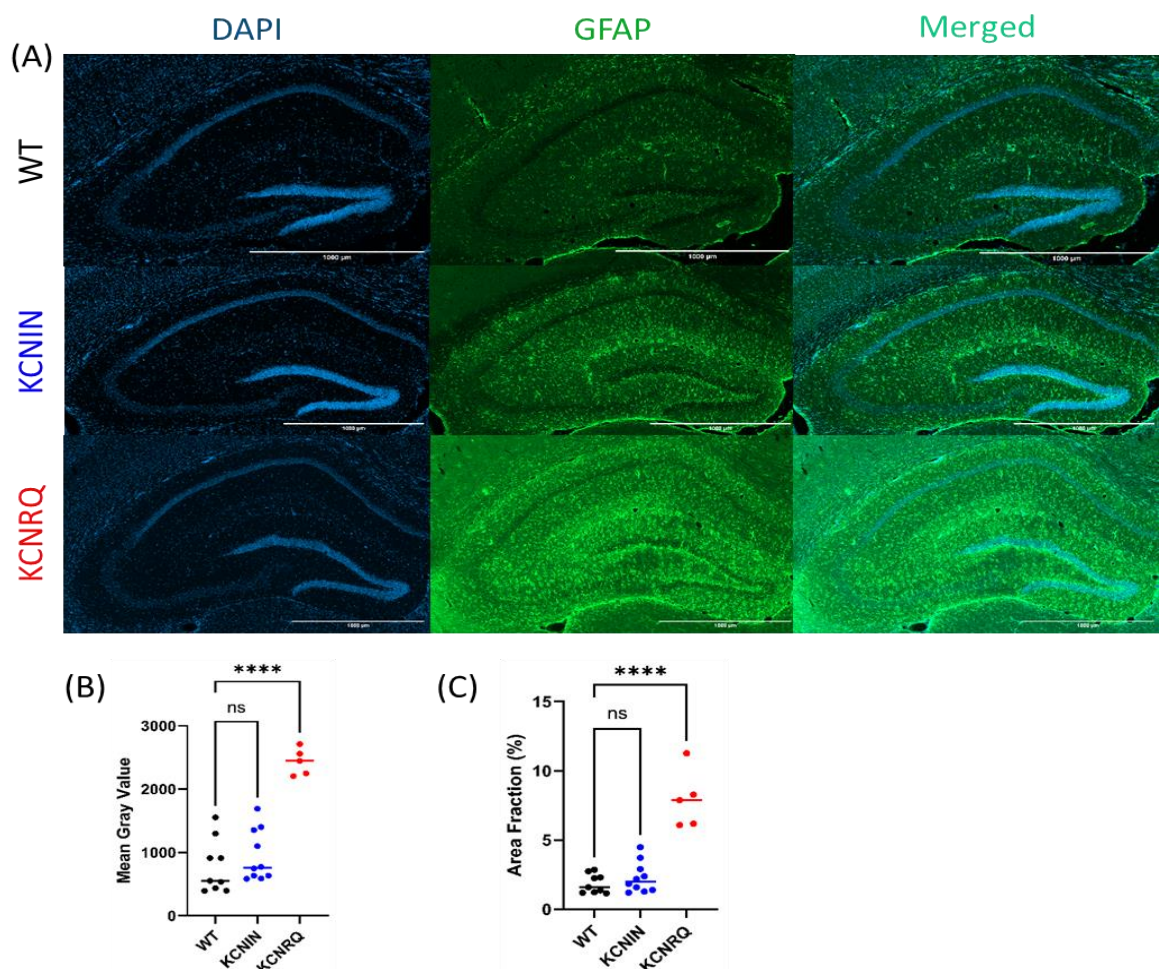


**Figure 21: Enhanced astrocytic reactivity in the hippocampal area of KCNRQ homozygous animals and a trend toward increased astrogliosis in KCNIN heterozygotes.** (A) Example images of the hippocampal area stained with DAPI (first column), GFAP (second column), and merged images (third column). WT images are shown in the first row, KCNIN heterozygote images in the second row, and KCNRQ homozygote images in the third row, illustrating increased GFAP signal intensity in mutant animals. (B) Mean gray value comparisons of GFAP signal intensity: KCNRQ homozygous animals exhibited significantly increased signal intensity compared to WT, while KCNIN heterozygous animals showed a trend toward increased values, though not statistically significant. (C) Area fraction of GFAP signal intensity for the whole hippocampal area: KCNRQ homozygous animals displayed a significant increase in the area fraction, reflecting elevated astrocytic reactivity and widespread astrogliosis. KCNIN heterozygous animals demonstrated a non-significant trend toward increased area fraction. These findings indicate heightened astrocytic reactivity in KCNRQ homozygous animals and a milder, non-significant trend in KCNIN heterozygotes. Animal numbers used for the analysis are WT (n = 9), KCNIN (n = 10), and KCNRQ (n = 5). Data are presented as mean  $\pm$  SEM, with statistical analyses performed using one-way ANOVA (ns = not significant, \*\*\*\* p < 0.0001).

trend toward increased astrocytic reactivity indicating widespread astrogliosis, whereas KCNIN heterozygotes showed a non-significant trend toward increased astrocytic reactivity.

These histological findings underscore the hippocampus as a key region affected by KCNT1 mutations, demonstrating significant morphological changes including altered PNN density, increased NPY levels, and heightened astrocytic reactivity. These alterations are reflecting the protective effect of PNN density and NPY expression as an attempt of dentate gyrus to counteract cortical excitability and the response of astrocytes against local hyperexcited neurons.

### **3.6 | Pimozide Treatment in Adult KCNT1 Mutants**

#### **3.6.1 | Pimozide Treatment in Adult KCNIN Heterozygous Animals**

The impact of pimozide treatment on seizure frequency and interictal brain oscillations was assessed in adult KCNIN heterozygous animals using telemetric ECoG recordings (Figures 22 and 23). Pimozide was administered intraperitoneally (i.p.) at a dose of 1 mg/kg in the morning and 1.5 mg/kg in the evening for 7 consecutive days, following an initial 5-day vehicle treatment phase. Seizure activity was monitored across three phases: vehicle-treated, pimozide-treated, and post-treatment washout. The seizure incidences illustrated with heat maps revealed no changes between the vehicle and pimozide treatment phases, despite achieving the targeted serum pimozide levels of 10-20 ng/ml (Figure 22A-B). Seizure

activity remained consistent during the washout phase (Figure 22C), indicating that pimoziide treatment did not reduce seizure frequency in KCNIN heterozygous animals.

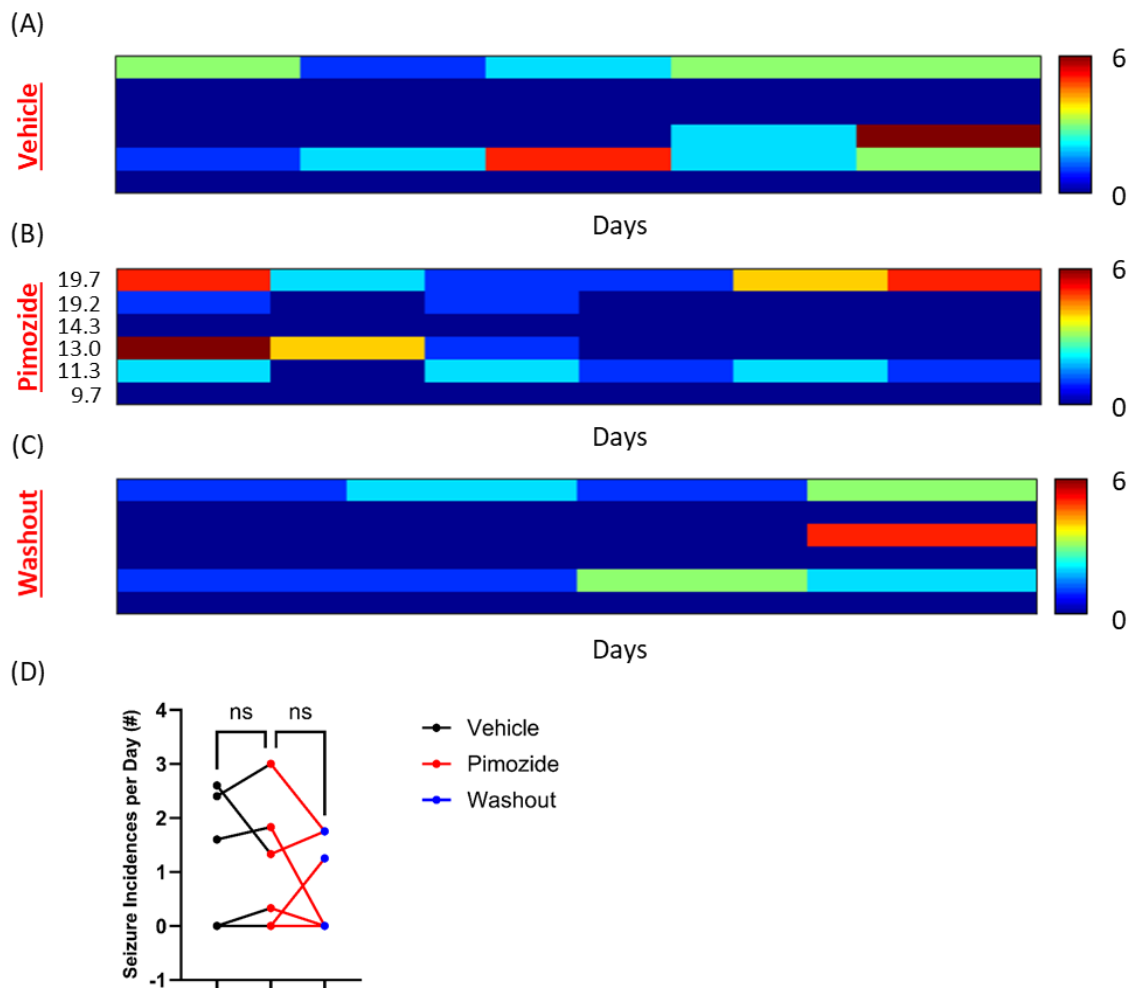


**Figure 22: Pimoziide treatment did not affect seizure incident rates in adult KCNIN heterozygous animals.** Heat maps illustrating seizure activity across treatment phases in adult heterozygous KCNIN mice (13–17 weeks old). **(A)** Vehicle-treated phase: animals received intraperitoneal (i.p.) injections of vehicle solution (5% DMSO in 0.9% NaCl) twice daily for 5 days. **(B)** Pimoziide-treated phase: animals were treated with pimoziide dissolved in the vehicle solution at doses of 1 mg/kg body weight in the morning and 1.5 mg/kg in the evening for 5 days. Numbers on the left side of the heat map indicate serum pimoziide levels (ng/ml), measured 1.5 hours after the final morning injection on the last day of treatment. **(C)** Post-treatment washout phase: animals underwent a 4-day period without injections, followed by resumption of ECoG recordings. Each column represents a recording day, and each row represents an individual animal. Warm colors represent higher seizure frequency, while colder colors represent lower seizure frequency. **(D)** The average seizure incidences per day for each group. Despite achieving the targeted serum pimoziide levels, treatment did not alter seizure frequency compared to the vehicle phase. Seizures remained consistent during the washout phase as well. Statistical analysis was performed using one-way ANOVA Kruskal-Wallis tests (ns = not significant).

PSD analysis was performed to investigate the effects of pimoziide on interictal brain oscillations during REM sleep, SWS, and wakefulness (Figure 23). The PSD plots showed no changes in oscillatory power across theta, beta, and low gamma frequency bands during

any of the treatment phases (Figure 23A). Individual trends depicted by scatter plots further confirmed the absence of treatment-induced changes in oscillatory frequencies and power values for theta, beta, and low gamma oscillations (Figure 23B–D). Statistical analysis revealed no significant differences across phases, suggesting that chronic pimoizide treatment did not affect interictal dynamics regarding the power and frequency of oscillation in KCNIN heterozygote animals. On the other hand, the contingency analysis performed for the

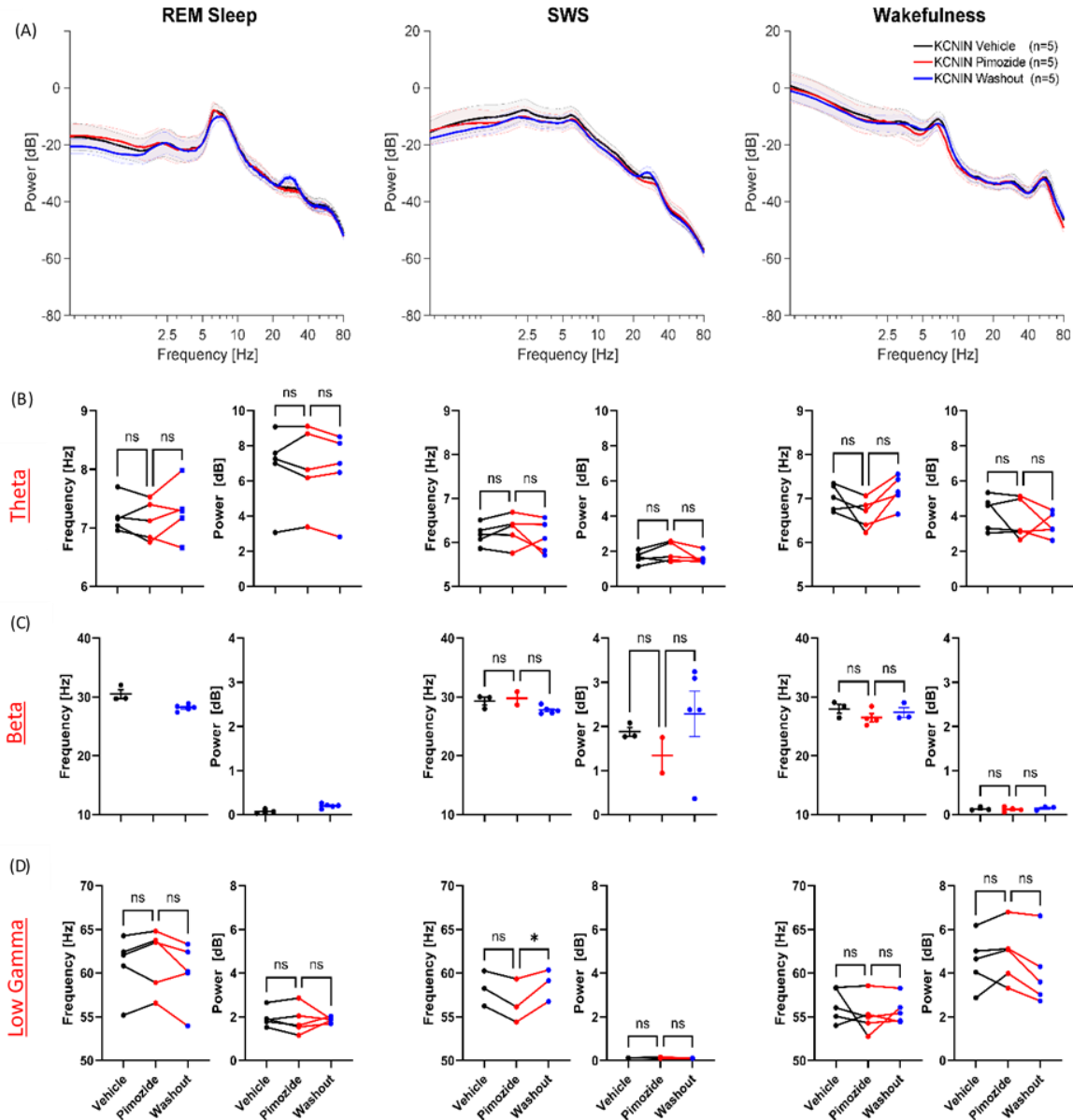


**Figure 23 Chronic pimoizide treatment normalized the aberrant beta oscillations during REM sleep in adult KCNIN heterozygous animals.** (A) Power spectral density (PSD) plots showing power (dB) and frequency (Hz) for KCNIN heterozygous animals during REM sleep, SWS, and wakefulness across treatment phases. Shaded areas represent mean  $\pm$  SEM, with the number of animals indicated in the legend. (B–D) Scatter plots for theta (B), beta (C), and low gamma (D) oscillations, showing frequency peaks and corresponding power values for REM sleep (left column), SWS (middle column), and wakefulness (right column). Each dot represents an individual animal, with  $\pm$  SEM plotted. Statistical analysis was performed using one-way ANOVA Kruskal-Wallis tests (ns = not significant, \*  $p < 0.05$ ).

occurrences of beta oscillations during REM sleep revealed a significant dependence of beta occurrence from genotype (Chi-square test,  $p=0.006$ ). The absence of aberrant beta oscillations might indicate a treatment effect on the severity of epileptic activity.

### 3.6.2 | Pimozide Treatment in Adult KCNRQ Homozygous Animals

Seizure frequency and interictal oscillatory activity were evaluated in KCNRQ homozygous animals using telemetric ECoG recordings across vehicle, pimozide, and washout phases (Figures 24 and 25). Pimozide was administered intraperitoneally at a dose of 1.5 mg/kg in the morning and 2 mg/kg in the evening for 7 consecutive days, following an initial 5-day vehicle treatment phase. Heat maps demonstrated no significant differences in seizure frequency between the vehicle and pimozide treatment phases, despite achieving therapeutic serum pimozide levels (Figure 24A, B). Seizure activity remained stable during the washout phase as well (Figure 24C), indicating that pimozide treatment failed to reduce seizure frequency in KCNRQ homozygous animals (Figure 24D).

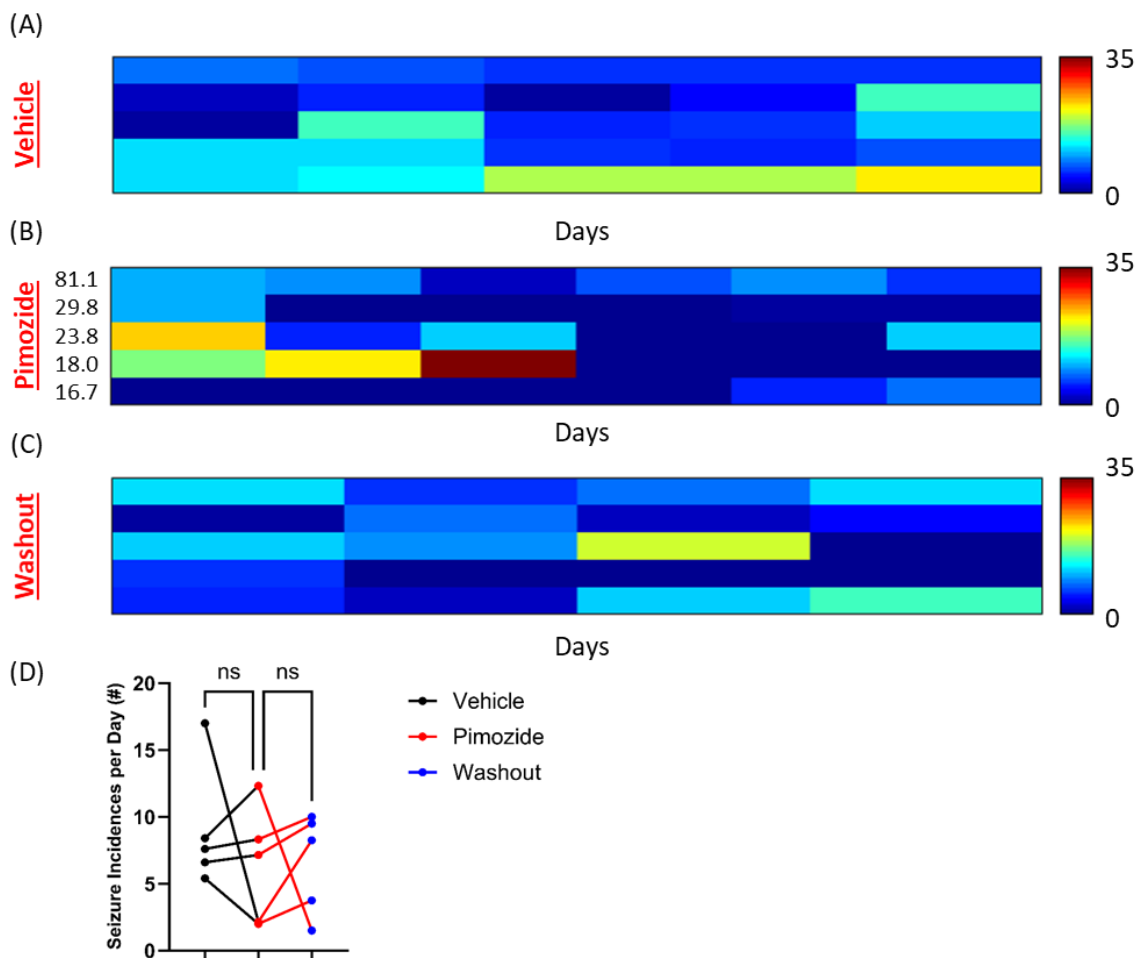


**Figure 24: Pimozide treatment did not affect seizure frequency in adult KCNRQ homozygous animals.** Heat maps illustrating seizure activity across treatment phases in adult homozygous KCNRQ mice (14–18 weeks old). **(A)** Vehicle-treated phase: animals received intraperitoneal (i.p.) injections of vehicle solution (5% DMSO in 0.9% NaCl) twice daily for 5 consecutive days. **(B)** Pimozide-treated phase: animals were treated with pimozide dissolved in the vehicle solution at doses of 1.5 mg/kg body weight in the morning and 2 mg/kg in the evening for 7 days. Numbers on the left side of the heat map indicate serum pimozide levels (ng/ml), measured 1.5 hours after the final evening injection on the last day of treatment. **(C)** Post-treatment washout phase: animals underwent a 7-day period without injections, followed by resumption of ECoG recordings to assess post-treatment neural activity. Each column represents a recording day, and each row represents an individual animal. Warm colors represent higher seizure frequency, while colder colors represent lower seizure frequency. **(D)** The average seizure incidences per day for each group. Despite achieving the targeted serum pimozide levels, treatment did not alter seizure frequency compared to the vehicle phase. Seizure activity remained consistent during the washout phase as well. Statistical analysis was performed using one-way ANOVA Kruskal-Wallis tests (ns = not significant).

PSD analysis was performed to investigate the effects of pimozide on interictal brain oscillations in KCNRQ homozygous animals during REM sleep, SWS, and wakefulness (Figure 25). The PSD plots showed no changes in oscillatory power across theta, beta, and low gamma frequency bands during any of the treatment phases (Figure 25A). Individual trends depicted by scatter plots further confirmed the absence of treatment-induced changes in oscillatory frequencies and power values for theta, beta, and low gamma oscillations (Figure 25B–D). Statistical analysis revealed no significant differences across phases, suggesting that chronic pimozide treatment did not affect interictal oscillatory dynamics in KCNRQ homozygous animals. The contingency analysis performed for the occurrences of beta oscillations during REM sleep revealed no significant dependence of beta occurrence from genotype (Chi-square test,  $p=0.99$ ).

Together, these results demonstrate that pimozide treatment in adult KCNT1 mutant models does not mitigate seizure incidence rate or alter interictal oscillatory activity, underscoring its limited efficacy in rescuing the epileptic phenotype.

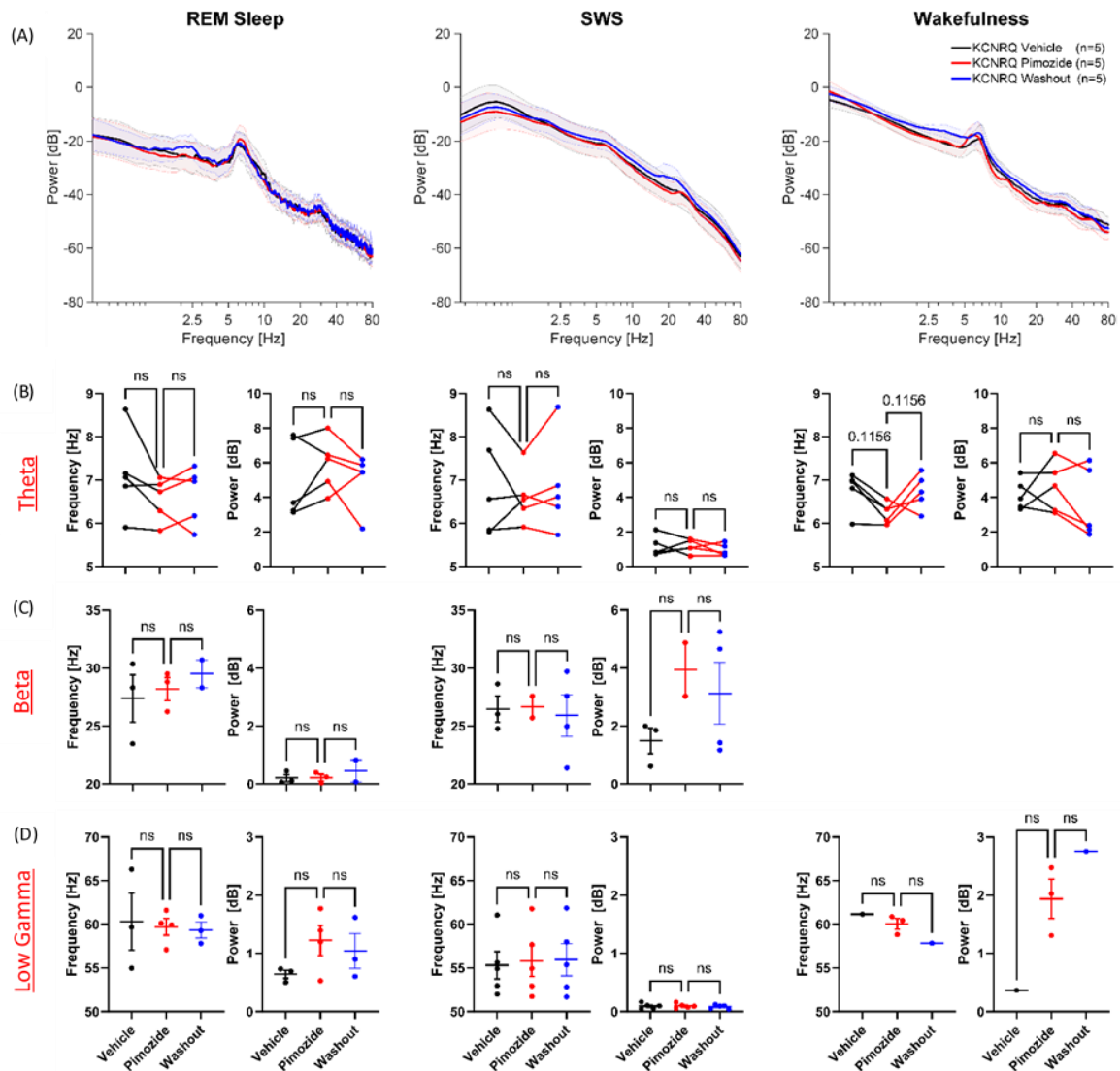


**Figure 25: Chronic pimoziide treatment did not alter interictal oscillations in adult KCNRQ homozygous animals.** (A) Power spectral density (PSD) plots for REM sleep, SWS, and wakefulness in KCNRQ homozygous animals during interictal periods, illustrating oscillatory power distribution across frequency bands. Shaded areas represent mean  $\pm$  SEM, with the number of animals indicated in the legend. (B–D) Scatter plots for theta (B), beta (C), and low gamma (D) oscillations, showing frequency peaks and corresponding power values for REM sleep (left column), SWS (middle column), and wakefulness (right column). Each dot represents an individual animal, with  $\pm$  SEM plotted. Statistical analysis was performed using one-way ANOVA Kruskal-Wallis tests (ns = not significant).

### 3.7 | Carvedilol Treatment in Adult KCNIN Mutants

The effects of chronic carvedilol treatment on seizure frequency were assessed in adult KCNIN heterozygous animals using telemetric ECoG recordings (Figure 26). Seizure activity was monitored across four phases: vehicle-treated, first carvedilol treatment, second carvedilol treatment, and post-treatment washout. Carvedilol was continuously delivered via subcutaneously implanted Alzet® Osmotic Pumps, with a daily dosage of 8 mg/kg body

weight. Heat maps of seizure frequency showed no significant changes between the vehicle and carvedilol treatment phases (Figure 26A–C). Seizure activity remained consistent during the washout phase as well (Figure 26D). These results indicate that carvedilol treatment did not reduce seizure frequency in adult KCNIN heterozygous animals.

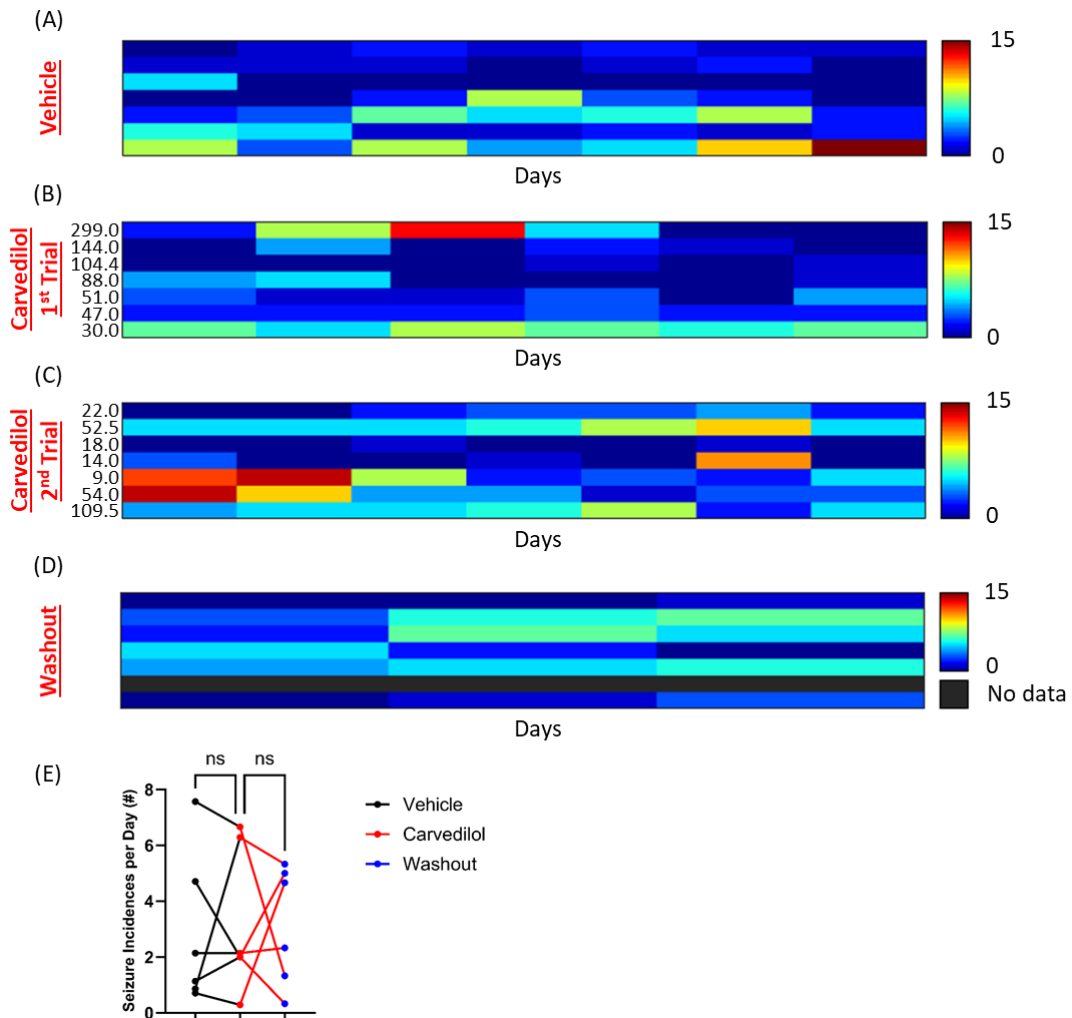


**Figure 26: Chronic carvedilol treatment did not affect seizure frequency in adult KCNIN heterozygous animals.** Heat maps illustrating seizure frequency across treatment phases in adult heterozygous KCNIN mice (12–17 weeks old) treated with carvedilol via subcutaneously implanted Alzet© Osmotic Pumps. **(A)** Vehicle-treated phase: seizure activity during baseline recordings, with pumps delivering vehicle solution (20% hydroxypropyl- $\beta$ -cyclodextrin in 1% glacial acetic acid). **(B)** First carvedilol treatment phase: pumps delivered carvedilol at 8 mg/kg body weight daily, with serum carvedilol levels (ng/mL) indicated on the left side of the heat map. **(C)** Second carvedilol treatment phase: an additional carvedilol treatment was conducted after optimizing the solution, with serum drug levels (ng/mL) shown on the left side of the heat map. **(D)** Washout phase: seizure activity recorded over 3 days following a 3-day period without drug administration. Each column represents a recording day, and each row represents an individual animal. Warm colors indicate higher seizure frequency, while colder colors represent lower seizure frequency. **(E)** The average seizure incidences per day for each group. For Carvedilol group, the 2<sup>nd</sup> trial seizure rate was considered due to targeted therapeutic range except the fifth animal which has a lower serum level than the 1<sup>st</sup> trial. Despite continuous carvedilol delivery and achieving serum drug levels, no significant changes in seizure frequency were observed during or after treatment in adult KCNIN heterozygous animals. Statistical analysis was performed using one-way ANOVA Kruskal-Wallis tests (ns = not significant).

To investigate whether carvedilol influences cortical activity, PSD analysis was performed on ECoG recordings during REM sleep, SWS, and wakefulness (Figure 27). PSD plots revealed no significant differences in oscillatory power across theta, beta, and low gamma frequency bands during or after carvedilol treatment (Figure 27A). Scatter plots of oscillatory frequencies and power values confirmed the absence of treatment-induced changes in cortical activity across all phases (Figure 27B–D). Statistical analysis using one-way ANOVA Kruskal-Wallis tests showed no significant differences, suggesting that chronic carvedilol administration did not alter interictal oscillatory dynamics in KCNIN heterozygous animals. Furthermore, the contingency analysis performed for the occurrences

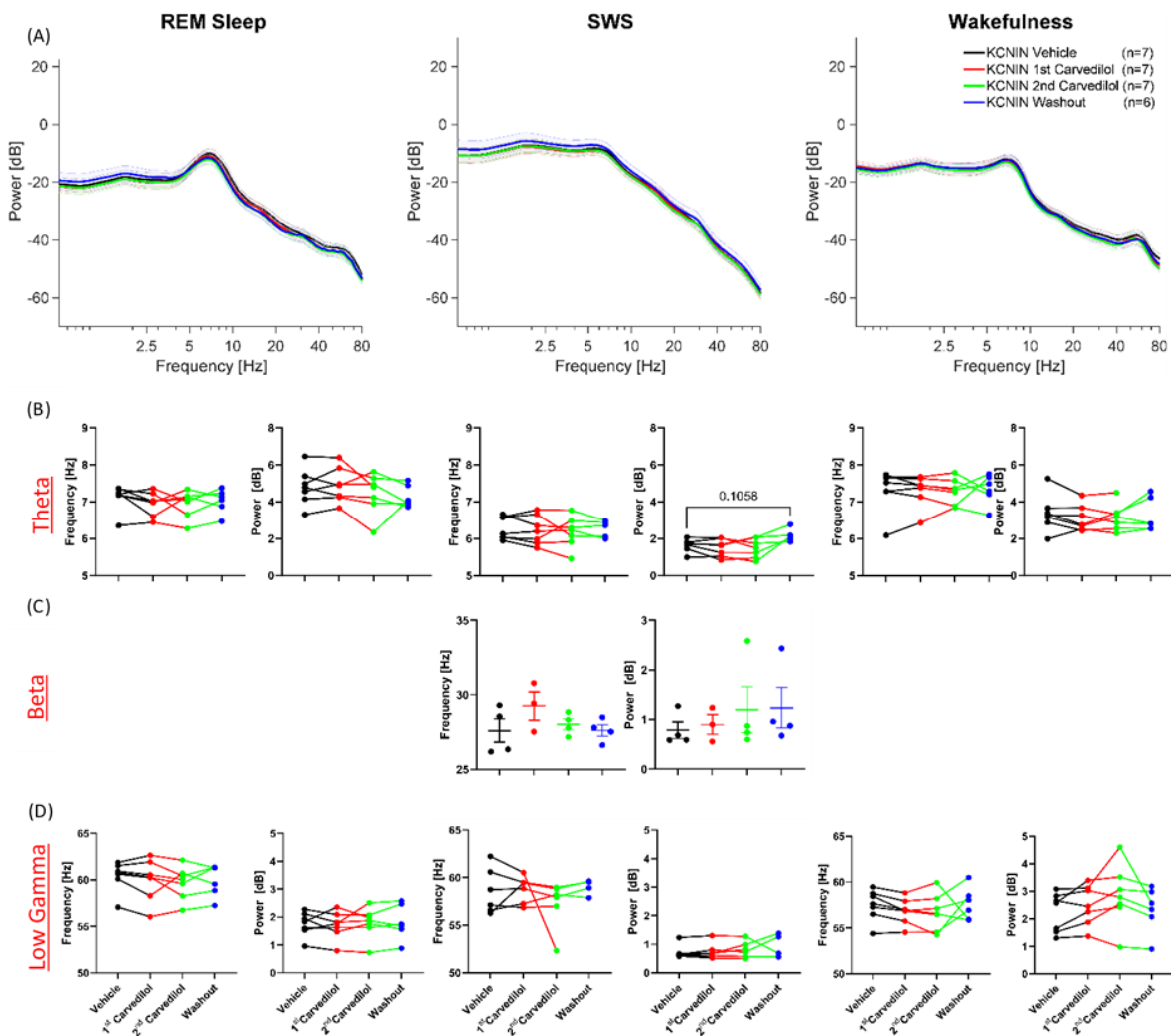


**Figure 27: Chronic carvedilol treatment did not alter interictal oscillations in adult KCNIN heterozygous animals.** (A) Power spectral density (PSD) plots for REM sleep, SWS, and wakefulness, illustrating oscillatory power distribution across frequency bands. Shaded areas represent mean  $\pm$  SEM, with the number of animals indicated in the legend. (B–D) Scatter plots for theta (B), beta (C), and low gamma (D) oscillations, showing frequency peaks and corresponding power values for REM sleep (left column), SWS (middle column), and wakefulness (right column). Each dot represents an individual animal, with  $\pm$  SEM plotted. Statistical analysis was performed using one-way ANOVA Kruskal-Wallis tests. Despite chronic carvedilol administration, interictal oscillations showed no significant changes during or after treatment.

of beta oscillations during SWS sleep revealed no significant dependence of beta occurrence from genotype (Chi-square test,  $p=0.86$ ).

Together, these results demonstrate that carvedilol treatment in adult KCNIN heterozygous animals has no effect on seizure frequency or cortical activity, underscoring its limited efficacy in mitigating the epileptic phenotype.

### **3.8 | Preventive Carvedilol Treatment in Neonatal KCNIN Mutants**

Epileptic encephalopathies associated with KCNT1 mutations typically manifest in human infants around three months of age. Early diagnosis and intervention are essential for preventing the progression of these severe disorders. However, genetic tests, which could enable earlier diagnosis, are not routinely performed for every newborn, and their availability remains limited in many regions. Consequently, diagnosis often occurs only after the onset of clinical symptoms. Given this challenge, neonatal carvedilol treatment was investigated in a mouse model, with administration beginning at postnatal day 7 (P7). This time point was chosen because P7 represents a critical developmental period for interneurons in mice and corresponds to the late prenatal stage in human brain development. By intervening during this sensitive window, the study aimed to evaluate whether early pharmacological treatment could prevent seizure onset and mitigate associated cortical excitability. The preventive study in neonatal KCNIN heterozygous animals were conducted together with Nele Bohne in the framework of her master's thesis (Thesis 2023).

#### **3.8.1 | Positive Effects of Early Carvedilol Treatment on Seizures and Cortical Excitability**

Neonatal carvedilol treatment was assessed for its potential to prevent seizures and modulate cortical excitability in juvenile KCNIN heterozygous animals (Figures 28 and 29). Carvedilol was administered via intraperitoneal injections from postnatal day 7 (P7) to P21, followed by chow embedding from P21 to P35, ensuring consistent drug delivery during critical developmental periods. Representative ECoG recordings highlighted spontaneous seizure activity in vehicle-treated animals, whereas carvedilol-treated animals demonstrated reduced seizure frequency (Figure 28A, B). Statistical analysis of seizure-free ratios using

Kaplan-Meier survival analysis showed a significantly higher proportion of seizure-free animals in the carvedilol-treated group compared to vehicle-treated controls (\* $p < 0.05$ ; Figure 28C). These findings suggest that carvedilol can effectively reduce seizure onset in a subset of juvenile KCNIN heterozygotes, likely by modulating early neural excitability.

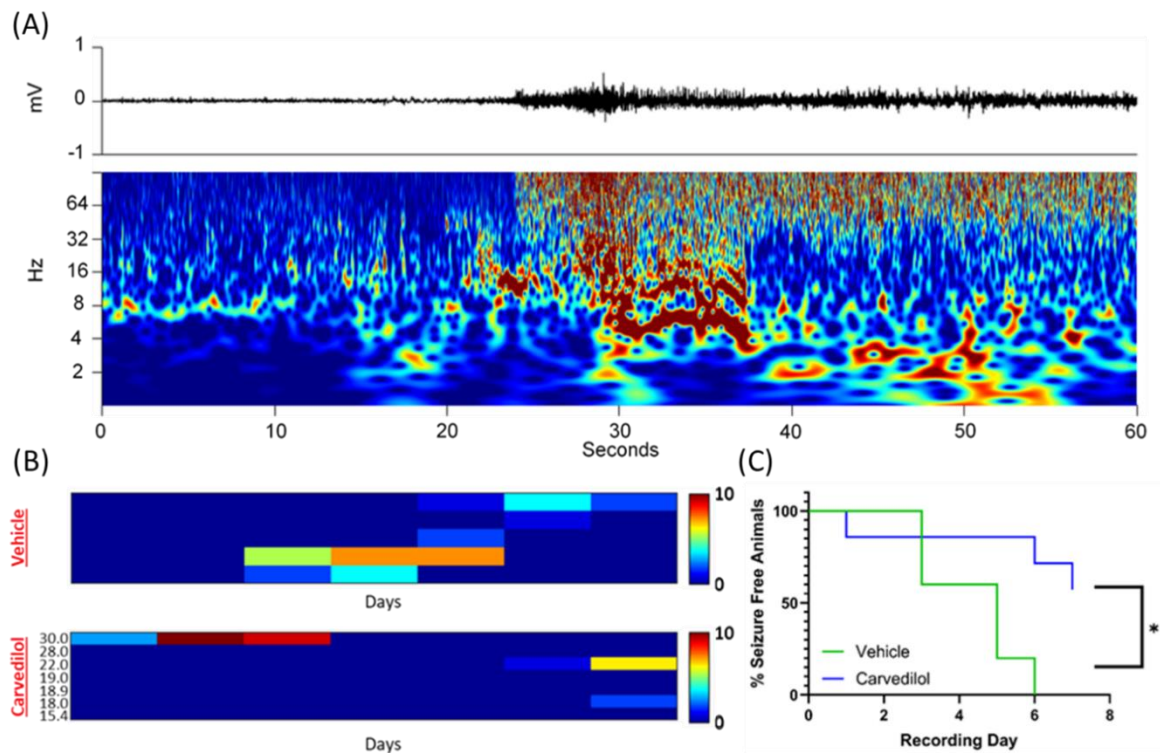


**Figure 28: Early carvedilol treatment prevents seizures in a subset of juvenile KCNIN heterozygous animals.** (A) Representative example of a spontaneous seizure event in a juvenile KCNIN heterozygous animal. Top: Raw ECoG signal in mV of seizure activity. Bottom: Time-frequency wavelet spectrogram showing the power distribution across time and frequencies. (B) Heatmaps illustrating seizure frequency in juvenile KCNIN animals treated with vehicle (upper heatmap) and carvedilol (lower heatmap). Carvedilol was administered via intraperitoneal injections from postnatal day 7 (P7) to P21 (pre-weaning phase) and through chow embedding from P21 to P35 (post-weaning phase). Serum carvedilol levels (ng/mL) at the end of the treatment are shown on the left side of the carvedilol heatmap. Each column represents a recording day, and each row represents an individual animal. (C) Ratio of seizure-free animals during the ECoG recording period: carvedilol-treated animals showed a higher proportion of seizure-free animals compared to vehicle-treated animals, indicating that starting treatment at an earlier age effectively prevented seizures in a subset of animals. Statistical analysis was performed using Kaplan-Meier survival analysis (\* $p < 0.05$ ). These results highlight a potential benefit of early carvedilol treatment in mitigating seizure onset in neonatal KCNIN heterozygous animals.

Cortical excitability was further analyzed through PSD measurements during REM sleep, SWS, and wakefulness (Figure 29). While the PSD plots revealed no statistically significant differences across groups, there was a notable trend toward increased aperiodic exponent

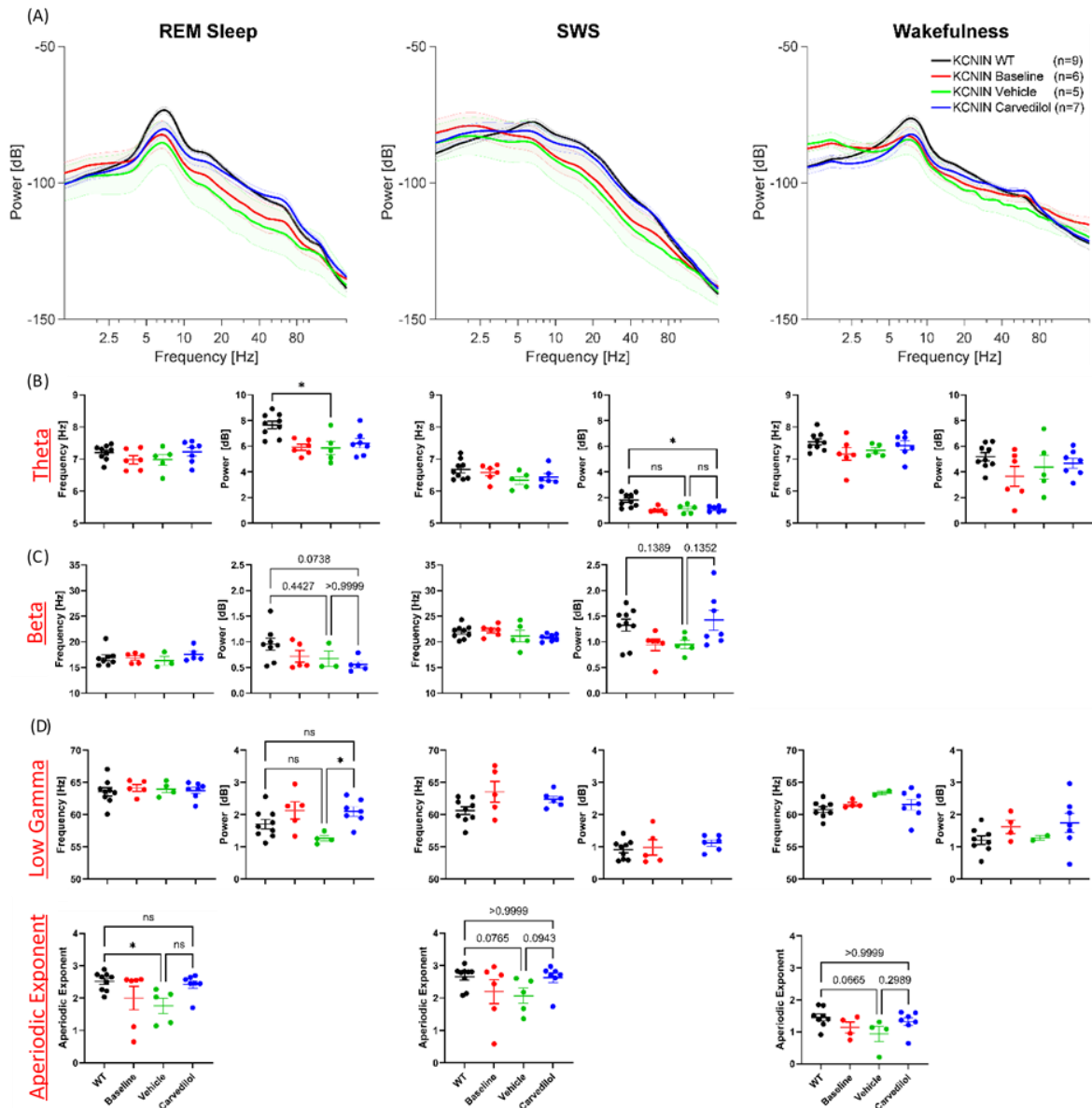


**Figure 29: Early carvedilol treatment shows a trend toward reduced cortical excitability in juvenile KCNIN heterozygous animals.** (A) Power spectral density (PSD) plots for REM sleep, SWS, and wakefulness, illustrating oscillatory power distribution across frequency bands. Shaded areas represent mean  $\pm$  SEM, with the number of animals indicated in the legend. (B–D) Scatter plots for theta (B), beta (C), and low gamma (D) oscillations, showing frequency peaks and corresponding power values for REM sleep (left column), SWS (middle column), and wakefulness (right column). (E) Aperiodic exponent across brain states, reflecting cortical excitability: carvedilol-treated animals showed a trend toward increased aperiodic exponent values at each brain state compared to vehicle-treated animals, suggesting a potential decrease in cortical excitability. Each dot represents an individual animal, with mean  $\pm$  SEM plotted. Statistical analysis was performed using one-way ANOVA Kruskal-Wallis tests (ns = not significant, \*  $p < 0.05$ ). These findings indicate a trend toward a positive treatment effect of early carvedilol in reducing cortical excitability in juvenile KCNIN heterozygous animals.

values in carvedilol-treated animals, indicating a possible reduction in cortical excitability (Figure 29A, E). Scatter plots for theta, beta, and low gamma oscillations similarly showed consistent patterns across treatment phases (Figure 29B–D). Furthermore, the contingency analysis performed for the occurrences of beta oscillations during REM sleep revealed no significant dependence of beta occurrence from genotype (Chi-square test,  $p=0.69$ ). Together, these data suggest that early carvedilol treatment may exert subtle but positive effects on cortical network dynamics.

### 3.8.2 | Mild Sleep Architecture Alterations Unaffected by Carvedilol Treatment

Sleep architecture was evaluated by analyzing key metrics, including mean episode duration, percentage of total recording time spent in each state, and episode frequency for REM sleep, SWS, and wakefulness in juvenile KCNIN heterozygous animals (Figure 30). Compared to

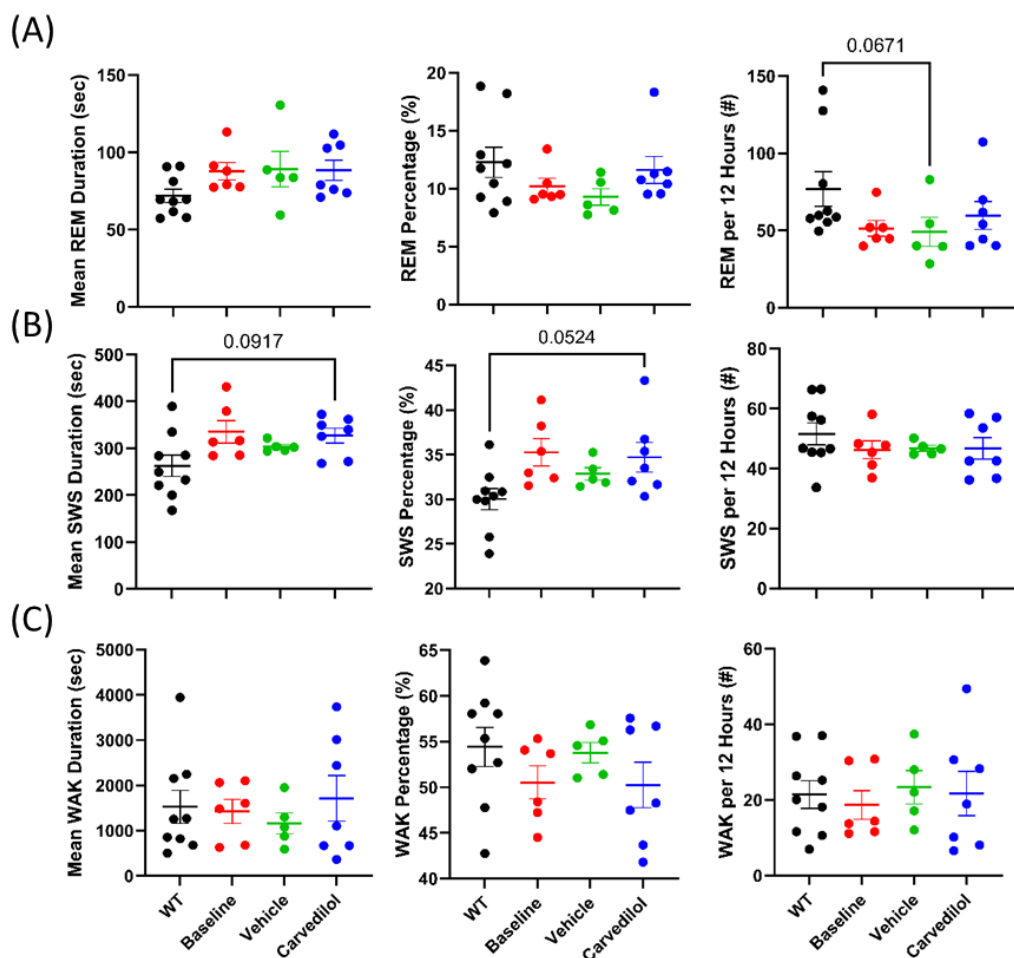


**Figure 30: Mild alterations in sleep architecture in juvenile KCNIN heterozygous animals with no significant effect of carvedilol treatment.** (A) REM sleep, (B) SWS, and (C) wakefulness were analyzed for mean episode duration (left), percentage of total recording time spent in each state (middle), and number of episodes per 12-hour period (right). Juvenile KCNIN heterozygous animals exhibited mild alterations in sleep architecture compared to WT animals, including increased mean REM duration and slightly higher percentage of SWS episodes, but these differences were not statistically significant. Carvedilol treatment did not result in any significant changes in sleep metrics for mutant animals. Data are presented as mean  $\pm$  SEM. Statistical significance was assessed using one-way ANOVA. Animal numbers used for analysis: WT (n = 9), non-treated KCNIN (n=6), vehicle-treated KCNIN (n = 5), and carvedilol-treated KCNIN (n = 7).

WT animals, mutant animals exhibited mild alterations such as increased mean REM duration and a slightly higher percentage of SWS episodes. However, these differences did not reach statistical significance. Carvedilol-treated animals showed sleep patterns similar to non-treated and vehicle-treated animals, indicating that neonatal carvedilol administration did not significantly affect sleep architecture. These findings suggest that sleep architecture was not altered in juvenile KCNIN heterozygous animals and carvedilol treatment does not change it.

### 3.8.3 | Reduction in Anxiety-Like Behavior Following Carvedilol Treatment

Carvedilol's effects on anxiety-like behavior were evaluated using the open field test (Figure 31). This test measures locomotor activity and anxiety levels based on exploratory behavior. Total distance moved and activity patterns over time revealed no significant differences in locomotion between carvedilol-treated, vehicle-treated, and non-treated animals (Figure

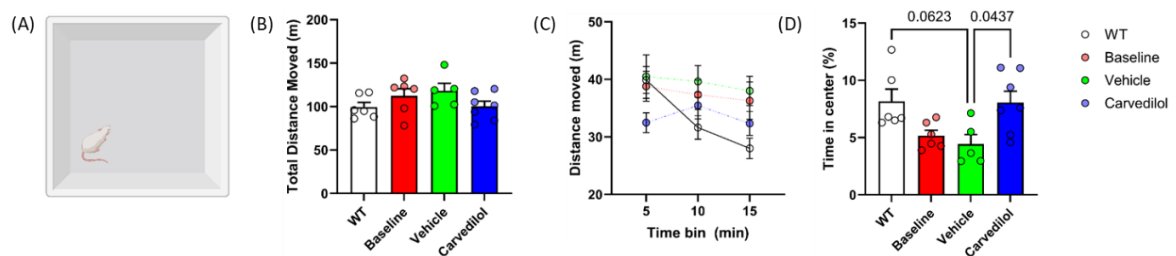


**Figure 31: Carvedilol treatment reduces anxiety-like behavior in juvenile KCNIN heterozygous animals.** (A) Schematic view of the open field test arena (created with BioRender.com). (B) Total distance moved (m) over a 15-minute session, comparing WT (n = 6), non-treated KCNIN (n = 6), vehicle-treated KCNIN (n = 5), and carvedilol-treated KCNIN (n = 7) heterozygous juvenile animals. No significant differences in locomotion were observed between groups. (C) Distance moved per 5-minute time bin, illustrating activity patterns over time and reflecting habituation. Non-treated and vehicle-treated animals did not exhibit habituation, regardless of carvedilol treatment. (D) Percentage of time spent in the center of the arena, indicative of anxiety-like behavior. Non-treated and vehicle-treated animals showed increased anxiety-like behavior, while carvedilol treatment prevented this behavioral change. Each dot represents an individual animal, with data presented as mean  $\pm$  SEM. Statistical analysis was performed using one-way ANOVA Kruskal-Wallis tests (\*  $p < 0.05$ ).

31B, C). However, carvedilol-treated animals spent a significantly higher percentage of time in the center of the arena compared to non-treated and vehicle-treated animals, reflecting reduced anxiety-like behavior (\* $p < 0.05$ ; Figure 31D). These findings suggest that neonatal carvedilol treatment normalizes anxiety-like behavior in KCNIN heterozygous animals, potentially through modulation of anxiety-related neural circuits.

### 3.8.4 | Perineuronal Nets Remain Unaltered by Carvedilol Treatment

The integrity of perineuronal nets (PNNs) was evaluated using WFA staining in the dentate gyrus molecular layer (Figure 32). PNNs are critical for maintaining neuronal stability and

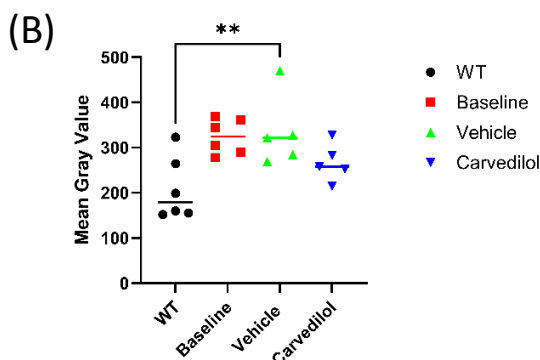
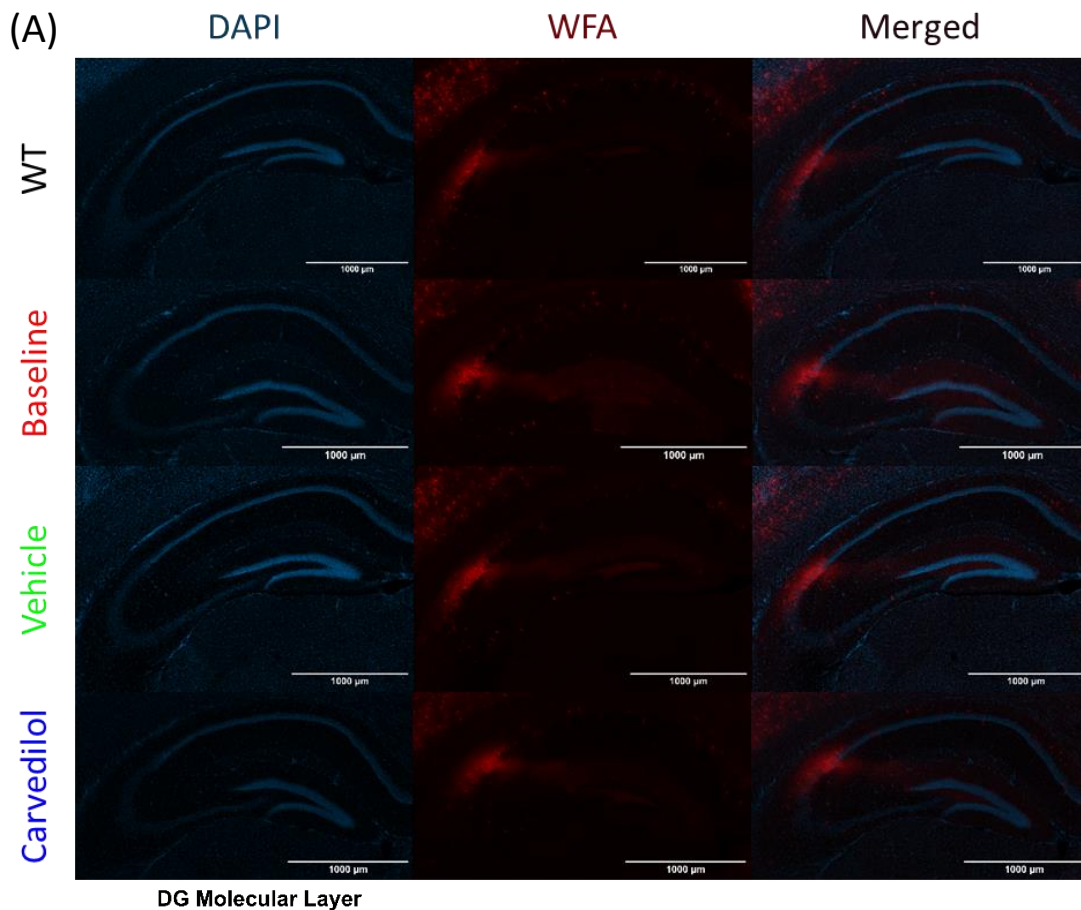


**Figure 32: Increased perineuronal nets in the dentate gyrus molecular layer of non-treated KCNIN heterozygous animals are not prevented by carvedilol treatment. (A)** Representative images of the dentate gyrus molecular layer stained with DAPI (first column), WFA (second column), and merged images (third column). WT images are shown in the first row, non-treated KCNIN in the second row, vehicle-treated KCNIN in the third row, and carvedilol-treated KCNIN in the fourth row. **(B)** Mean gray value comparisons of WFA signal intensity across groups. Non-treated KCNIN heterozygous juvenile animals exhibited increased perineuronal nets in the dentate gyrus molecular layer compared to WT animals, but carvedilol treatment did not significantly reduce WFA signal intensity. Data are presented as mean  $\pm$  SEM, with statistical analysis performed using one-way ANOVA (\*\*  $p < 0.01$ ).

regulating synaptic plasticity. Non-treated KCNIN heterozygous animals displayed significantly increased WFA signal intensity compared to WT controls, indicative of enhanced PNN formation (Figure 32A). However, carvedilol treatment did not significantly reduce WFA intensity, suggesting that neonatal carvedilol administration does not influence PNN alterations associated with the epileptic phenotype (Figure 32B). These results highlight the persistence of PNN changes in KCNIN heterozygotes despite pharmacological intervention.

### **3.8.5 | Normal Astroglia Levels in Juvenile KCNIN Heterozygotes**

Reactive astrogliosis, a key indicator of glial response to neuronal stress, was assessed in the hippocampal region using GFAP staining (Figure 33). Representative images demonstrated no significant differences in GFAP signal intensity or area fraction among non-treated, vehicle-treated, and carvedilol-treated KCNIN heterozygous animals compared to WT controls (Figure 33A–C). The astroglial level in juvenile animals was at the normal level and the statistical analysis confirmed that carvedilol treatment during the neonatal phase did not alter the astroglial level, indicating that glial activation remains unaffected by the intervention. These results suggest that carvedilol shows promise in modulating seizures, cortical excitability, and no effect on astroglial level in this model.

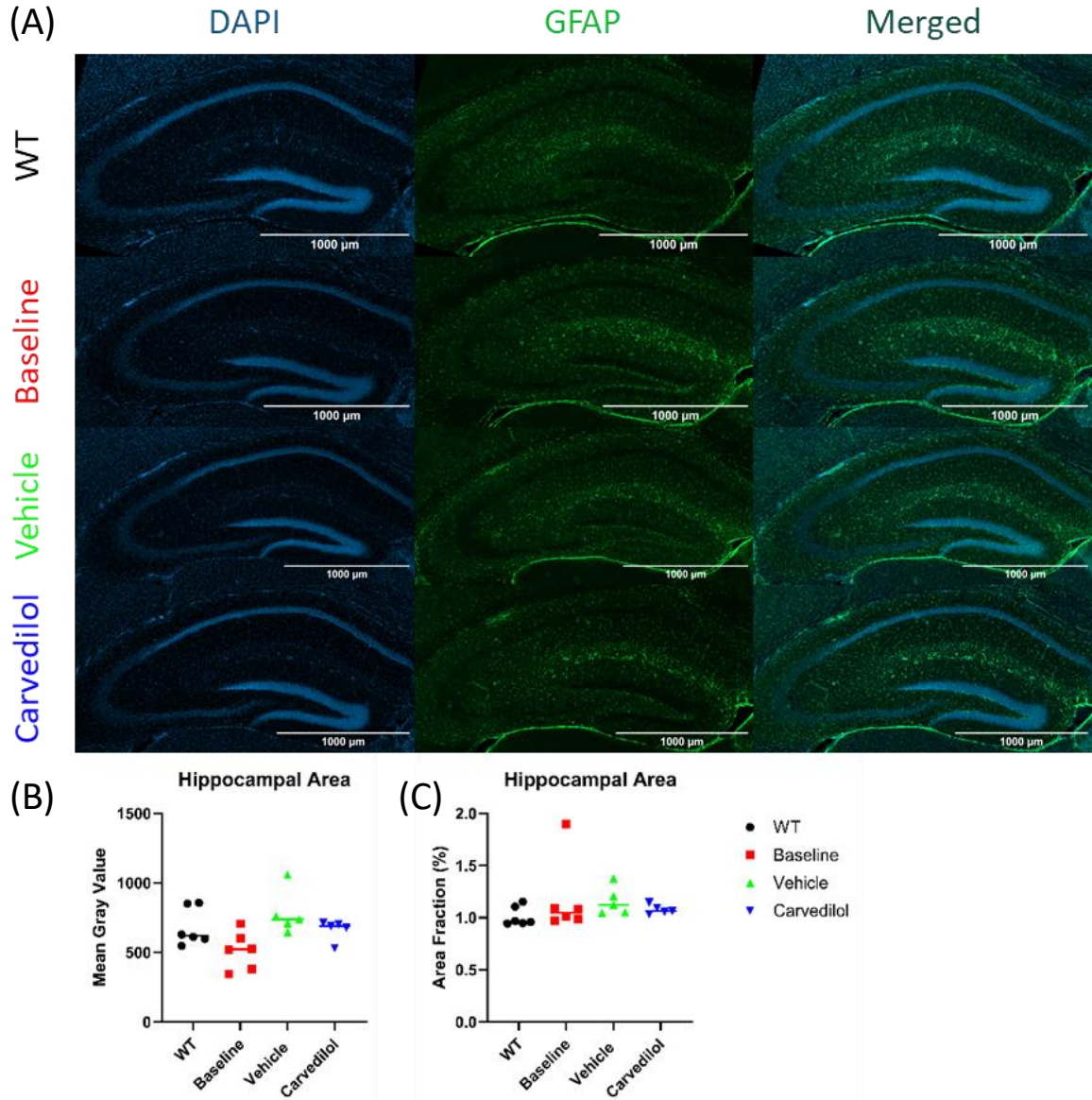


**Figure 33: Normal Astroglia Levels in Juvenile KCNIN Heterozygotes.** (A) Representative images of the hippocampal area showing DAPI (first column), GFAP (second column), and merged images (third column). WT images are in the first row, non-treated KCNIN in the second, vehicle-treated KCNIN in the third, and carvedilol-treated KCNIN in the fourth. (B) Mean gray value comparisons of GFAP signal intensity across groups. (C) Area fraction of GFAP signal intensity in the hippocampal region. Neither non-treated nor vehicle-treated KCNIN juvenile animals exhibited significant alterations in astrocytic reactivity compared to WT animals. Carvedilol treatment during the neonatal phase did not influence astrocytic reactivity. Data are presented as mean  $\pm$  SEM, with statistical analysis performed using one-way ANOVA (ns = not significant).

## 4. | Discussion

Epileptic encephalopathies represent a group of severe neurological disorders characterized by early-onset seizures, significant developmental delays, and profound cognitive impairments. KCNT1-associated epileptic encephalopathies in particular present with high seizure frequency and resistance to conventional treatments (Lim et al. 2016; Bonardi et al. 2021; Barcia et al. 2019). These disorders stem from gain-of-function mutations in the *KCNT1* gene, which encode hyperactive Na<sup>+</sup>-activated K<sup>+</sup> channels, leading to destabilized neural networks and excessive excitatory activity that drive pathological hyperexcitability (Barcia et al. 2012; Heron et al. 2012).

This thesis investigates the phenotypic impact of KCNT1 mutations using two patient-derived mouse models: KCNIN (p.I296N) and KCNRQ (p.R911Q). Through an integrative approach encompassing behavioural, electrophysiological, and morphological analyses, the study provides a detailed characterization of the epileptic phenotypes associated with these mutations. The key areas of focus included the frequency of seizures, changes in interictal cortical oscillations, somatomotor development, behavioural impairments, and structural changes in brain morphology. Additionally, treatment studies were conducted to evaluate the effectiveness of KCNT1 channel blockers in mitigating the epileptic phenotype, shedding light on potential therapeutic strategies.

The results revealed specific epilepsy phenotypes depending on the location of the mutation on the channel for the disease severity. KCNIN heterozygotes exhibited relatively mild phenotypes, characterized by subtle behavioural and developmental disruptions, while KCNRQ homozygotes displayed more severe seizures which is in line with the level of GoF measured in vitro, marked cortical oscillatory disturbances, and significant network dysfunction. Treatment studies conducted in adult animals proved largely ineffective, underscoring the necessity of early therapeutic intervention to prevent irreversible network remodelling and disease progression. Notably, early pharmacological intervention with KCNT1 blockers demonstrated partial efficacy in preventing epileptogenesis in KCNIN heterozygotes. The evaluation of pharmacological interventions in patient-derived disease models offers valuable insights into the development of targeted treatments for these debilitating conditions, emphasizing the critical importance of early and precise therapeutic strategies.

## 4.1 | KCNT1 Mutations Cause Severe Epileptic Phenotypes, Altered Oscillatory Dynamics, and Disrupted Sleep Architecture

The defining feature of KCNT1-associated epileptic encephalopathies is the presence of frequent and severe spontaneous seizures (Lim et al. 2016; Bonardi et al. 2021; Barcia et al. 2019), as observed in both KCNIN and KCNRQ mutant mouse models (Figure 8, 9). While KCNIN heterozygotes demonstrated moderate seizure frequency, KCNRQ homozygotes exhibited significantly higher seizure severity and frequency. Electrocorticographic (ECoG) recordings identified distinct epileptiform patterns, including high-amplitude rhythmic discharges, postictal depression, beta bursts, and sporadic interictal spikes in KCNRQ homozygotes (Figure 8B-D). These findings are consistent with clinical observations in human patients, where increased seizure burden often correlates with mutation severity (McTague et al. 2018).

Beyond seizures, KCNT1 mutations profoundly disrupt cortical oscillatory dynamics, reflecting widespread disturbances in network stability. KCNIN heterozygotes showed a trend towards reduction in theta power during sleep, along with unexpected beta oscillations (Figure 10), while KCNRQ homozygotes exhibited more pronounced reductions in theta power and interictal beta oscillations (Figure 11). Theta oscillations, crucial for hippocampal-dependent cognitive functions, rely on synchronized activity between pyramidal cells and inhibitory interneurons, particularly parvalbumin (PV)-expressing cells (Stark et al. 2013). These PV interneurons play a critical role in timing and synchronizing theta rhythms by providing precise perisomatic inhibition, which ensures proper coordination of neuronal firing during memory-related processes (Sohal et al. 2009). Sirota et al. (Sirota et al. 2008) demonstrated that hippocampal theta coordinates neocortical gamma oscillators, and its impairment in mutant animals may disrupt interregional synchrony. In another study, Siapas et al. (Siapas, Lubenov, and Wilson 2005) showed that hippocampal-prefrontal theta phase-locking facilitates memory consolidation. The reduction in theta power, especially in KCNRQ homozygote animals, likely result from impaired synchronization within hippocampal circuits and disrupting temporal coding necessary for memory processes.

The unexpected beta oscillations observed in KCNIN heterozygous and KCNRQ homozygous animals during sleep, typically associated with sensorimotor and cognitive

maintenance, may stem from hyperactive somatostatin (SOM)-expressing interneurons (Chen et al. 2017; Veit et al. 2017). Chen et al. (Chen et al. 2017) elaborated on the roles of SOM+ and PV+ interneurons, showing that SOM+ cells primarily drive beta oscillations and are critical for their modulation during visual stimulation. Veit et al. (Veit et al. 2017) demonstrated that SOM+ interneurons are essential for generating rhythmic activity in the gamma and beta frequency ranges. Although their study referred to these oscillations as gamma, the frequency (~30 Hz) aligns more with beta activity. Beyond synaptic mechanisms, Roopun et al. (Roopun et al. 2006) highlighted that beta oscillations in layer V of the somatosensory cortex are driven by nonsynaptic gap-junction coupling between intrinsically bursting pyramidal neurons. These oscillations, independent of synaptic transmission, suggest an alternative mechanism for beta rhythm generation. Supporting this hypothesis, Mancilla et al. (Mancilla et al. 2007) showed that electrical coupling between inhibitory interneurons robustly synchronizes beta rhythms, emphasizing the importance of gap junctions in maintaining oscillatory coherence. Changes in oscillation patterns including beta and theta abnormalities, may contribute to the impaired excitation-inhibition (E/I) balance and cognitive deficits observed in these models.

Sleep architecture, an essential component of neuronal homeostasis (Girardeau and Lopes-Dos-Santos 2021), was affected in both models, with more severe disturbances observed in KCNRQ homozygotes. Increased NREM sleep duration and reduced REM sleep percentage in these mutant animals showed altered sleep cycles which are critical for maintaining neuronal and cognitive functions (Figure 12). The reduction in REM sleep percentage, a state characterized by theta and gamma rhythms originating from hippocampal and cortical networks (Montgomery, Sirota, and Buzsáki 2008), points to impairments in the coordination between these regions in line with the interictal power spectral density analyses. Grosmark et al. (Grosmark et al. 2012) highlight the critical role of REM sleep in reorganizing hippocampal excitability. During REM, theta oscillations and reduced firing rates facilitate the refinement of synaptic connectivity, contributing to firing rate homeostasis. According to Miyawaki and Diba (Miyawaki and Diba 2016), NREM sleep plays a pivotal role in reducing hippocampal firing rates through oscillatory events such as spindles and sharp-wave ripples (SWRs). The prolonged NREM sleep in the epileptic mutants may represent a compensatory mechanism to counteract heightened baseline excitability and excessive synaptic activity caused by the epileptic condition. Additionally, the prolonged NREM sleep may reflect an adaptive mechanism to stabilize hyperexcitable

thalamocortical circuits (Fernandez and Lüthi 2020). Sleep spindles, generated by these circuits, may play a compensatory role by promoting synaptic downscaling and protecting against cortical overactivation. Disruptions in sleep likely exacerbate seizure susceptibility, as seizures were frequently observed during or shortly after sleep in both models. This bidirectional interaction between sleep disruptions and epileptic activity is a hallmark of several epilepsy syndromes (Sinha 2011; Roliz and Kothare 2022), emphasizing the need to explore further the role of sleep-dependent oscillatory dynamics in epilepsy pathophysiology.

Overall, these findings underscore the multifaceted impact of KCNT1 mutations on neural networks. The disruptions in oscillatory dynamics, spanning theta, beta, and gamma rhythms, reflect a broad disturbance in the coordination of neural circuits responsible for cognitive and emotional regulation. These results highlight the critical need for therapeutic approaches that target not only seizure reduction but also the restoration of oscillatory and sleep stability. Addressing these broader dysfunctions may provide a pathway toward more effective management of KCNT1-associated epilepsies.

## **4.2 | Developmental and Behavioural Deficits Reflect Genotype-Specific Neurological Impairments**

KCNT1 mutations result profound developmental and behavioural changes. Analyses of KCNIN and KCNRQ mouse models reveal distinct differences in growth trajectories, sensory-motor functions, and cognitive performance, underscoring the diverse neurological impacts of these mutations. Both KCNIN and KCNRQ mutants exhibited significantly reduced body weight compared to WT controls, with KCNRQ homozygotes showing the most severe deficits (Figure 13B). These animals displayed visibly smaller body size and altered posture, indicative of pronounced developmental delays (Figure 13A). Such growth impairments may reflect disruptions in metabolic regulations or energy homeostasis (Brüning and Fenselau 2023). While basic motor reflexes, such as righting and geotactic reflexes, remained intact across genotypes, KCNRQ homozygous females exhibited significant delays in the cliff avoidance reflex, pointing to impaired sensory-motor integration and spatial awareness (Figure 13F). This finding might be a result of cerebellar circuit dysfunction considering high-expression levels of KCNT1 in cerebellum, contributing to deficits in sensorimotor coordination (Bausch et al. 2015).

Behavioural evaluations in the open field test revealed hyperactivity and impaired habituation in KCNIN heterozygotes, consistent with increased locomotion (Figure 14B). In contrast, KCNRQ homozygotes, particularly males, displayed reduced exploratory activity and time spent in center (Figure 14E and 14G). On the other hand, the observed effect in these animals might not be concluded as behavioural impairment due to their unresponsiveness period at the beginning of the experiment when they were first introduced to an open field arena. Female KCNRQ homozygotes exhibited impaired habituation without overt anxiety, suggesting sex-specific differences in behavioural phenotypes (Figure 14F). Anxiety profiles were further assessed using the elevated plus maze, where KCNIN heterozygotes spent significantly more time in the open arms, reflecting reduced anxiety and increased exploratory behaviour (Figure 15B). Interestingly, KCNRQ homozygotes exhibited an even stronger preference for open arms, potentially reflecting abnormal risk assessment rather than a simple reduction in anxiety (Figure 15D). This behavioural pattern likely stems from disruptions in amygdala-hippocampus circuitry, which parallels observations in other KCNT1 epilepsy models (Q. Zhang et al. 2022).

Working memory was assessed using the Y-maze test. KCNIN heterozygotes demonstrated intact performance, with alternation percentages comparable to WT controls (Figure 16B-C). In contrast, KCNRQ homozygotes, particularly males, exhibited significant impairments, indicating genotype-specific deficits in cognitive processes dependent on the prefrontal cortex, with contributions from the hippocampus for spatial working memory. These findings align with studies showing that KCNT1 mutations impair synaptic plasticity within the prefrontal-hippocampal circuits, leading to compromised memory functions (Matt et al. 2021; Wu, El-Hassar, et al. 2024). KCNRQ homozygotes performed well in recognition memory task, indicating preserved recognition memory, while KCNRQ heterozygotes showed a trend towards a mild impairment (Figure 17E). On the other hand, further investigation is required to make a conclusion regarding spatial and recognition memories in these models considering the limited sample size in our experiments.

Long-term memory, evaluated through the step-through passive avoidance test, revealed severe impairments in both models. KCNIN heterozygotes and KCNRQ homozygotes exhibited significantly reduced latencies to enter the dark compartment, indicating impaired retention of aversive stimuli (Figure 18). Notably, non-epileptic KCNRQ heterozygotes performed similarly to WT controls, indicating genotype dependent deficits in KCNRQ

homozygotes. These observations align with studies linking the impact of KCNT1 on memory-related mechanism and the intellectual disability observed in human patients (Bausch et al. 2015; Wu, El-Hassar, et al. 2024; Kim and Kaczmarek 2014).

KCNIN heterozygotes exhibited a relatively milder phenotype characterized by hyperactivity, reduced anxiety-like behaviour. Learning and memory performance in these animals was severely impaired, while maintaining cognitive performance in working memory task. Conversely, KCNRQ homozygotes displayed a broader range of impairments, including reduced locomotion, reduced anxiety-like behaviour, and significant memory deficits. These results highlight the genotype-specific impact of KCNT1 mutations on developmental, motor, and cognitive functions, providing critical insights into the pathophysiological mechanisms underlying KCNT1-associated epileptic encephalopathies. These findings underscore the importance of developing targeted therapeutic strategies aimed at preserving cognitive and behavioural functions in affected individuals.

### **4.3 | Morphological Changes Correlate with Epileptic Phenotype**

The morphological changes identified in KCNT1 mutant models provide essential insights into the structural alterations in the hippocampal area. Alterations in perineuronal nets, NPY expression, and glial activation underscore the intricate interactions between neuronal, glial, and extracellular matrix components in the pathophysiology of KCNT1-associated epilepsies.

The increased WFA signal intensity observed in the dentate gyrus molecular layer in both KCNIN and KCNRQ mutants, with more pronounced enhancement in KCNRQ homozygotes, suggests extensive PNN remodelling. These extracellular matrix structures are crucial for regulating synaptic plasticity and neuronal excitability by stabilizing synaptic contacts and modulating ion diffusion (Wen et al. 2018). Cabungcal et al demonstrated the protective role of perineuronal nets against oxidative stress on PV+ interneurons (Cabungcal et al. 2013). In contrast, enhanced PNN density may impair synaptic flexibility and limit dendritic spine remodelling, thereby fostering a hyperexcitable network and increasing seizure susceptibility (Pollock et al. 2014). At this point, it is not clear that either PNN remodelling is an attempt to counterbalance hyperexcited network activity or it contributes to the pathogenesis of KCNT1-associated epilepsies by reinforcing aberrant circuit dynamics and maintaining hyperexcitability.

Analysis of NPY staining demonstrated genotype-specific alterations, with notably elevated expression in mossy fibers of the CA3 stratum lucidum. While increased NPY levels were detected in both KCNIN heterozygotes and KCNRQ homozygotes, the variability was greater in KCNIN heterozygotes, and the effect was more pronounced in KCNRQ homozygotes. NPY plays a critical inhibitory role by suppressing excitatory neurotransmitter release, and its upregulation likely represents a compensatory response to prolonged epileptic activity (Cattaneo et al. 2020). Despite this adaptive mechanism, the persistent epileptic phenotype in KCNRQ homozygotes indicates that increased NPY expression alone is insufficient to fully restore the excitation-inhibition balance.

Astroglial activation, as evidenced by enhanced GFAP staining in the hippocampus, highlights the response of astrocytes against hyperexcited network. Both KCNIN and KCNRQ mutants exhibited increased GFAP expression, with a more pronounced astrogliosis response in KCNRQ homozygotes. Astrocytes are essential for maintaining extracellular ion homeostasis, modulating synaptic activity, and responding to neuronal injury. Elevated GFAP levels might be a response against increased network activity. However, it may participate in a neuroinflammatory response, which may exacerbate excitatory signalling (Hayatdavoudi et al. 2022). Notably, the Nissl and Isolectin B4 stainings in our models did not show cellular loss or microglial activation. Hence, our data is supporting the hypothesis that the elevated GFAP levels reflects hyperexcited network activity.

Collectively, the increased PNN density, elevated NPY expression, and enhanced GFAP levels highlight significant structural and cellular remodelling in the hippocampus. These morphological changes likely protective against to the persistence of hyperexcitable neural networks in KCNT1 mutant models. The findings underscore the dynamic interplay between neuronal, glial, and extracellular matrix components in sustaining epileptic activity and emphasize the therapeutic potential of targeting these structural changes to alleviate network hyperexcitability in KCNT1-associated epilepsies.

## 4.4 | KCNT1 Blocker Treatment in Adult Mice Fails to Reverse Epileptic Phenotypes

The administration of KCNT1 blockers in adult KCNIN and KCNRQ mutant mice demonstrated minimal efficacy in addressing established epileptic phenotypes. Despite targeting hyperactive KCNT1 channels pharmacologically, neither Pimozide nor Carvedilol significantly reduced seizure activity.

Pimozide, identified through a high-throughput thallium flux assay as a candidate KCNT1 inhibitor, was selected for its robust inhibition of KCNT1-mediated currents and favourable pharmacokinetics. Although its ability to cross the blood-brain barrier suggests therapeutic potential, Pimozide treatment in adult KCNIN heterozygotes and KCNRQ homozygotes failed to reduce seizure frequency (Figures 22 and 24). Electrocorticogram (ECoG) analyses revealed persistent epileptiform discharges and disrupted cortical oscillations throughout the treatment period (Figures 23 and 25). One possible explanation for its inefficacy is Pimozide's lack of specificity, as it also antagonizes dopamine D2 receptors (Tecott et al. 1986). This unintended activity may alter neuronal excitability and synaptic dynamics, counteracting its intended effects on KCNT1-mediated hyperexcitability. Furthermore, advanced disease progression and prolonged exposure to hyperexcitable states may have led to irreversible circuit alterations, such as synaptic remodelling and gliosis.

Carvedilol, another repurposed compound identified via the high-throughput screening and validated through patch-clamp electrophysiology, similarly exhibited no discernible therapeutic benefit in adult animals. Known for its beta-adrenergic blocking properties, Carvedilol also modulates potassium channels and acts as a functional antagonist of serotonin 5-HT<sub>2A</sub> receptors, offering the potential for broader modulation of neuronal excitability (Murnane et al. 2019; Benkel et al. 2022). Nevertheless, Carvedilol failed to reduce seizure frequency or alleviate cortical hyperexcitability markers (Figures 26 and 27). These results underscore the challenges of treating chronic epilepsy, where long-standing maladaptive changes in neuronal and glial networks limit the efficacy of ion channel modulation alone.

Several factors may explain the limited success of these treatments. Foremost, the therapeutic serum levels required for KCNT1-associated epileptic encephalopathy remain undefined. The pharmacokinetics of these drugs, including their metabolism and distribution

to target sites, are incompletely understood. Moreover, metabolic rates likely differ between younger and older animals, potentially influencing drug efficacy. In this study, drug levels were measured only at the end of the treatment period, leaving gaps in understanding the pharmacodynamic profiles during earlier phases. The inability to monitor drug levels continuously throughout treatment introduces further uncertainty. Additionally, chronic epilepsy induces irreversible neuronal circuit changes, including maladaptive synaptic plasticity, gliosis, and PNN remodelling, which sustain the hyperexcitable network. KCNT1's widespread expression across various brain regions adds complexity to the therapeutic landscape, as it remains unclear whether specific regions or distributed network alterations primarily drive hyperactivity. Furthermore, our non-region-specific drug delivery approach may have diluted the therapeutic effect. Given the potential for cell-type-specific impacts of KCNT1 mutations, uniformly targeting all neuronal subtypes may not effectively rescue the phenotype. Epigenetic modifications and altered gene expression in adult animals likely further reduce the efficacy of KCNT1 blockers.

These findings highlight the mechanistic limitations of late-stage interventions and underscore the diminished network plasticity in adult animals. The reduced capacity for functional recovery emphasizes the need for timely therapeutic intervention to prevent irreversible circuit dysfunctions. Clinically, these results stress the importance of early diagnosis and intervention to promote normal brain development and slow disease progression.

#### **4.5 | Early Treatment Reduces the Severity of Epileptic Phenotypes**

Neonatal intervention with Carvedilol in KCNIN heterozygotes demonstrated a reduction in the severity of epileptic phenotypes, underscoring the importance of early therapeutic intervention in KCNT1-associated disorders. Administered via intraperitoneal injections pre-weaning and chow embedding post-weaning, Carvedilol significantly increased the proportion of seizure-free animals compared to untreated animals. Power spectral density analyses revealed a trend toward reduced cortical excitability in carvedilol-treated juvenile KCNIN heterozygote animals. Specifically, SWS beta oscillatory power tended towards normalization compared to vehicle-treated animals. The aperiodic exponent values indicated a potential decrease in overall cortical excitability across brain states, including REM sleep, SWS, and wakefulness (Figure 29). These findings suggest that early carvedilol treatment

partially modulates cortical network dynamics, reducing hyperexcitability and stabilizing some aspects of oscillatory function. However, the observed effects remained trends rather than statistically significant changes, emphasizing the need for further studies with larger cohorts to confirm the efficacy of early intervention in altering cortical excitability.

Sleep architecture analysis in juvenile KCNIN heterozygote animals revealed mild alterations compared to WT controls, including increased mean REM duration, mean SWS duration, a slightly higher percentage of SWS episodes, and a reduced number of REM events, although none of these differences reached statistical significance. Carvedilol treatment did not result in significant changes to any of these sleep metrics, suggesting that while early intervention may modulate some aspects of network excitability, it is insufficient to restore normal sleep architecture. This highlights the need for more comprehensive strategies targeting the underlying network dysfunctions contributing to sleep disturbances in KCNT1-associated epilepsies.

Early intervention significantly impacted behavioural outcomes, particularly as demonstrated by the open-field test. Non-treated and vehicle-injected animals exhibited a slight but non-significant increase in locomotion, which was normalized by Carvedilol treatment. However, untreated and vehicle-injected animals also showed a lack of habituation, and early treatment did not effectively address this genotype-associated deficit. Importantly, the heightened anxiety-like behaviour, characterized by increased thigmotaxis, observed in non-treated and vehicle-injected animals was significantly reduced by early Carvedilol intervention. This finding suggests that early treatment mitigates anxiety-like behaviour, which contrasts with the normal anxiety-like behaviour of older adult KCNIN animals in open-field experiments. The heightened anxiety in vehicle-treated animals during the early treatment study may be attributed to age-related factors and the potential stress effects of repeated injections. These results highlight the selective efficacy of early treatment in addressing specific behavioural parameters while leaving others unaffected.

Histological analyses provided further insights into the limited efficacy of early intervention. WFA staining revealed that increased PNN density in the dentate gyrus molecular layer of non-treated KCNIN heterozygote animals was not significantly reduced by Carvedilol treatment (Figure 32). GFAP staining showed normal astroglia in all treatment groups (Figure 33). Notably, the absence of astrogliosis in these juvenile animals suggests that early

intervention occurs before significant glial activation can develop, which may be a positive indicator of the timing and potential benefits of early treatment.

Despite its benefits, the early intervention did not fully normalize electrophysiological, behavioural, or structural outcomes, reflecting the multifactorial nature of KCNT1-associated epilepsies. While early treatment effectively increased the ratio of seizure-free animals, anxiety-like behaviour, and cortical excitability, ongoing residual sleep disturbances, persistent PNN density, and incomplete behavioural recovery suggest that further investigation is required. The limited sample size in this study complicates definitive conclusions about the effectiveness of Carvedilol in preventing the disorder in KCNIN heterozygote animals. To maximize therapeutic efficacy, further investigation into the optimal timing and dosage of early Carvedilol treatment is essential. Additionally, studies in KCNRQ homozygotes and other KCNT1 variants could provide valuable insights into the broader applicability of early intervention strategies.

#### **4.6 | Synaptic Transmission Alterations Highlight E/I Balance Shift in KCNT1 Mutants**

The synaptic transmission findings in KCNT1 mutant models reveal alterations in excitatory and inhibitory balance (E/I balance) that correlate with genotype severity and developmental progression. Electrophysiological analyses across age groups and brain regions, conducted by our collaborators Dr. Kunihiro Araki from Prof. Dr. Heinz Beck's lab, provide critical insights into the mechanisms driving KCNT1-associated epileptic phenotypes. Spontaneous synaptic currents, which include action potential-dependent vesicle release, provide a broad measure of overall synaptic activity. In contrast, miniature synaptic currents, recorded under conditions that block action potentials, isolate action potential-independent vesicle release events and reflect the properties of individual synapses. Together, these approaches offer complementary perspectives on synaptic transmission dynamics.

**Table 6: Synaptic transmission alterations in KCNT1 mutants.**

<b>Genotype</b>	<b>Region of Interest</b>	<b>Age (Weeks)</b>	<b>Synaptic Measure</b>	<b>Amplitude Changes</b>	<b>E/I Balance</b>
<b>KCNIN heterozygote</b>	CA1 Pyramidal Cells	8	Spontaneous	No change	Stable
<b>KCNIN heterozygote</b>	Sensory-Motor Cortex Layer 2/3	8-9	Miniature	mEPSC: n.s. ↑	Subtle shift toward excitation
<b>KCNIN heterozygote</b>	Sensory-Motor Cortex Layer 2/3	13	Spontaneous	sEPSC: n.s. ↑	Mild excitatory trend
<b>KCNRQ homozygote</b>	Sensory-Motor Cortex Layer 2/3	10	Miniature	mEPSC: ** ↑ mIPSC: * ↑	Predominant excitation

In 8-week-old KCNIN heterozygote animals, recordings from CA1 pyramidal cells showed no significant changes in spontaneous IPSC or EPSC amplitude and frequency. This stability indicates that synaptic transmission within the CA1 region is relatively unaffected. The lack of detectable synaptic alterations suggests that early hyperexcitability in KCNIN mutants may instead stem from disruptions in network excitability or broader connectivity deficits rather than local synaptic transmission dysfunction.

In the sensory-motor cortex layer 2/3 of KCNIN heterozygotes, synaptic transmission remained relatively stable, as evidenced by the absence of significant changes in spontaneous IPSC or EPSC metrics at 13 weeks. However, a non-significant increase in sEPSC amplitude at 13 weeks, along with similar trends in mEPSC amplitude and E/I balance amplitude at 8–9 weeks, points to subtle shifts toward increased excitatory input over time. These mild excitatory trends align with cortical oscillatory disruptions and behavioural impairments observed in these mutants. Together, these findings highlight a gradual evolution of synaptic transmission alterations, with small excitatory shifts potentially predisposing the network to hyperexcitability.

In contrast, 10-week-old KCNRQ homozygotes displayed pronounced synaptic changes in the sensory-motor cortex layer 2/3 (Figure 34). Significant increases in mIPSC and mEPSC amplitudes suggest heightened excitatory and inhibitory synaptic drive, a hallmark of severe hyperexcitability (Figure 34A-D). Although the increase in E/I balance amplitude was not statistically significant, the data point to a predominant excitatory drive relative to inhibition, correlating with severe seizure activity and disrupted cortical dynamics observed in this genotype (Figure 34E). These synaptic alterations underscore the distinct and severe phenotype of KCNRQ homozygotes, contrasting sharply with the relatively stable synaptic profile in KCNIN heterozygotes.

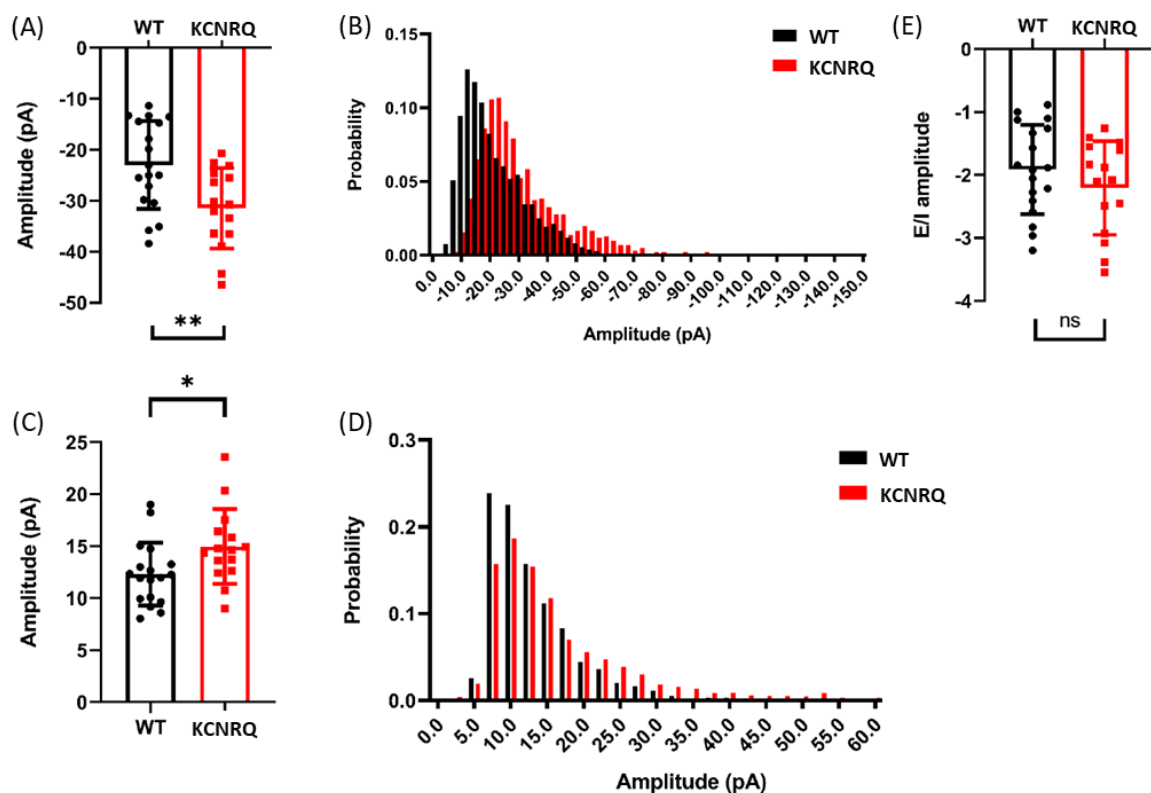


**Figure 34. Pronounced synaptic transmission alterations in the sensory-motor cortex layer 2/3 of KCNRQ homozygote animals.** (A) Increased mEPSC amplitude (pA) in KCNRQ homozygote animals compared to WT animals, highlighting heightened excitatory synaptic drive. (B) Probability distribution of excitatory current amplitudes (pA), showing a shift toward larger excitatory events in KCNRQ homozygotes. (C) Increased mIPSC amplitude (pA) in KCNRQ homozygote animals compared to WT animals, indicating enhanced inhibitory synaptic input. (D) Probability distribution of inhibitory current amplitudes (pA), demonstrating altered inhibitory event dynamics in KCNRQ homozygotes. (E) E/I balance amplitude comparison between KCNRQ homozygote and WT animals, showing a trend toward increased excitatory drive relative to inhibition, although not statistically significant. These measurements were obtained from 9–10-week-old animals. For WT animals, 18 patches were performed across 6 animals, with 2037 mIPSCs and 1080 mEPSCs recorded. For KCNRQ homozygote animals, 15 patches were performed across 4 animals, with 1761 mIPSCs and 1012 mEPSCs recorded. Statistical analysis was conducted using an unpaired two-tailed t-test; \* $p < 0.05$ . These results underscore the severe synaptic transmission alterations in KCNRQ homozygotes, reflecting heightened cortical hyperexcitability.

The synaptic changes in KCNT1 mutants likely result from a combination of intrinsic alterations caused by gain-of-function mutations and compensatory mechanisms aimed at stabilizing network activity. In KCNRQ homozygotes, these pronounced synaptic abnormalities may be exacerbated by structural changes such as increased PNN density and astrogliosis, which contribute to severe hyperexcitability. These findings align with histological evidence of extracellular matrix remodelling and neuroinflammation, emphasizing the multifaceted nature of synaptic transmission disruptions in KCNT1-associated epilepsies.

## 4.7 | Future Directions

Several critical directions for future research have emerged to address the limitations of the current study and can deepen our understanding of KCNT1-associated epileptic encephalopathies. Investigating sex-specific differences might be critical, as sex hormones may significantly influence seizure phenotypes, cortical dynamics, sleep disruptions, and morphological changes. Evaluation of sex-specific differences could impact our treatment efficacy and help to refine personalized medicine approaches and optimize patient outcomes. One major limitation of this study is the relatively small sample size, particularly for the KCNRQ line, which may have reduced the statistical power and generalizability of certain findings. Expanding the sample size will be essential to confirm the trends observed and validate the efficacy of early treatment interventions. Larger sample sizes will allow for more robust conclusions regarding therapeutic potential and their broader applicability.

Electrocorticogram analyses could be extended to include interictal epileptiform discharges, which are critical markers of hyperexcited neural networks. Quantifying these discharges would provide a complementary measure of epileptic severity and allow for a more precise evaluation of treatment effects. Moreover, current analyses focused exclusively on the right hemisphere; future studies should include the left hemisphere and investigate inter-hemispheric interactions to provide a more comprehensive understanding of network dysfunctions and potential asymmetric epileptic burden.

This study provides critical insights into the functional consequences of KCNT1 mutations beyond seizure activity by investigating behavioral comorbidities. On the other hand, it requires further exploration to improve our understanding about the comorbidities of KCNT1-associated epileptic encephalopathy. For instance, in the Object Location Memory

test, the WT females did not show a preference for exploring the displaced object as expected and failed to perform above the chance level. This raises questions about the validity of the current findings and underscores the need for more rigorous experimental replication. Additionally, recognition memory deficits have not yet been evaluated in KCNIN heterozygote animals, leaving a gap in our understanding of potential cortex-associated memory impairments. Furthermore, given the high expression of KCNT1 in the piriform cortex and considering its role in the olfactory system, it is likely that mutations could affect social interactions. Similarly, as it has been demonstrated before for a different variant of KCNT1 (Shore et al. 2020), nest-building experiments could offer valuable insights into innate behaviour and the stress level of the animals, adding another layer to the functional characterization of these animal models.

DeltaFos-B staining, a marker of epileptic activity, could provide valuable region-specific insights into the effects of these mutations. This transcription factor accumulates in response to sustained or repeated neural activity, making it particularly useful for identifying regions of chronic hyperexcitability. By utilizing deltaFos-B staining, future studies could pinpoint hyperactive regions, assess their contribution to seizure propagation, and evaluate the regional efficacy of therapeutic interventions. Advanced brain-wide imaging techniques, such as brain clearing with subsequent light-sheet microscopy or functional ultrasound imaging, could help identify epileptic loci and elucidate functional changes in greater detail. These techniques will be particularly valuable for our research as they enable comprehensive mapping of neural circuits and identification of hyperexcited regions.

The scope of this research, which focused primarily on cortical and hippocampal alterations, should be broadened to investigate other brain regions. For instance, sleep architecture disruptions point to impairments in cortico-thalamic circuits. These circuits play a pivotal role in regulating sleep stages by generating and maintaining slow-wave activity and sleep spindles during NREM sleep. Additionally, reductions in body weight suggest altered hypothalamic activity, which could be linked to metabolic changes. Chronic stress and elevated glucocorticoid levels, often associated with epilepsy, may further exacerbate metabolic dysregulation (Brüning and Fenselau 2023).

Further studies are needed to investigate how p.I335N and p.R950Q mutations affect the intrinsic properties of the KCNT1 channels. While the effects of KCNT1 mutations on intrinsic channel properties have been demonstrated for other variants (Wu, Quraishi, et al.

2024), the specific impact of mutations used in this study remains unexplored. Addressing this gap will provide valuable information on how these particular mutations influence neuronal excitability and network behavior. Similarly, the cell-type-specific effects of these mutations remain unclear. While other KCNT1 variants have been studied, the impact of these specific mutations on distinct neuronal subpopulations could illuminate important aspects of their functional consequences (Shore et al. 2020; Wu, Quraishi, et al. 2024).

The positive effects of Carvedilol observed in the early treatment study necessitate further validation to determine its specific action on KCNT1 channels. Carvedilol is known to interact with other targets, including beta-adrenergic receptors and serotonin 5-HT<sub>2A</sub> receptors, which may contribute to its observed effects. Exploring these off-target interactions is essential to isolate their specific role in modulating KCNT1 activity and to clarify whether these additional mechanisms influence its therapeutic efficacy. Given that knock-out generated and ready-to-use mice in our lab could be utilized to isolate its KCNT1-specific effects through patch-clamp experiments on primary cortical cultures. Such studies would clarify its mechanism of action and establish its potential as a targeted therapeutic agent.

The efficacy of the early treatment study should be demonstrated in KCNRQ homozygote animals using matrix-driven timed-release pellets implanted subcutaneously from P7 until weaning. Replicating the study in KCNRQ homozygotes is essential to evaluate whether early intervention can mitigate even more severe epileptic phenotype. The use of matrix-driven timed-release pellets offers significant advantages by ensuring consistent and controlled drug delivery over the treatment period, thereby reducing variability in drug administration and enhancing the reliability of treatment outcomes. This approach would provide more definitive conclusions regarding the efficacy of early intervention.

Finally, molecular mechanistic studies are essential to complement the morphological and electrophysiological findings. Transcriptomic profiling can reveal cell-type-specific gene expression changes associated with KCNT1 mutations, shedding light on how these mutations affect distinct neuronal and glial populations. This approach can identify dysregulated signaling pathways, providing insights into how specific cellular mechanisms contribute to hyperexcitability and seizure susceptibility. Integrating transcriptomic data with functional and structural findings will offer a comprehensive understanding of the

molecular underpinnings of KCNT1-associated epilepsies, guiding the development of more effective and targeted treatment strategies.

## 5. | Conclusion

This thesis provides a detailed phenotypic characterization of KCNT1-associated epileptic encephalopathies using two patient-derived mouse models harbouring single-point mutations: p.I335N and p.R950Q. These gain-of-function mutations in *KCNT1* result in the hyperactivity of Na<sup>+</sup>-activated K<sup>+</sup> channels, driving pathological hyperexcitability and severe epileptic phenotypes. Through comprehensive assessments of neural activity, early development, behaviour, and brain morphology, this research enhances our understanding of disease pathology, progression and comorbidities. Moreover, the targeted therapeutic approach by repurposing FDA approved drugs recently identified as KCNT1 blockers has underscored the importance of intervention timing for these debilitating conditions.

The findings reveal that both KCNIN and KCNRQ models experience spontaneous seizures, with KCNRQ homozygotes displaying markedly higher seizure frequency and severity. Beyond seizures, significant changes in cortical oscillatory dynamics and sleep architecture were observed. While KCNIN heterozygotes exhibited moderate oscillatory disturbances, KCNRQ homozygotes demonstrated pronounced reductions in theta power, elevated beta oscillations, and severe sleep impairments, reflecting the imbalance of excitation and inhibition that underpins epileptogenesis.

Developmental and behavioural experiments revealed the impact of the mutations on body weight and sensory-motor reflexes, with KCNRQ homozygotes experiencing more severe impairments. A battery of behavioural testing demonstrated altered anxiety-like behaviour and memory impairments in both epileptic lines. Furthermore, KCNIN heterozygous animals showed hyperactivity and working memory deficits, while KCNRQ homozygotes exhibited reduced locomotion. Morphological evaluations further revealed enhanced PNN density, increased NPY expression, and increased astrogliosis in the hippocampal area, indicating extensive structural remodelling.

Targeted therapeutic interventions employing repurposed drugs as KCNT1 blockers, such as Pimozide and Carvedilol, showed partial efficacy in preventing seizure burden and network instability when administered before the disorder manifestation in KCNIN heterozygote

animals. However, these treatments were ineffective in reversing established epileptic phenotypes in adult mice, underscoring the critical importance of early intervention to avert irreversible circuit remodelling.

In conclusion, this research significantly advances the understanding of KCNT1-associated epileptic encephalopathies by delineating the epileptic phenotypes. It highlights the intrinsic heterogeneity of these disorders, which carries profound implications for personalized medicine. Additionally, the pharmacological findings reveal both, the promise and limitations of current therapeutic strategies, emphasizing the urgent need for early targeted interventions. By characterizing the phenotypic features, this work establishes a foundation for developing more effective and personalized treatment strategies, offering hope for enhancing the quality of life for affected individuals and their families.

## References

- AA Pharma Inc. 2014. “Pimozide Product Monograph,” March.
- Barcia, Giulia, Nicole Chemaly, Mathieu Kuchenbuch, Monika Eisermann, Stéphanie Gobin-Limballe, Viorica Ciorna, Alfons Macaya, et al. 2019. “Epilepsy with Migrating Focal Seizures: KCNT1 Mutation Hotspots and Phenotype Variability.” *Neurology. Genetics* 5 (6): e363. <https://doi.org/10.1212/NXG.0000000000000363>.
- Barcia, Giulia, Matthew R Fleming, Aline Deligniere, Valeswara-Rao Gazula, Maile R Brown, Maeva Langouet, Haijun Chen, et al. 2012. “De Novo Gain-of-Function KCNT1 Channel Mutations Cause Malignant Migrating Partial Seizures of Infancy.” *Nature Genetics* 44 (11): 1255–59. <https://doi.org/10.1038/ng.2441>.
- Barger, Zeke, Charles G Frye, Danqian Liu, Yang Dan, and Kristofer E Bouchard. 2019. “Robust, Automated Sleep Scoring by a Compact Neural Network with Distributional Shift Correction.” *Plos One* 14 (12): e0224642. <https://doi.org/10.1371/journal.pone.0224642>.
- Bausch, Anne E, Rebekka Dieter, Yvette Nann, Mario Hausmann, Nora Meyerdierks, Leonard K Kaczmarek, Peter Ruth, and Robert Lukowski. 2015. “The Sodium-Activated Potassium Channel Slack Is Required for Optimal Cognitive Flexibility in Mice.” *Learning & Memory* 22 (7): 323–35. <https://doi.org/10.1101/lm.037820.114>.
- Bausch, Anne E, Rebekka Ehinger, Julia Straubinger, Patrick Zerfass, Yvette Nann, and Robert Lukowski. 2018. “Loss of Sodium-Activated Potassium Channel Slack and FMRP Differentially Affect Social Behavior in Mice.” *Neuroscience* 384 (August): 361–74. <https://doi.org/10.1016/j.neuroscience.2018.05.040>.
- Benkel, Tobias, Mirjam Zimmermann, Julian Zeiner, Sergi Bravo, Nicole Merten, Victor Jun Yu Lim, Edda Sofie Fabienne Matthees, et al. 2022. “How Carvedilol Activates B2-Adrenoceptors.” *Nature Communications* 13 (1): 7109. <https://doi.org/10.1038/s41467-022-34765-w>.
- Bhattacharjee, Arin, Li Gan, and Leonard K Kaczmarek. 2002. “Localization of the Slack Potassium Channel in the Rat Central Nervous System.” *The Journal of Comparative Neurology* 454 (3): 241–54. <https://doi.org/10.1002/cne.10439>.
- Bhattacharjee, Arin, William J Joiner, Meilin Wu, Youshan Yang, Fred J Sigworth, and Leonard K Kaczmarek. 2003. “Slick (Slo2.1), a Rapidly-Gating Sodium-Activated Potassium Channel Inhibited by ATP.” *The Journal of Neuroscience* 23 (37): 11681–91. <https://doi.org/10.1523/JNEUROSCI.23-37-11681.2003>.
- Boillot, Morgane, and Stéphanie Baulac. 2016. “Genetic Models of Focal Epilepsies.” *Journal of Neuroscience Methods* 260 (February): 132–43. <https://doi.org/10.1016/j.jneumeth.2015.06.003>.
- Bonardi, Claudia M, Henrike O Heyne, Martina Fiannacca, Mark P Fitzgerald, Elena Gardella, Boudewijn Gunning, Kern Olofsson, et al. 2021. “KCNT1-Related Epilepsies and Epileptic Encephalopathies: Phenotypic and Mutational Spectrum.” *Brain: A Journal of Neurology* 144 (12): 3635–50. <https://doi.org/10.1093/brain/awab219>.
- Borlot, Felipe, Ahmed Abushama, Nadine Morrison-Levy, Puneet Jain, Kollencheri Puthenveetil Vinayan, Musaad Abukhalid, Hesham M Aldhalaan, et al. 2020. “KCNT1-

- Related Epilepsy: An International Multicenter Cohort of 27 Pediatric Cases.” *Epilepsia* 61 (4): 679–92. <https://doi.org/10.1111/epi.16480>.
- Brüning, Jens C, and Henning Fenselau. 2023. “Integrative Neurocircuits That Control Metabolism and Food Intake.” *Science* 381 (6665): eabl7398. <https://doi.org/10.1126/science.abl7398>.
- Burbano, Lisseth Estefania, Melody Li, Nikola Jancovski, Paymaan Jafar-Nejad, Kay Richards, Alicia Sedo, Armand Soriano, et al. 2022. “Antisense Oligonucleotide Therapy for KCNT1 Encephalopathy.” *Journal of Clinical Investigation Insight* 7 (23). <https://doi.org/10.1172/jci.insight.146090>.
- Cabungcal, Jan-Harry, Pascal Steullet, Hirofumi Morishita, Rudolf Kraftsik, Michel Cuenod, Takao K Hensch, and Kim Q Do. 2013. “Perineuronal Nets Protect Fast-Spiking Interneurons against Oxidative Stress.” *Proceedings of the National Academy of Sciences of the United States of America* 110 (22): 9130–35. <https://doi.org/10.1073/pnas.1300454110>.
- Cataldi, Matteo, Lino Nobili, Federico Zara, Romina Combi, Giulia Prato, Thea Giacomini, Valeria Capra, Patrizia De Marco, Luigi Ferini-Strambi, and Maria Margherita Mancardi. 2019. “Migrating Focal Seizures in Autosomal Dominant Sleep-Related Hypermotor Epilepsy with KCNT1 Mutation.” *Seizure* 67 (April): 57–60. <https://doi.org/10.1016/j.seizure.2019.02.019>.
- Cattaneo, Stefano, Gianluca Verlengia, Pietro Marino, Michele Simonato, and Barbara Bettegazzi. 2020. “NPY and Gene Therapy for Epilepsy: How, When,... and Y.” *Frontiers in Molecular Neuroscience* 13: 608001. <https://doi.org/10.3389/fnmol.2020.608001>.
- Chapron, Brian D, Jean C Dinh, Paul C Toren, Andrea Gaedigk, and J Steven Leeder. 2020. “The Respective Roles of CYP3A4 and CYP2D6 in the Metabolism of Pimozide to Established and Novel Metabolites.” *Drug Metabolism and Disposition: The Biological Fate of Chemicals* 48 (11): 1113–20. <https://doi.org/10.1124/dmd.120.000188>.
- Chaunsali, Lata, Bhanu P Tewari, and Harald Sontheimer. 2021. “Perineuronal Net Dynamics in the Pathophysiology of Epilepsy.” *Epilepsy Currents* 21 (4): 273–81. <https://doi.org/10.1177/15357597211018688>.
- Chen, Guang, Yuan Zhang, Xiang Li, Xiaochen Zhao, Qian Ye, Yingxi Lin, Huizhong W Tao, Malte J Rasch, and Xiaohui Zhang. 2017. “Distinct Inhibitory Circuits Orchestrate Cortical Beta and Gamma Band Oscillations.” *Neuron* 96 (6): 1403–1418.e6. <https://doi.org/10.1016/j.neuron.2017.11.033>.
- Cole, Bethan A, Rachel M Johnson, Hattapark Dejakaisaya, Nadia Pilati, Colin W G Fishwick, Stephen P Muench, and Jonathan D Lippiat. 2020. “Structure-Based Identification and Characterization of Inhibitors of the Epilepsy-Associated KNa1.1 (KCNT1) Potassium Channel.” *IScience* 23 (5): 101100. <https://doi.org/10.1016/j.isci.2020.101100>.
- Delanty, Norman, and Gianpiero Cavalleri. 2017. “Genomics-Guided Precise Anti-Epileptic Drug Development.” *Neurochemical Research* 42 (7): 2084–88. <https://doi.org/10.1007/s11064-017-2312-y>.
- Donoghue, Thomas, Matar Haller, Erik J Peterson, Paroma Varma, Priyadarshini Sebastian, Richard Gao, Torben Noto, et al. 2020. “Parameterizing Neural Power Spectra into Periodic

- and Aperiodic Components.” *Nature Neuroscience* 23 (12): 1655–65. <https://doi.org/10.1038/s41593-020-00744-x>.
- Fang, Zhi-Xu, Ling-Ling Xie, Li-Si Yan, Huan Lin, Ya-Nan Pan, Ben-Ke Liu, Yan Jiang, Min Cheng, Xiu-Juan Li, and Li Jiang. 2021. “Clinical and Genetic Characteristics of Epilepsy of Infancy with Migrating Focal Seizures in Chinese Children.” *Epilepsy Research* 174 (August): 106669. <https://doi.org/10.1016/j.eplepsyres.2021.106669>.
- Fernandez, Laura M J, and Anita Lüthi. 2020. “Sleep Spindles: Mechanisms and Functions.” *Physiological Reviews* 100 (2): 805–68. <https://doi.org/10.1152/physrev.00042.2018>.
- Gao, Kai, Zehong Lin, Sijia Wen, and Yuwu Jiang. 2022. “Potassium Channels and Epilepsy.” *Acta Neurologica Scandinavica* 146 (6): 699–707. <https://doi.org/10.1111/ane.13695>.
- Gertler, Tracy, David Bearden, Arin Bhattacharjee, and Gemma Carvill. 2018. “KCNT1-Related Epilepsy.” In *GeneReviews®*, edited by Margaret P Adam, Holly H Ardinger, Roberta A Pagon, Stephanie E Wallace, Lora JH Bean, Karen Stephens, and Anne Amemiya. Seattle (WA): University of Washington, Seattle.
- Gertler, Tracy S, Suraj Cherian, Jean-Marc DeKeyser, Jennifer A Kearney, and Alfred L George. 2022. “KNa1.1 Gain-of-Function Preferentially Dampens Excitability of Murine Parvalbumin-Positive Interneurons.” *Neurobiology of Disease* 168 (June): 105713. <https://doi.org/10.1016/j.nbd.2022.105713>.
- Girardeau, Gabrielle, and Vitor Lopes-Dos-Santos. 2021. “Brain Neural Patterns and the Memory Function of Sleep.” *Science* 374 (6567): 560–64. <https://doi.org/10.1126/science.abi8370>.
- Goldberg, Ethan M. 2021. “Rational Small Molecule Treatment for Genetic Epilepsies.” *Neurotherapeutics* 18 (3): 1490–99. <https://doi.org/10.1007/s13311-021-01110-w>.
- Griffin, Andrew M, Kristopher M Kahlig, Robert John Hatch, Zoë A Hughes, Mark L Chapman, Brett Antonio, Brian E Marron, Marion Wittmann, and Gabriel Martinez-Botella. 2021. “Discovery of the First Orally Available, Selective Kna1.1 Inhibitor: In Vitro and in Vivo Activity of an Oxadiazole Series.” *ACS Medicinal Chemistry Letters* 12 (4): 593–602. <https://doi.org/10.1021/acsmchemlett.0c00675>.
- Grosmark, Andres D, Kenji Mizuseki, Eva Pastalkova, Kamran Diba, and György Buzsáki. 2012. “REM Sleep Reorganizes Hippocampal Excitability.” *Neuron* 75 (6): 1001–7. <https://doi.org/10.1016/j.neuron.2012.08.015>.
- Hayatdavoudi, Parichehr, Mahmoud Hosseini, Vahid Hajali, Azar Hosseini, and Arezoo Rajabian. 2022. “The Role of Astrocytes in Epileptic Disorders.” *Physiological Reports* 10 (6): e15239. <https://doi.org/10.14814/phy2.15239>.
- Helbig, Ingo, and Colin A Ellis. 2020. “Personalized Medicine in Genetic Epilepsies - Possibilities, Challenges, and New Frontiers.” *Neuropharmacology* 172 (August): 107970. <https://doi.org/10.1016/j.neuropharm.2020.107970>.
- Heron, Sarah E, Katherine R Smith, Melanie Bahlo, Lino Nobili, Esther Kahana, Laura Licchetta, Karen L Oliver, et al. 2012. “Missense Mutations in the Sodium-Gated Potassium Channel Gene KCNT1 Cause Severe Autosomal Dominant Nocturnal Frontal Lobe Epilepsy.” *Nature Genetics* 44 (11): 1188–90. <https://doi.org/10.1038/ng.2440>.

- Hinckley, Christopher A, Zhonghua Zhu, Jen-Hwa Chu, Cynthia Gubbels, Timm Danker, Jonathan J Cherry, Christopher D Whelan, Sandra J Engle, and Viet Nguyen. 2023. "Functional Evaluation of Epilepsy-Associated KCNT1 Variants in Multiple Cellular Systems Reveals a Predominant Gain of Function Impact on Channel Properties." *Epilepsia* 64 (8): 2126–36. <https://doi.org/10.1111/epi.17648>.
- Hite, Richard K, Peng Yuan, Zongli Li, Yichun Hsuing, Thomas Walz, and Roderick MacKinnon. 2015. "Cryo-Electron Microscopy Structure of the Slo2.2 Na(+)-Activated K(+) Channel." *Nature* 527 (7577): 198–203. <https://doi.org/10.1038/nature14958>.
- Iraci, Nunzio, Lidia Carotenuto, Tania Ciaglia, Giorgio Belperio, Francesca Di Matteo, Ilaria Mosca, Giusy Carleo, et al. 2024. "In Silico Assisted Identification, Synthesis, and In Vitro Pharmacological Characterization of Potent and Selective Blockers of the Epilepsy-Associated KCNT1 Channel." *Journal of Medicinal Chemistry* 67 (11): 9124–49. <https://doi.org/10.1021/acs.jmedchem.4c00268>.
- Ishii, Atsushi, Mutsuki Shioda, Akihisa Okumura, Hiroyuki Kidokoro, Masako Sakauchi, Shino Shimada, Toshiaki Shimizu, Makiko Osawa, Shinichi Hirose, and Toshiyuki Yamamoto. 2013. "A Recurrent KCNT1 Mutation in Two Sporadic Cases with Malignant Migrating Partial Seizures in Infancy." *Gene* 531 (2): 467–71. <https://doi.org/10.1016/j.gene.2013.08.096>.
- Joshi, Charuta. 2022. "Zeroing in on Phenotypes While Also Broadening Our Understanding of KCNT1-Related Epilepsy." *Epilepsy Currents* 22 (5): 291–93. <https://doi.org/10.1177/15357597221096002>.
- Kaczmarek, Leonard K. 2013. "Slack, Slick and Sodium-Activated Potassium Channels." *ISRN Neuroscience* 2013 (2013). <https://doi.org/10.1155/2013/354262>.
- Kameyama, M, M Kakei, R Sato, T Shibasaki, H Matsuda, and H Irisawa. 1984. "Intracellular Na<sup>+</sup> Activates a K<sup>+</sup> Channel in Mammalian Cardiac Cells." *Nature* 309 (5966): 354–56. <https://doi.org/10.1038/309354a0>.
- Kim, Grace E, and Leonard K Kaczmarek. 2014. "Emerging Role of the KCNT1 Slack Channel in Intellectual Disability." *Frontiers in Cellular Neuroscience* 8 (July): 209. <https://doi.org/10.3389/fncel.2014.00209>.
- Kim, Grace E, Jack Kronengold, Giulia Barcia, Imran H Quraishi, Hilary C Martin, Edward Blair, Jenny C Taylor, et al. 2014. "Human Slack Potassium Channel Mutations Increase Positive Cooperativity between Individual Channels." *Cell Reports* 9 (5): 1661–72. <https://doi.org/10.1016/j.celrep.2014.11.015>.
- Kohli, Utkarsh, Chitra Ravishankar, and Douglas Nordli. 2020. "Cardiac Phenotypic Spectrum of KCNT1 Mutations." *Cardiology in the Young* 30 (12): 1935–39. <https://doi.org/10.1017/S1047951120002735>.
- Kuchenbuch, Mathieu, Giulia Barcia, Nicole Chemaly, Emilie Carme, Agathe Roubertie, Marc Gibaud, Patrick Van Bogaert, et al. 2019. "KCNT1 Epilepsy with Migrating Focal Seizures Shows a Temporal Sequence with Poor Outcome, High Mortality and SUDEP." *Brain: A Journal of Neurology* 142 (10): 2996–3008. <https://doi.org/10.1093/brain/awz240>.
- Lim, Chiao Xin, Michael G Ricos, Leanne M Dibbens, and Sarah E Heron. 2016. "KCNT1 Mutations in Seizure Disorders: The Phenotypic Spectrum and Functional Effects."

- Journal of Medical Genetics* 53 (4): 217–25. <https://doi.org/10.1136/jmedgenet-2015-103508>.
- Liu, Ru, Lei Sun, Yunfu Wang, Qun Wang, and Jianping Wu. 2023. “New Use for an Old Drug: Quinidine in KCNT1-Related Epilepsy Therapy.” *Neurological Sciences* 44 (4): 1201–6. <https://doi.org/10.1007/s10072-022-06521-x>.
- Los Angeles Tejada, Maria de, Kathleen Stolpe, Anne-Kristine Meinild, and Dan A Klaerke. 2012. “Clofilium Inhibits Slick and Slack Potassium Channels.” *Biologics : Targets & Therapy* 6 (December): 465–70. <https://doi.org/10.2147/BTT.S33827>.
- Lu, Jinyu, Gaohua Zhao, Dayao Lv, Lanxiao Cao, and Guohua Zhao. 2022. “Autosomal Dominant Sleep-Related Hypermotor Epilepsy Associated with a Novel Mutation of KCNT1.” *Translational Neuroscience* 13 (1): 240–45. <https://doi.org/10.1515/tnsci-2022-0241>.
- M Qunies, Alshaima’a, and Kyle A Emmitte. 2022. “Small-Molecule Inhibitors of Slack Potassium Channels as Potential Therapeutics for Childhood Epilepsies.” *Pharmaceutical Patent Analyst* 11 (2): 45–56. <https://doi.org/10.4155/ppa-2022-0002>.
- Mancilla, Jaime G, Timothy J Lewis, David J Pinto, John Rinzel, and Barry W Connors. 2007. “Synchronization of Electrically Coupled Pairs of Inhibitory Interneurons in Neocortex.” *The Journal of Neuroscience* 27 (8): 2058–73. <https://doi.org/10.1523/JNEUROSCI.2715-06.2007>.
- Matt, Lucas, Thomas Pham, David Skrabak, Felix Hoffmann, Philipp Eckert, Jiaqi Yin, Miriam Gisevius, et al. 2021. “The Na<sup>+</sup>-Activated K<sup>+</sup> Channel Slack Contributes to Synaptic Development and Plasticity.” *Cellular and Molecular Life Sciences* 78 (23): 7569–87. <https://doi.org/10.1007/s00018-021-03953-0>.
- McTague, Amy, Katherine B Howell, J Helen Cross, Manju A Kurian, and Ingrid E Scheffer. 2016. “The Genetic Landscape of the Epileptic Encephalopathies of Infancy and Childhood.” *Lancet Neurology* 15 (3): 304–16. [https://doi.org/10.1016/S1474-4422\(15\)00250-1](https://doi.org/10.1016/S1474-4422(15)00250-1).
- McTague, Amy, Umesh Nair, Sony Malhotra, Esther Meyer, Natalie Trump, Elena V Gazina, Apostolos Papanthou, et al. 2018. “Clinical and Molecular Characterization of KCNT1-Related Severe Early-Onset Epilepsy.” *Neurology* 90 (1): e55–66. <https://doi.org/10.1212/WNL.0000000000004762>.
- Milligan, Carol J, Melody Li, Elena V Gazina, Sarah E Heron, Umesh Nair, Chantel Trager, Christopher A Reid, et al. 2014. “KCNT1 Gain of Function in 2 Epilepsy Phenotypes Is Reversed by Quinidine.” *Annals of Neurology* 75 (4): 581–90. <https://doi.org/10.1002/ana.24128>.
- Miyawaki, Hiroyuki, and Kamran Diba. 2016. “Regulation of Hippocampal Firing by Network Oscillations during Sleep.” *Current Biology* 26 (7): 893–902. <https://doi.org/10.1016/j.cub.2016.02.024>.
- Miziak, Barbara, and Stanisław J Czuczwar. 2022. “Approaches for the Discovery of Drugs That Target K Na 1.1 Channels in KCNT1-Associated Epilepsy.” *Expert Opinion on Drug Discovery* 17 (12): 1313–28. <https://doi.org/10.1080/17460441.2023.2150164>.

- Mochol, Monika, Erik Taubøll, Pål Aukrust, Thor Ueland, Ole A. Andreassen, and Sigrid Svalheim. 2023. "Serum Markers of Neuronal Damage and Astrocyte Activity in Patients with Chronic Epilepsy: Elevated Levels of Glial Fibrillary Acidic Protein." *Acta Neurologica Scandinavica* 2023 (February): 1–5. <https://doi.org/10.1155/2023/7246373>.
- Montgomery, Sean M, Anton Sirota, and György Buzsáki. 2008. "Theta and Gamma Coordination of Hippocampal Networks during Waking and Rapid Eye Movement Sleep." *The Journal of Neuroscience* 28 (26): 6731–41. <https://doi.org/10.1523/JNEUROSCI.1227-08.2008>.
- Murnane, Kevin Sean, Osman F Guner, J Phillip Bowen, Kalyn M Rambacher, Nader H Moniri, Tyler J Murphy, Cedrick Maceo Daphney, Aboagyewaah Oppong-Damoah, and Kenner C Rice. 2019. "The Adrenergic Receptor Antagonist Carvedilol Interacts with Serotonin 2A Receptors Both in Vitro and in Vivo." *Pharmacology, Biochemistry, and Behavior* 181 (June): 37–45. <https://doi.org/10.1016/j.pbb.2019.04.003>.
- Niday, Zachary, and Anastasios V Tzingounis. 2018. "Potassium Channel Gain of Function in Epilepsy: An Unresolved Paradox." *The Neuroscientist* 24 (4): 368–80. <https://doi.org/10.1177/1073858418763752>.
- Pollock, Emily, Michelle Everest, Arthur Brown, and Michael O Poulter. 2014. "Metalloproteinase Inhibition Prevents Inhibitory Synapse Reorganization and Seizure Genesis." *Neurobiology of Disease* 70 (October): 21–31. <https://doi.org/10.1016/j.nbd.2014.06.003>.
- Qunies, Alshaima'a M, Brittany D Spitznagel, Yu Du, C David Weaver, and Kyle A Emmitte. 2023. "Design, Synthesis, and Biological Evaluation of a Novel Series of 1,2,4-Oxadiazole Inhibitors of SLACK Potassium Channels: Identification of in Vitro Tool VU0935685." *Bioorganic & Medicinal Chemistry* 95 (November): 117487. <https://doi.org/10.1016/j.bmc.2023.117487>.
- Qunies, Alshaima'a M, Brittany D Spitznagel, Yu Du, Paul K Peprah, Yasmeeen K Mohamed, C David Weaver, and Kyle A Emmitte. 2024. "Structure-Activity Relationship Studies in a Series of Xanthine Inhibitors of SLACK Potassium Channels." *Molecules* 29 (11). <https://doi.org/10.3390/molecules29112437>.
- Quraishi, Imran H, Shani Stern, Kile P Mangan, Yalan Zhang, Syed R Ali, Michael R Mercier, Maria C Marchetto, et al. 2019. "An Epilepsy-Associated KCNT1 Mutation Enhances Excitability of Human iPSC-Derived Neurons by Increasing Slack KNa Currents." *The Journal of Neuroscience* 39 (37): 7438–49. <https://doi.org/10.1523/JNEUROSCI.1628-18.2019>.
- Rizzi, Sandra, Hans-Günther Knaus, and Christoph Schwarzer. 2016. "Differential Distribution of the Sodium-Activated Potassium Channels Slick and Slack in Mouse Brain." *The Journal of Comparative Neurology* 524 (10): 2093–2116. <https://doi.org/10.1002/cne.23934>.
- Rizzo, Francesca, Paolo Ambrosino, Anna Guacci, Massimiliano Chetta, Giovanna Marchese, Teresa Rocco, Maria Virginia Soldovieri, et al. 2016. "Characterization of Two de Novo KCNT1 Mutations in Children with Malignant Migrating Partial Seizures in Infancy." *Molecular and Cellular Neurosciences* 72 (April): 54–63. <https://doi.org/10.1016/j.mcn.2016.01.004>.

- Roliz, Annie H, and Sanjeev Kothare. 2022. "The Interaction between Sleep and Epilepsy." *Current Neurology and Neuroscience Reports* 22 (9): 551–63. <https://doi.org/10.1007/s11910-022-01219-1>.
- Roopun, Anita K, Steven J Middleton, Mark O Cunningham, Fiona E N LeBeau, Andrea Bibbig, Miles A Whittington, and Roger D Traub. 2006. "A Beta2-Frequency (20-30 Hz) Oscillation in Nonsynaptic Networks of Somatosensory Cortex." *Proceedings of the National Academy of Sciences of the United States of America* 103 (42): 15646–50. <https://doi.org/10.1073/pnas.0607443103>.
- Sacco, Sandra M, Caitlin Saint, Paul J LeBlanc, and Wendy E Ward. 2017. "Maternal Consumption of Hesperidin and Naringin Flavanones Exerts Transient Effects to Tibia Bone Structure in Female CD-1 Offspring." *Nutrients* 9 (3). <https://doi.org/10.3390/nu9030250>.
- Schaefer, W H, J Politowski, B Hwang, F Dixon, A Goalwin, L Gutzait, K Anderson, C DeBrosse, M Bean, and G R Rhodes. 1998. "Metabolism of Carvedilol in Dogs, Rats, and Mice." *Drug Metabolism and Disposition: The Biological Fate of Chemicals* 26 (10): 958–69.
- Shore, Amy N, Sophie Colombo, William F Tobin, Sabrina Petri, Erin R Cullen, Soledad Dominguez, Christopher D Bostick, et al. 2020. "Reduced GABAergic Neuron Excitability, Altered Synaptic Connectivity, and Seizures in a KCNT1 Gain-of-Function Mouse Model of Childhood Epilepsy." *Cell Reports* 33 (4): 108303. <https://doi.org/10.1016/j.celrep.2020.108303>.
- Shore, Amy N, Keyong Li, Mona Safari, Alshaima'a M Qunies, Brittany D Spitznagel, C David Weaver, Kyle Emmitte, Wayne Frankel, and Matthew C Weston. 2024. "Heterozygous Expression of a Kcnt1 Gain-of-Function Variant Has Differential Effects on Somatostatin- and Parvalbumin-Expressing Cortical GABAergic Neurons." *ELife* 13 (October). <https://doi.org/10.7554/eLife.92915>.
- Siapas, Athanassios G, Evgueniy V Lubenov, and Matthew A Wilson. 2005. "Prefrontal Phase Locking to Hippocampal Theta Oscillations." *Neuron* 46 (1): 141–51. <https://doi.org/10.1016/j.neuron.2005.02.028>.
- Sinha, Saurabh R. 2011. "Basic Mechanisms of Sleep and Epilepsy." *Journal of Clinical Neurophysiology* 28 (2): 103–10. <https://doi.org/10.1097/WNP.0b013e3182120d41>.
- Sirota, Anton, Sean Montgomery, Shigeyoshi Fujisawa, Yoshikazu Isomura, Michael Zugaro, and György Buzsáki. 2008. "Entrainment of Neocortical Neurons and Gamma Oscillations by the Hippocampal Theta Rhythm." *Neuron* 60 (4): 683–97. <https://doi.org/10.1016/j.neuron.2008.09.014>.
- Sohal, Vikaas S, Feng Zhang, Ofer Yizhar, and Karl Deisseroth. 2009. "Parvalbumin Neurons and Gamma Rhythms Enhance Cortical Circuit Performance." *Nature* 459 (7247): 698–702. <https://doi.org/10.1038/nature07991>.
- Spitznagel, Brittany D, Nigam M Mishra, Alshaima'a M Qunies, Francis J Prael, Yu Du, Krystian A Kozek, Roman M Lazarenko, Jerod S Denton, Kyle A Emmitte, and C David Weaver. 2020. "VU0606170, a Selective Slack Channels Inhibitor, Decreases Calcium Oscillations in Cultured Cortical Neurons." *ACS Chemical Neuroscience* 11 (21): 3658–71. <https://doi.org/10.1021/acscchemneuro.0c00583>.

- Stark, Eran, Ronny Eichler, Lisa Roux, Shigeyoshi Fujisawa, Horacio G Rotstein, and György Buzsáki. 2013. "Inhibition-Induced Theta Resonance in Cortical Circuits." *Neuron* 80 (5): 1263–76. <https://doi.org/10.1016/j.neuron.2013.09.033>.
- Tang, Qiong-Yao, Fei-Fei Zhang, Jie Xu, Ran Wang, Jian Chen, Diomedes E Logothetis, and Zhe Zhang. 2016. "Epilepsy-Related Slack Channel Mutants Lead to Channel Over-Activity by Two Different Mechanisms." *Cell Reports* 14 (1): 129–39. <https://doi.org/10.1016/j.celrep.2015.12.019>.
- Tecott, L H, L L Kwong, S Uhr, and S J Peroutka. 1986. "Differential Modulation of Dopamine D2 Receptors by Chronic Haloperidol, Nitrendipine, and Pimozide." *Biological Psychiatry* 21 (12): 1114–22. [https://doi.org/10.1016/0006-3223\(86\)90219-2](https://doi.org/10.1016/0006-3223(86)90219-2).
- TEVA PHARMACEUTICALS. 2008. "ORAP (Pimozide) Tablets - Clinical Pharmacology and Indications," January.
- Thesis, Nele Bohne. 2023. "Assessing Novel Therapies for KCNT1 Channelopathies in Mice Harboring Patient-Derived Pathogenic Sequence Variants." Master thesis, University Duisburg-Essen.
- Veit, Julia, Richard Hakim, Monika P Jadi, Terrence J Sejnowski, and Hillel Adesnik. 2017. "Cortical Gamma Band Synchronization through Somatostatin Interneurons." *Nature Neuroscience* 20 (7): 951–59. <https://doi.org/10.1038/nn.4562>.
- Villa, Chiara, and Romina Combi. 2016. "Potassium Channels and Human Epileptic Phenotypes: An Updated Overview." *Frontiers in Cellular Neuroscience* 10 (March): 81. <https://doi.org/10.3389/fncel.2016.00081>.
- Wen, Teresa H, Devin K Binder, Iryna M Ethell, and Khaleel A Razak. 2018. "The Perineuronal 'safety' Net? Perineuronal Net Abnormalities in Neurological Disorders." *Frontiers in Molecular Neuroscience* 11 (August): 270. <https://doi.org/10.3389/fnmol.2018.00270>.
- Wu, Jing, Lynda El-Hassar, Dibyadeep Datta, Merrilee Thomas, Yalan Zhang, David P Jenkins, Nicholas J DeLuca, et al. 2024. "Interaction Between HCN and Slack Channels Regulates MPFC Pyramidal Cell Excitability in Working Memory Circuits." *Molecular Neurobiology* 61 (4): 2430–45. <https://doi.org/10.1007/s12035-023-03719-8>.
- Wu, Jing, Imran H Quraishi, Yalan Zhang, Mark Bromwich, and Leonard K Kaczmarek. 2024. "Disease-Causing Slack Potassium Channel Mutations Produce Opposite Effects on Excitability of Excitatory and Inhibitory Neurons." *Cell Reports* 43 (3): 113904. <https://doi.org/10.1016/j.celrep.2024.113904>.
- Xu, Da, Shuang Chen, Jun Yang, Xiufeng Wang, Zhi Fang, and Man Li. 2022. "Precision Therapy with Quinidine of KCNT1-Related Epileptic Disorders: A Systematic Review." *British Journal of Clinical Pharmacology* 88 (12): 5096–5112. <https://doi.org/10.1111/bcp.15479>.
- Xu, Jie, Yan-Tian Lv, Xiao-Yun Zhao, Jing-Jing Wang, Zhong-Shan Shen, Jian Li, Fei-Fei Zhang, et al. 2023. "Identification of Sodium- and Chloride-Sensitive Sites in the Slack Channel." *The Journal of Neuroscience* 43 (15): 2665–81. <https://doi.org/10.1523/JNEUROSCI.1365-22.2023>.

- Yamamoto, Kaoru, Shimpei Baba, Takashi Saito, Eiji Nakagawa, Kenji Sugai, Masaki Iwasaki, Atsushi Fujita, et al. 2023. “Synchronous Heart Rate Reduction with Suppression-Burst Pattern in KCNT1-Related Developmental and Epileptic Encephalopathies.” *Epilepsia Open* 8 (2): 651–58. <https://doi.org/10.1002/epi4.12705>.
- Yang, Haiyan, Xiaofan Yang, Fang Cai, Siyi Gan, Sai Yang, and Liwen Wu. 2022. “Analysis of Clinical Phenotypic and Genotypic Spectra in 36 Children Patients with Epilepsy of Infancy with Migrating Focal Seizures.” *Scientific Reports* 12 (1): 10187. <https://doi.org/10.1038/s41598-022-13974-9>.
- Yuan, Alex, Celia M Santi, Aguan Wei, Zhao Wen Wang, Kelly Pollak, Michael Nonet, Leonard Kaczmarek, C Michael Crowder, and Lawrence Salkoff. 2003. “The Sodium-Activated Potassium Channel Is Encoded by a Member of the Slo Gene Family.” *Neuron* 37 (5): 765–73. [https://doi.org/10.1016/s0896-6273\(03\)00096-5](https://doi.org/10.1016/s0896-6273(03)00096-5).
- Zhang, Jiangtao, Shiqi Liu, Junping Fan, Rui Yan, Bo Huang, Feng Zhou, Tian Yuan, Jianke Gong, Zhuo Huang, and Daohua Jiang. 2023. “Structural Basis of Human Slo2.2 Channel Gating and Modulation.” *Cell Reports* 42 (8): 112858. <https://doi.org/10.1016/j.celrep.2023.112858>.
- Zhang, Qi, Shun-Heng Gao, Zhong-Shan Shen, Yun Wang, Su-Wan Hu, Guang-Bing Duan, Ye Liu, et al. 2022. “The Slack Channel Regulates Anxiety-Like Behaviors via Basolateral Amygdala Glutamatergic Projections to Ventral Hippocampus.” *The Journal of Neuroscience* 42 (14): 3049–64. <https://doi.org/10.1523/JNEUROSCI.2027-21.2022>.

## **Acknowledgement**

First, I would like to express my gratitude to Prof. Dr. Dirk Isbrandt for welcoming me into his research group and guiding me through this challenging journey with patience and support. He was always there for me when I needed him and motivated me to keep pushing forward.

I am deeply indebted to Dr. Malte Stockebrand for his wholehearted help without hesitation in the path of this thesis. I am genuinely thankful to Prof. Dr. Matteo Bergami and Prof. Dr. Tatiana Korotkova for accepting to be a tutor for my journey. Their expertise and dedication to advancing my understanding in our annual meetings have been invaluable.

I would like to extend my sincere gratitude to my collaborators, including Dr. Fabio Morellini, Dr. Kunihiko Araki and Prof. Dr. Heinz Beck, for their meaningful contributions to this work. Their expertise and the additional data they provided have been instrumental in deepening the scope and impact of my research.

With all my soul, I would like to thank Hanna Oelßner, who brightened my days with her smile and stood by me through the most stressful moments. Your support has been a source of strength, and this thesis would have never been possible without you.

To my friends and colleagues, Grusha Mathias, Daniil Kirianov, and Nele Bohne, you have been more than just co-workers; you've been my companions in this journey. Thank you for being there to share the laughter, frustrations, and victories along the way.

A special thanks to Christopher Schühlein for being a great friend everyone wishes they had. Your unwavering friendship, humor, and support helped me to navigate the emotional rollercoaster of these years.

Last but not least, I am eternally grateful to my family. Your love and encouragement have been my anchor throughout this journey. Thank you for believing in me unconditionally and for your sacrifices that made this path possible.

## Statutory Declaration

Ich versichere, dass ich die von mir vorgelegte Dissertation selbstständig angefertigt, die benutzten Quellen und Hilfsmittel vollständig angegeben und die Stellen der Arbeit - einschließlich Tabellen, Karten und Abbildungen -, die anderen Werken im Wortlaut oder dem Sinn nach entnommen sind, in jedem Einzelfall als Entlehnung kenntlich gemacht habe; dass diese Dissertation noch keiner anderen Fakultät oder Universität zur Prüfung vorgelegen hat; dass sie - abgesehen von unten angegebenen Teilpublikationen - noch nicht veröffentlicht worden ist sowie, dass ich eine solche Veröffentlichung vor Abschluss des Promotionsverfahrens nicht vornehmen werde. Die Bestimmungen dieser Promotionsordnung sind mir bekannt. Die von mir vorgelegte Dissertation ist von Prof. Dr. Dirk Isbrandt betreut worden.

Ich versichere, dass ich alle Angaben wahrheitsgemäß nach bestem Wissen und Gewissen gemacht habe und verpflichte mich, jedmögliche, die obigen Angaben betreffenden Veränderungen, dem Promotionsausschuss unverzüglich mitzuteilen.

14.04.2025

Datum

Timucin Bas

Unterschrift